Large-scale Investigation of Memory Circuits

Prawesh Dahal

Submitted in partial fulfillment of the
requirements for the degree of
Doctor of Philosophy
under the Executive Committee
of the Graduate School of Arts and Sciences

COLUMBIA UNIVERSITY

2023

Abstract

Large-scale Investigation of Memory Circuits

Prawesh Dahal

The human brain relies on the complex interactions of distinct brain regions to support cognitive processes. The interplay between the hippocampus and neocortical regions plays a key role in the formation, storage, and retrieval of long-term episodic memories. Oscillatory activities during sleep are a fundamental mechanism that binds distributed neuronal networks into functionally coherent ensembles. However, the large-scale hippocampal-neocortical oscillatory mechanisms that support flexible modulation of long-term memory remain poorly understood. Furthermore, alterations to physiologic spatiotemporal patterns that are essential for intact memory function can result in pathophysiology in brain disorders such as focal epilepsy. Investigating how epileptic network activity disrupts connectivity in distributed networks and the organization of oscillatory activity are additional crucial areas that require further research. Our experiments on rodents and human patients with epilepsy have provided valuable insights into these mechanisms. In rodents, we used high-density microelectrode arrays in tandem with hippocampal probes to analyze intracranial electroencephalography (iEEG) from multiple cortical regions and the hippocampus. We identified key hippocampal-cortical oscillatory biomarkers that were differentially coordinated based on the age, strength, and type of memory. We also analyzed iEEG from patients with focal epilepsy and demonstrated how individualized pattern of pathologic-physiologic coupling can disrupt large-scale memory circuits. Our findings may offer new opportunities for therapies aimed at addressing distributed network dysfunction in various neuropsychiatric disorders.

Table of Contents

Chapter 1: Memory Circuits of the Brain

1.1 Multiple Memory Systems

Human memory can be broadly categorized into two main types: short-term memory (STM) and long-term memory (LTM). STM or working memory is responsible for holding a limited amount of information for a brief period, typically seconds to minutes. On the other hand, LTM can hold an unlimited amount of information for an extended period, ranging from minutes to years. LTM can be further divided into nondeclarative memory and declarative memory. Nondeclarative memory, also known as implicit memory, includes memory for skills, habits, and conditioned responses. Declarative memory involves conscious recollection of information and can be further divided into episodic memory (memory for personal experiences) and semantic memory (memory for general knowledge and facts). These different types of memory are processed in different brain regions and involve different neural mechanisms.

1.2 Declarative Memory and Hippocampus

The hippocampal region has been identified as fundamental to our capacity for declarative memory. The important principle in declarative memory is the ability to encode the uniqueness of a single event in place and time. Episodic memory is the specific form of long-term declarative memory that allows us to learn, store, and recall everyday events within a spatiotemporal context. Decades of neurobiological studies have established that this memory function is supported by the medial temporal lobe (MTL) memory system which includes the hippocampus, the parahippocampal region and neocortical areas.[1] In 1957, Scoville and Milner conducted a groundbreaking study on the renowned patient H. M. and provided the first detailed analysis of the effects of damage to the hippocampal region on long-term episodic memory.[2] H. M., who

underwent bilateral remove of the medial temporal lobes to alleviate epilepsy, suffered from severe amnesia as a result. Continuing study of H. M. [3],[4] and other amnesic patients [5], [6] revealed that damage to the MTL, or specifically the hippocampus, impedes the ability to remember recent autobiographical memories as well as causes deficits in long-term spatial memory. [7] However, short-term memories, the learning of skills, and general knowledge and facts are not affected. These findings suggest that hippocampal regions function predominantly for one type of memory processing – memory of places and events. Notably, these amnesic patients had no difficulty recalling remote memories formed well before the lesion, indicating that the hippocampus may also have a time-limited role in memory processing.

Further research on animal models has been instrumental in dissecting the hippocampal memory system and characterizing the neural circuitry and information processing mechanisms that mediate long-term memory processing. These studies have provided supportive evidence for the hypothesis generated by the early studies that the hippocampus plays a critical role in initial episodic memory formation. However, over time, memories appear to be reorganized somewhere outside of the hippocampal network, where they may become resistant to disruption caused by hippocampal damage.

1.3 Lesions in Animal Models

Animal models have played a crucial role in establishing a consensus on the function of the hippocampal memory system by enabling invasive experiments with interventions such as lesions. In nonhuman primates and rodents, damage to the hippocampal region has resulted in findings similar to human amnesia and has supported the hippocampus's time-limited and memory-specific roles. For example, monkeys trained in multiple object discrimination tasks showed better recall for problems learned 12 weeks before the lesion than those learned just before the lesion.[8],[9]

Similarly, rats with hippocampal lesions 28 days after contextual fear conditioning continued to exhibit fear in the conditioning chamber, unlike rats trained just one day before the lesion. [10] Additionally, hippocampal lesions resulted in impairments in rodents' spatial working memory [11] and navigation skills to hidden spatial goals in a water maze.[12]

These neurophysiologic lesion studies in animals suggested that episodic memory becomes less dependent on the hippocampal region over time. Based on these findings, researchers proposed the influential theory of the two-stage model of systems consolidation [13],[14], according to which initial hippocampal memory traces are reactivated offline to transfer and gradually strengthen memory representations in the neocortex.

1.4 Hippocampal – Neocortical Circuitry

To understand the nature of memory consolidation, it is crucial to first delineate the anatomical organization of the hippocampal memory system and its signaling pathways to the neocortex. Given that the formation and storage of memory involve an interplay between the MTL and neocortex, it follows that there must be some kind of interaction between these two regions. By understanding the organization of the hippocampal memory system and the pathways through which it communicates with the neocortex, we can gain insight into the mechanisms underlying memory consolidation.

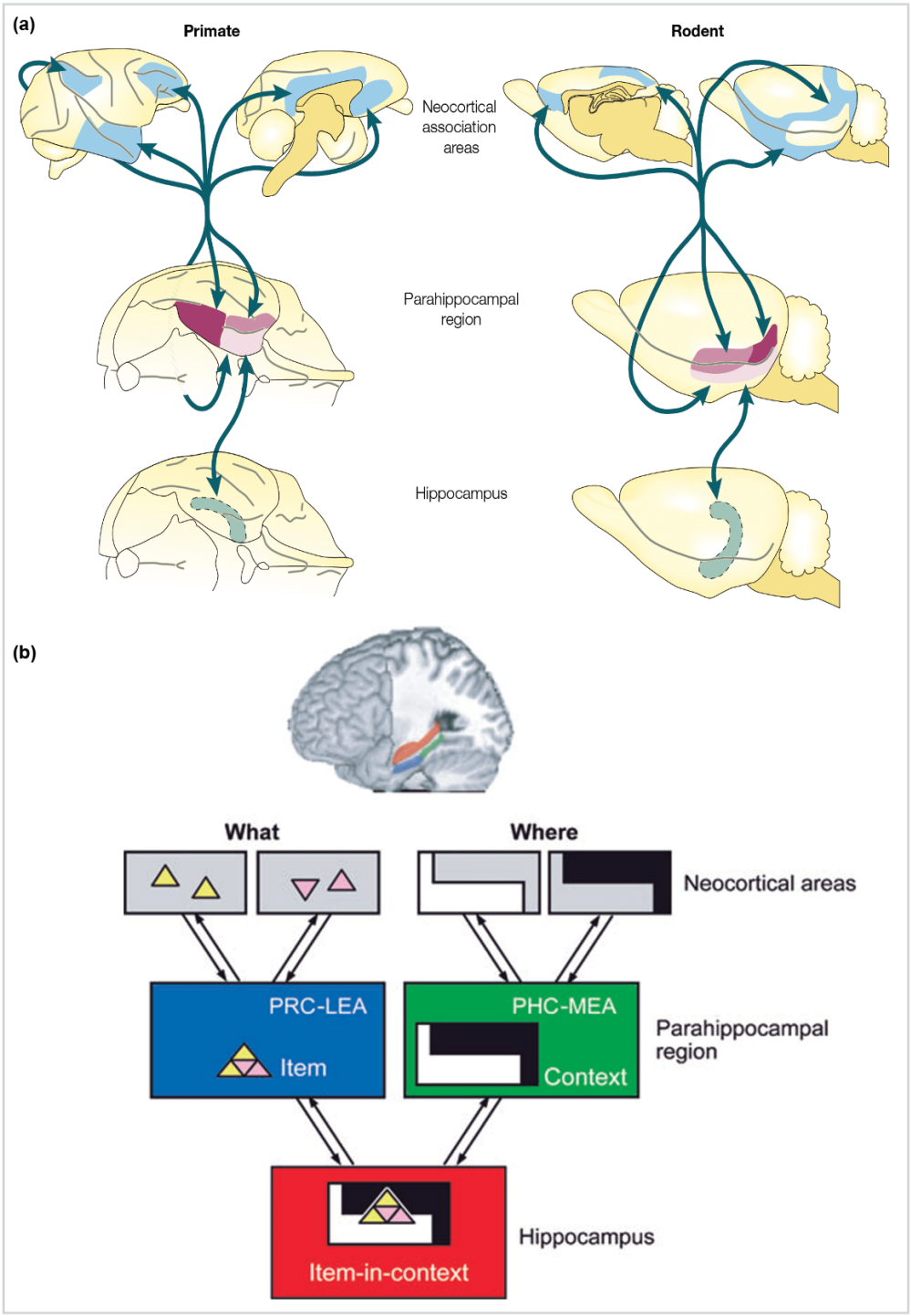

Figure 1: The anatomical and functional organization of the hippocampal memory system: **(a)**: The neocortical areas (blue), the perirhinal cortex (purple), the parahippocampal or postrhinal cortex (dark purple), the entorhinal cortex (light purple) and the hippocampus (green) form this memory system. Figure from [1] **(b)** Perirhinal Cortex (PRC) – Lateral entorhinal area (LEA), Parahippocampal cortex (PHC) – Medial entorhinal area (MEA).

As shown in both monkeys and rats [15]-[16], the hippocampus receives information from various areas of the neocortex through the parahippocampal region, which includes the perirhinal, parahippocampal (or postrhinal in rats), and entorhinal cortices (Figure 1). These subdivisions of the parahippocampal region are interconnected and serve as a convergence site for cortical input, distributing cortical afferents to different parts of the hippocampus, such as the dentate gyrus, CA3 and CA1 areas, and subiculum. Within the hippocampus, there are both divergent and convergent connections that could facilitate a large network of associations and support plasticity mechanisms for encoding new information. The parahippocampal region receives output from the hippocampus and projects back to the same areas of the neocortex that originally provided input to this region.[17]

The complex interactions between these regions governs declarative memories. The hippocampal memory system is functionally organized into distinct streams for processing spatial information and object features (Figure 1b). The cortical projections to the subregions of the MTL are streamed in two parallel pathways [18], characterized as relating to spatial and non-spatial features of sensory input. Neocortical input regarding object features ("what") are passed through the perirhinal cortex (PRC) and lateral entorhinal area (LEA), while spatial details, ("where") converge in the parahippocampal cortex (PHC) and medial entorhinal area (MEA). These pathways converge in the hippocampus which integrates and represents events in the context in which they were experienced. Reverse projections trace the same pathways back to the parahippocampal and neocortical regions. Back projections to the PHC-MEA may support recall of context, while back projections to the PHC-LEA may support recall of item associations. This functional organization allows for the integration of various types of information to form complex

memories, and for the retrieval of these memories through different pathways depending on the type of information being accessed.

1.5 Two-Stage Model of Memory Consolidation

The two-stage model of systems memory consolidation (Figure 2) is a widely accepted theory that explains the process by which newly encoded memories are gradually transferred and strengthened from the hippocampus to the neocortex. [19], [20] This process occurs in two stages - during the initial encoding, the hippocampus binds the different neocortical components of the experience into one unique episodic memory. However, these memories are not yet stable and are prone to interference. In the second stage, the hippocampus reactivates and replays the memory traces during periods of rest or sleep, which then propagates across the hippocampal memory network and reactivates the neocortical components. This coactivation triggers stabilization of local synaptic changes and strengthens the memory representations in the distributed neocortical networks, thus integrating them into long-term memories. These long-term memories become stable and resistant to interference, but remain susceptible to updating, weakening or modification post memory recall or retrieval in a mechanism called reconsolidation. [21], [22]

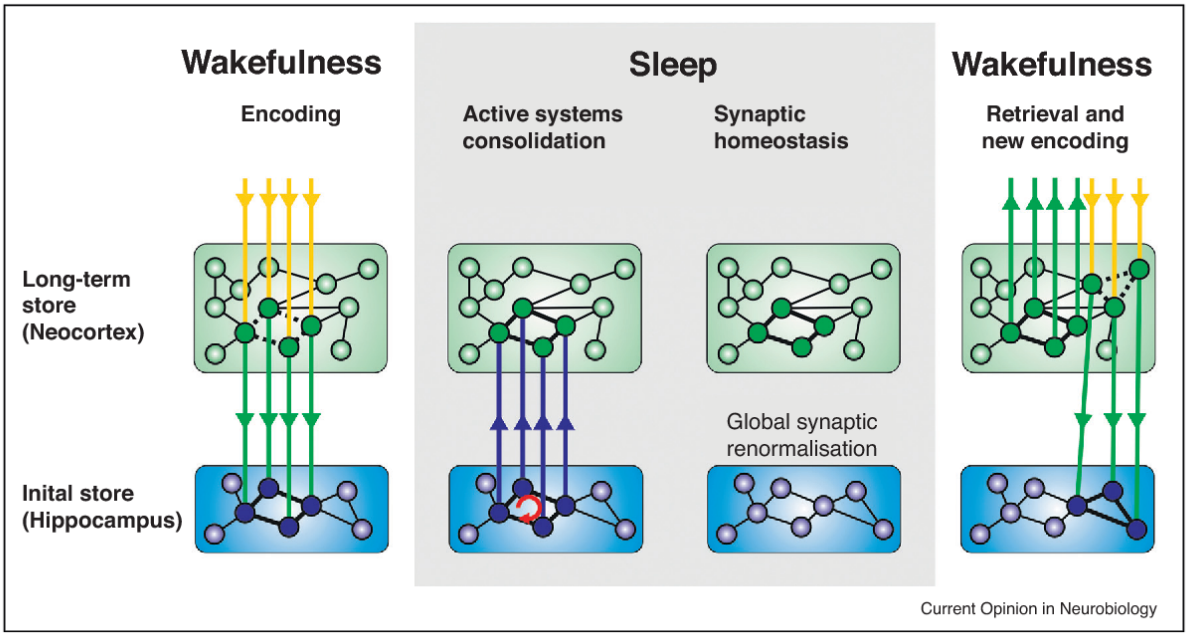

Figure 2: Schematic of process of memory consolidation: During wakefulness, external information (yellow arrows) flows through our sensory neocortical sites to the hippocampus that rapid binds it into a temporary unique representation. During sleep, these memory traces are repeatedly reactivated (red arrow) and transformed and integrated into neocortex (blue arrows). This process is called systems consolidation. Sleep also leads to global synaptic renormalization that could lead to the erasure of irrelevant information. Consolidated remote memories can be retrieved during wake again without involving the hippocampus (green upward arrows) and other new information can be encoded (yellow and green downward arrows) [20].

1.6 Stage I – Encoding

During wakefulness, the hippocampus is responsible for encoding novel episodic information. Studies using microdialysis measurements have shown that there are high levels of acetylcholine release in the hippocampus of freely moving rats during active wake behavior. [23] This release partially suppresses excitatory feedback connections in the hippocampus from CA1 neurons and favors information flow from the neocortex, thereby setting the appropriate dynamics for encoding. Hippocampus plays a fundamental role in spatial memory by mapping spatial layouts of the environment and encoding “sense of location”. For example, in rodents exploring their environment, researchers reported the observation of hippocampal pyramidal cells, called place

cells, that selectively fire when the rat is in particular zones of space ('place fields'). [24] These place cell discharges are organized in time-compressed sequences that are precisely embedded in particular phases of the ongoing theta oscillations (7-14 Hz) in the wake hippocampus.[24]-[26] As a result, theta oscillations provide a timing signal to place cell firings to facilitate sequence learning in the hippocampal network during encoding.

1.7 Stage 2 – Sleep

The second stage of memory consolidation relies on sleep where the hippocampus, through its interactions with the cortex, promotes information transfer. In humans, sleep is divided into several stages including non-rapid eye movement (NREM) and rapid eye movement (REM) sleep (Figure 3). In humans, the NREM sleep is divided into 3 stages. The deepest stages of NREM sleep (stage 3) is also referred as slow wave sleep (SWS). SWS dominates the first half of nocturnal sleep and has been shown to be a crucial stage for reprocessing of memory representations. The latter stages of sleep are dominated by REM sleep. Rodent studies also typically identify SWS and REM sleep as the main sleep stages. However, rodent sleep is more fragmented characterized with shorter sleep epochs and more frequent changes in stages and awakenings. [28]

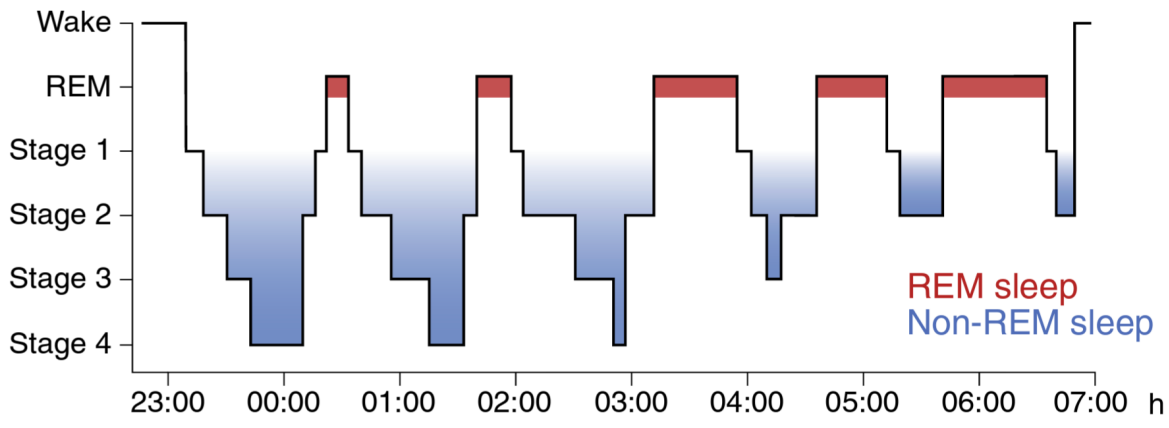

Figure 3: Sleep architecture in humans with cyclic occurrence of NREM and REM sleep. We can observe how NREM sleep phases are dominating the first half of the sleep whereas REM sleep the later stages. Figure from [28].

1.7.1 Hippocampal Neural Replay

During sleep, the brain is no longer exposed to external stimuli. This isolation is characterized by reduced level of acetylcholine in the hippocampus during SWS and quiet waking. [23] This might readjust the dynamics for the facilitation of consolidation of memory traces. The suppression of excitatory feedback connections of hippocampus during wake is now released, enhancing recurrent effective connectivity from hippocampus to extra-hippocampal networks. One way this could be achieved is through the phenomenon called neural replay. Neural replay is commonly observed during NREM sleep in rats where previously encoded spatial information (e.g., hippocampal place cell sequences during spatial exploration) is replayed by the hippocampus. [29]-[31] For example, compared to other cells, place cells activated during wake behavior increased their firing rate during subsequent sleep. Further studies confirmed strong correlations between spike trains of place cells observed during spatial exploration and those during sleep. In addition, these reactivated patterns during sleep also preserved the temporal order in which the cells fired during learning. Sequences of neural replay in the hippocampus are also coordinated with replay in the neocortex during SWS [32] suggesting the mediation of gradual redistribution of memory representations between these regions.

1.7.2 Sharp-wave Ripples

Importantly, this replay of firing patterns in hippocampal neuronal ensembles during sleep occurs predominantly during sharp-wave ripple oscillations (SPW-Rs; Figure 3). [33],[34] Sharp-wave ripples are caused by massive activation of a population of hippocampal neurons.[35] *Sharp-waves* localized in stratum radiatum reflect massive excitation of CA1 pyramidal neurons by synchronous

discharges of CA3 pyramidal cells via the Schaffer collaterals (Figure 4). The synchronization of the interneuron network at ~200 Hz generates fast field oscillations called *ripples* in the pyramidal layer. SPW-Rs occur during both SWS and non-exploratory wake states and have also been identified in macaques [36] and humans. [37]

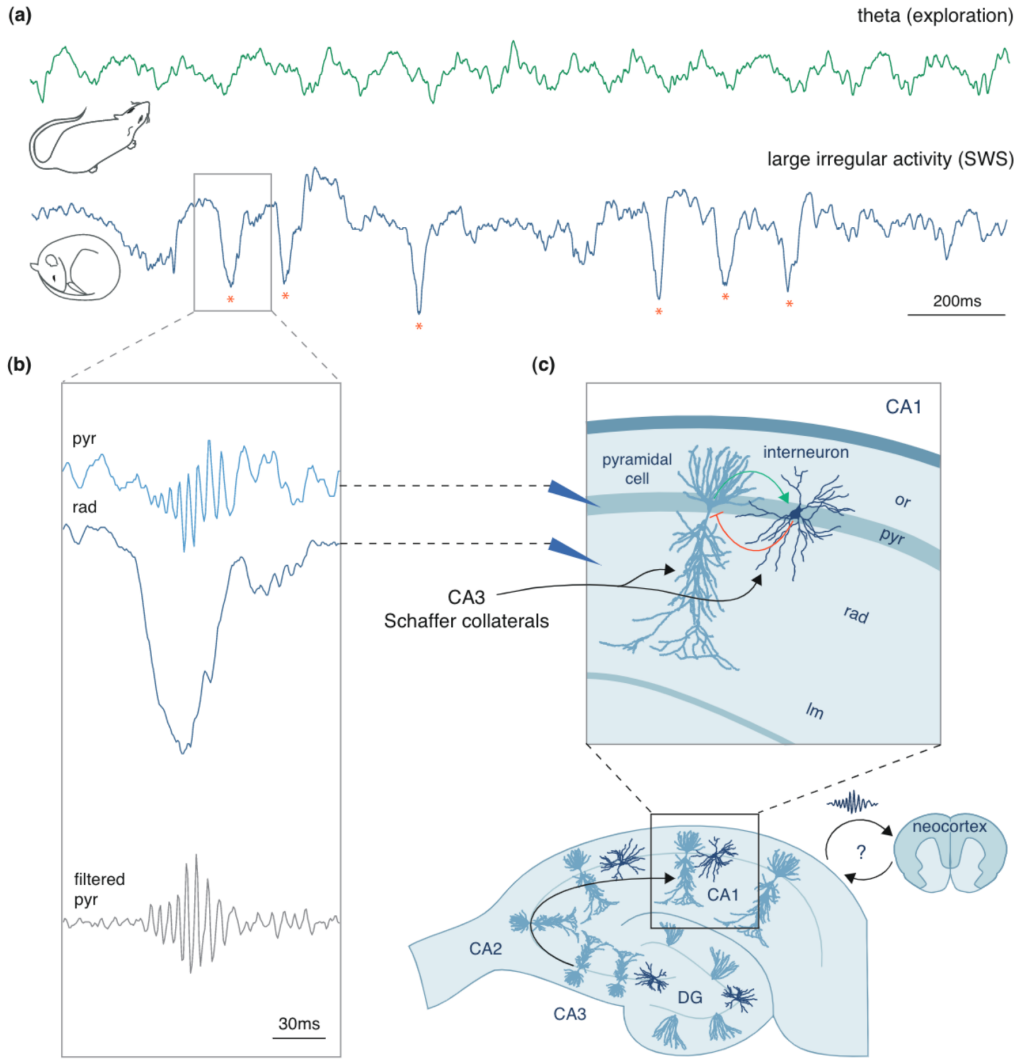

Figure 4: Hippocampal local field potentials (LFPs) during exploration and sleep. (a) Theta rhythm during exploration (green trace) and large irregular activity during SWS (blue trace) highlighting sharp wave events (red stars). **(b)** Zoomed view showing sharp wave in stratum radiatum (rad) and ripple oscillations in stratum pyramidale (pyr). Bottom trace is filtered SWR between 150-250 Hz. **(c)** Neuronal organization in the hippocampus (or: stratum oriens, lm: stratum lacunosum moleculare, CA1–3: cornu ammonis subfields of the hippocampus, DG: dentate gyrus).

Hippocampal replay events during sleep occurring during SPW-Rs are not only in strict temporal order, but also compressed in time by a factor of 5 to 20. [32]-[33] This has been demonstrated by employing methods like pattern-matching or sequence ranking in the firing trajectories. The temporal compression of neural replay makes it compatible with the typical time windows during which synaptic modifications and plasticity can be triggered, such as the induction of long-term potentiation (LTP) in the hippocampus. [38] Learning processes induce LTP in the hippocampus [40] that strengthens specific connections between neurons. Depolarization of the CA1 pyramidal cells during SPW-Rs also induces LTP [39] suggesting a potential mechanism utilized by SPW-Rs for memory consolidation.

1.7.3 Sharp-wave Ripples and Memory Consolidation

Several studies have demonstrated a strong correlation between SPW-Rs and memory consolidation. The occurrence rate of SPW-Rs has been shown to increase during sleep after learning and this increase seems to predict memory recall in rats as well as humans [42]-[43], suggesting that learning-dependent mechanisms can modulate SPW-Rs. One of the most influential studies that demonstrated the causal role of SPW-Rs in memory consolidation involved selectively suppressing ripples in rodents (Figure 5). This study, which used a hippocampal-dependent spatial memory task, detected ripples in the hippocampus during SWS after learning sessions and suppressed them through electrical stimulation. The disruption of ripples significantly impaired the animal's performance during recall, comparable to earlier effects observed in hippocampal lesion models. [44] Additional evidence was independently provided by another study which used a slightly different spatial learning task and stimulation protocol.[45] Therefore, these results provide direct evidence that SPW-Rs and its associated hippocampal neuronal reactivations in the off-line state play a causal role in the consolidation of memories.

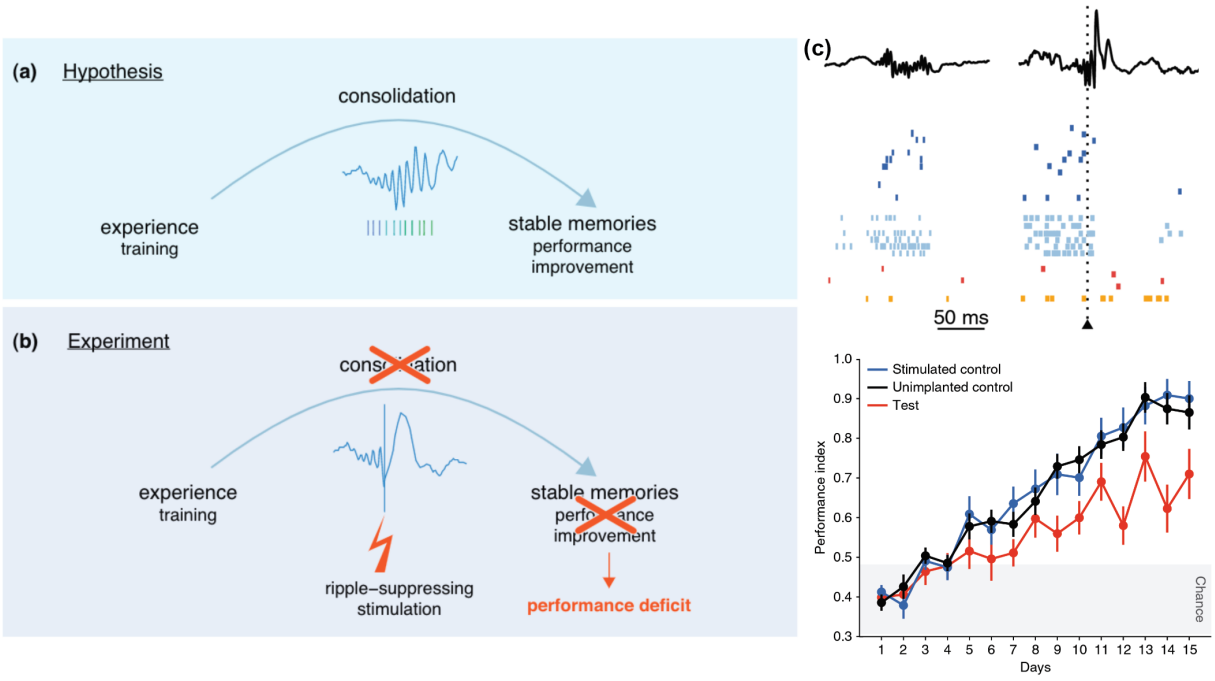

Figure 5: Causal role of SPW-Rs in memory consolidation. (a) Hypothesis – SPW-Rs and its associated neural replay is key to consolidation of memories. **(b)** Experiment to suppress ripples after learning and expect to induce a memory deficit. **(c)** Interruption of SPW-R and spiking activity in the hippocampus. LFPs (black traces), spiking activity (vertical ticks), time of stimulation (vertical dashed line) **(d)** Impaired performance in stimulated tests rats compared to controls. Figure from [45].

1.7.4 Hippocampal-Neocortical Transfer

According to the theory of consolidation, labile memory traces from the hippocampus are reorganized in the neocortical networks, leading to a retrieval process that gradually becomes independent of the hippocampus. Successful retrieval of remote memories is increasingly dependent on neocortical brain regions. For example, Takashima et al. showed using fMRI that hippocampal activation level during recognition memory tests declined over time accompanied by a progressively stronger activations in the medial prefrontal region, suggesting retrieval of remote memories can be executed without the hippocampus. [46] Changes such as synaptogenesis, increased gene expression, and laminar reorganization, occur in prefrontal and anterior cingulate cortex after spatial learning in mice, emphasizing the critical role of cortical sites in memory

storage and retrieval. [47] Multiple brain regions, including neocortical and subcortical regions, have also been shown to participate in neuronal ensemble reactivations during memory consolidation. These reactivations occur simultaneously with neuronal firings in the hippocampus, albeit with a slight delay of about 40-50 ms. [28],[32],[48] Taken together, these results suggests that there is a transfer of information between hippocampal and neocortex. Oscillations that occur during SWS have gathered strong evidence to be one of the driving mechanisms coordinating consolidation.

1.7.5 Role of Oscillations

Oscillations are produced predominantly by fluctuations in postsynaptic potentials. Oscillatory system, generated by local populations of neurons in one region can interact with neuronal assemblies in another remote but synaptically connected brain region through phase synchronization. [49] This phase synchrony allows neurons to open and close their window for sending and receiving information. [50] When the sending and receiving groups of neurons are excitable at the same times, communication and information transfer is facilitated. [51]-[53]

Oscillatory activities are key mechanisms of communication between distributed brain networks during wakefulness. [53] Studies on sensorimotor decision-making in primates and humans reveal that large-scale coherent oscillatory interactions, reflected by the phase coherence and amplitude correlation between brain regions, underlie neural mechanisms involved in different cognitive processes. Phase synchronization between the theta oscillations between prefrontal cortex and hippocampus has been implicated to modulate the retrieval of episodic memories in humans. [49] Oscillations have also been shown to travel across the cortical surface mediating intra- and inter-cortical information transfer. For example, beta oscillations (10-45 Hz) traveled as waves across motor cortices in monkeys performing a motor task. [52] In addition, these waves systematically

varied their spatiotemporal properties indicating that oscillatory activities can carry behaviorally relevant information. Beta traveling waves in the monkey frontoparietal network predict recent reward memory and the direction and timing of theta and alpha traveling waves in humans correlate with memory encoding and recall. Chapter 4 presents a novel finding on how pathological network in epilepsy can adopt similar properties of oscillations to alter the spatiotemporal patterns of physiologic memory circuits.

During slow-wave sleep, there are key oscillatory activities in the hippocampus and neocortex, the interplay of which is critical in memory consolidation. These oscillations regulate the timing of neural reactivations originating in the hippocampus in a manner capable of initiating synaptic changes in selected cortical sites. Oscillatory activity coordinated across multiple brain regions also creates a favorable context for the hippocampus to transfer and integrate information into relevant neocortical sites. This role of large-scale oscillatory orchestration for memory transfer is highlighted in Chapter 3.

1.7.6 Hippocampal-Cortical Oscillatory Coupling

Multiple studies have indicated that hippocampal-cortical dialogue might be facilitated through precise temporal coordination of hippocampal SPW-Rs oscillations with neocortical rhythms during sleep [56],[57] (Figure 5). The neocortical LFP oscillations present during SWS are slow oscillations (< 1 Hz) and thalamocortical spindles (12-15 Hz in humans and 8-20 Hz in rodents).

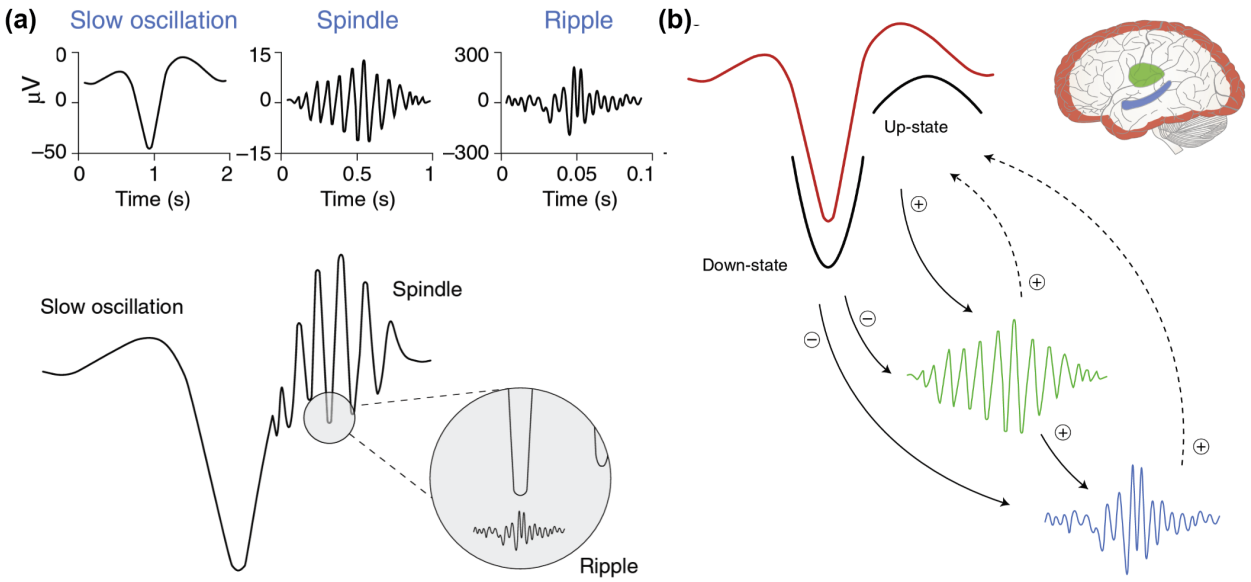

Figure 6: Temporal interplay of SPW-Rs with slow oscillations and spindles for systems consolidation. (a) Top: Relative amplitude and frequency of key SWS oscillations. Bottom: Spindles are nested in the up-state and ripples tend to nest in the troughs of spindles. **(b)** Brain regions involved in this process are neocortex (red), thalamus (green), and hippocampus (blue). Top-down and bottom-up loop-like model: Top-down (solid arrows): the down-state of neocortical SOs provides a general timing signal by suppressing thalamic spindles (green), hippocampal ripples (blue) and associated replay, as well as activity in multiple other brain areas suppresses thalamic spindles and ripple and brain activity in other regions. The recovery from it is the up-state which drives thalamocortical spindles and phase synchronizes ripple-spindle coupling. Bottom up (dashed line): Generated spindles target neocortical networks during up-state and facilitates synaptic plasticity. Both spindles and hippocampal ripples can also induce SOs in prefrontal cortex, hence creating a loop. Figure from [28].

Slow oscillations are synchronous alternations between down-states of membrane hyperpolarization and up-states of depolarization of widely distributed populations of neocortical neurons that correspond to periods of silence and high activity respectively. These oscillations are generated in cortical networks (layers 2/3 and 5) migrate mainly from anterior to posterior regions, and also reach subcortical structures including the hippocampus.[60]-[61] Human studies have shown that non-invasive brain stimulation that increased slow oscillation activity during post encoding SWS enhanced consolidation of declarative memories.[62]-[65]

Sleep spindle oscillations are synaptically generated in the thalamus through interactions between thalamic relay neurons and inhibitory reticular neurons.[68] The depolarization of thalamic relay

neurons activates T-type calcium channels, which then produce low-threshold calcium spikes. These spikes in turn activate reticular neurons, which inhibit and reset thalamic relay neurons creating a cyclic interplay to induce spindles. The reticular neurons receive excitatory inputs from thalamic neurons that project to cortex and vice versa influencing the flow of information between the thalamus and cerebral cortex. Thus, spindle oscillations can spread to multiple neocortical regions via thalamocortical fibers and even reach the hippocampus. [69] Spindles have been shown to play fundamental role in learning and memory. In both rats and humans, the rate and density of cortical spindles increases after learning and correlates with post-sleep retrieval performance. [66] The precise temporal nesting of spindles during the up-states of slow oscillations has shown to be effective in enhancing memory consolidation. Combined optogenetic and closed-loop experimentation in mice showed that only spindles that were induced in-phase with the up-states of slow oscillations, but not out-of-phase, enhanced consolidation of hippocampal-dependent memory in contextual fear-conditioning task. [55] In contrast, suppression of in-phase thalamic spindles impaired memory performance during the same task.

Hippocampal SPW-Rs coincide with neocortical spindles and tend to preferentially phase-lock to spindle troughs.[56]-[58] Ripples are synchronized to slow oscillations – they are suppressed during the slow oscillation down-state and enhanced during the slow oscillation up-state.[55], [59] However, hippocampal SPW-Rs also demonstrate a time-delayed coupling with slow oscillation-spindle activity in medial prefrontal cortex with ripples preceding slow oscillation-spindle coupled sequences by approximately 140 ms. [70] The fine temporal coordination of these three oscillations have been thus proposed as a mechanism of hippocampal-neocortical dialogue to transfer memory representations between the two regions. The causal link between the role of ripple-spindle coupling and memory consolidation was established by artificially enhancing the

pairing of SPW-Rs with cortical spindles in rodents during sleep following training on a spatial memory task. [70] Closed-loop stimulations at the time of SPW-Rs reliably induced down-up states and spindles in mPFC. These hippocampal-cortical coupled stimulations resulted in a successful consolidation of weak memory traces and predicted high recall performance. Furthermore, this coupling required fine temporal precision as random delays as short as 200 ms between SPW-Rs and cortical events restricted memory consolidation.

Ripple-band activity has also been identified in cortical regions in rats (cortical ripples, CXR). [80] These oscillations were predominantly observed in association cortices, particularly the posterior parietal cortex (PPC). Hippocampal SPW-Rs and spindles had close temporal association with CXRs. SPW-Rs were temporally coupled with CXRs and this magnitude of coupling was enhanced with learning during a spatial task. CXRs are also observed in humans and were correlated with successful verbal memory retrieval. [71] These results suggests that, in addition to SPW-Rs-spindle coupling, interactions between hippocampal and cortical ripples also form part of the hippocampal-cortical dialogue for long-term hippocampal-dependent memory

consolidation, allowing information transfer to association neocortical sites (Figure 6).

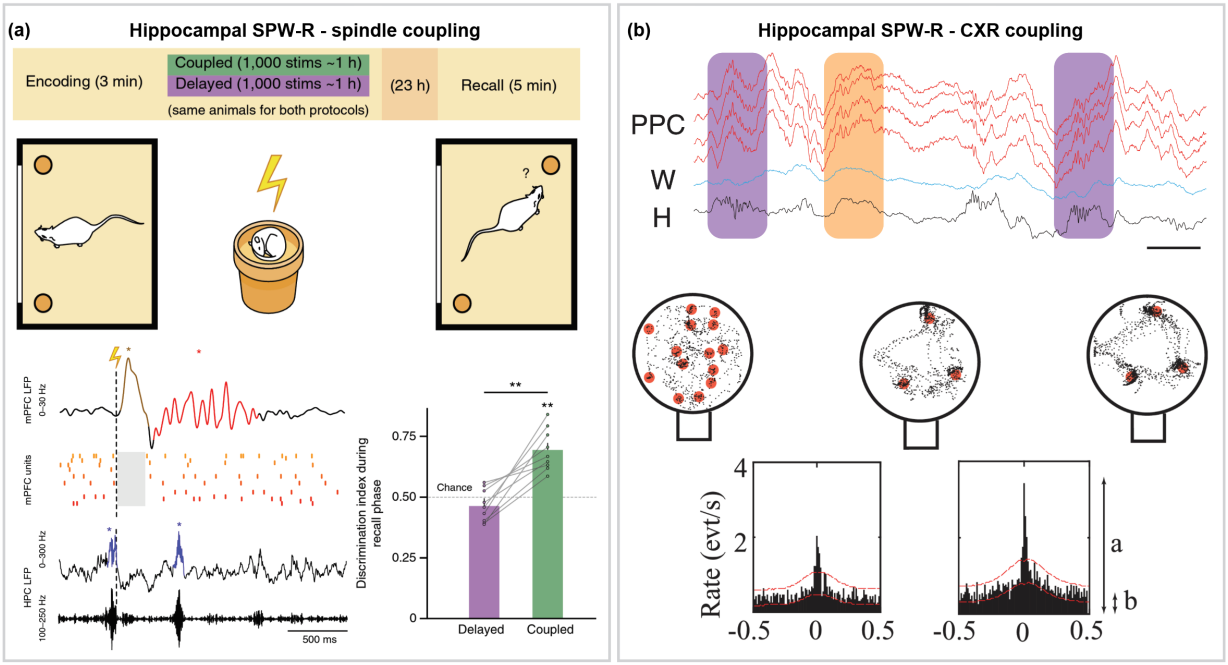

Figure 7: Key hippocampal-cortical oscillatory coupling important for memory consolidation. (a) Enhancement of hippocampal SPW-Rs and spindle coupling during post-encoding sleep enhances memory performance. Top: Stimulation protocol - rats ($n = 9$) were exposed for 3 min to two identical objects located in two adjacent corners of a familiar arena (encoding phase) and then underwent SPW-R–triggered cortical stimulation ($n =$ 1,000) during SWS following the task (~1 h). Coupled stimulation were delivered following SPW-Rs whereas delayed stimulation occurred (160-240 ms) delay. Bottom: Example SPW-R (blue) triggered stimulation (vertical dotted line) induced delta-wave (orange) followed by spindles (red) in mPFC. Increased memory recall following coupled (green bar) SPW-R-spindle stimulation (Maingret et al., 2016) **(b)** Coupling of hippocampal ripples and cortical ripples in the posterior parietal cortex (PPC) increases during sleep post-encoding of spatial maze. Top: LFP from PPC highlighting neocortical CXR (orange) and hippocampal ripples coupled with CXR (purple). (Scale bar 50 ms). Bottom: Sample trajectory of a rat (black) over maze surface relative to water reward locations (red) during exploration (left) and during training (middle, right). Sample CCGs between SPW-Rs and CXR showing increased coupling during post-training sleep compared to post-exploration sleep. Figures from [80]

1.8 Consolidation versus Reconsolidation

Newly formed memories become more stable and durable through memory consolidation. Retrieval of a consolidated memory can reopen a window of lability, after which the memory can be strengthened, updated, or weakened depending on the nature of the retrieval experience (Nader et al., 2000). This process of memory restabilization is called reconsolidation. Therefore, it has

been proposed that consolidation is not fixed, but a dynamic process wherein reactivation can flexibly modulate the lability of these memories. Over the years, several groups have investigated the molecular and cellular mechanisms behind reconsolidation to unravel whether it is simply a repetition of consolidation or in fact a distinct process.

1.8.1 Cellular and Molecular Machinery of Consolidation

It is crucial to distinguish between the concept of systems consolidation and that of "molecular" consolidation. Systems consolidation refers to the two-stage model, which emphasizes the interactions between brain regions, especially between the hippocampus and the neocortex, that allow for the transfer and stabilization of memory representations over time. In parallel, consolidation also occurs in the form of cellular and molecular changes within individual cells and synapses. [79] These two approaches are not mutually exclusive, but rather complement each other and offer different insights into the consolidation process.

Over the past decades, studies have suggested that following a learning experience, a cascade of specific molecular and cellular events mediates the induction of LTP in the hippocampus and this is widely considered to provide a basis for memory consolidation. [73]-[74] Synaptic changes necessary for memory were characterized by crucial phases of RNA and protein synthesis as well as enhanced gene expression. Most of these studies were based on administering protein synthesis inhibitors and drugs in animals after training on conditioned fear memory tasks (e.g., fear conditioning, inhibitory avoidance) at different time intervals. [76] Their findings demonstrated that molecular mechanisms are only required immediately after training and for a short period of time (approximately a few hours). Inhibition during this period does not affect learning of the task but impairs the recall memory, thereby supporting the role of these mechanisms in memory consolidation.

1.8.2 Cellular and Molecular Machinery of Reconsolidation

To determine whether consolidation and reconsolidation are similar or distinct processes, researchers have taken a direct approach by examining the involvement of specific molecules and brain regions in both processes. For instance, studies have investigated the effects of protein synthesis inhibitors after a consolidated memory was reactivated, as well as the inactivation of specific molecules and molecular pathways, or disruption of gene expression. [73] These investigations have revealed that general features such as protein synthesis, transcription, and translation are common to both consolidation and reconsolidation, suggesting similarities in the molecular processes underlying these long-term memory processes.

However, it has also been found that consolidation and reconsolidation require different molecular mechanisms and recruit distinct brain areas. For example, the activation of mitogen-activated protein (MAP) kinases in hippocampal circuits has been shown to differ between training and retrieval phases of an object recognition task in rodents. [77] Memory reconsolidation recruit different protein transcription factors and only engage a subset of immediate-early genes induced in consolidation, suggesting unique non-overlapping mechanisms between these memory processes. Using positron emission tomography in humans, another study revealed the recruitment of unique brain areas for encoding and retrieval. Left frontal brain regions were activated during initial encoding whereas right superior frontal regions were engaged during subsequent retrieval of information. [78] These findings suggest that while there are some common molecular processes, which mediate long-term synaptic plasticity, involved in both consolidation and reconsolidation, there are key differences in the specific molecular mechanisms and brain circuits engaged during these processes.

However, there is still limited understanding of the oscillatory mechanisms in the hippocampal-cortical network that underlie reconsolidation and how these processes differ from consolidation. Chapter 4 of this thesis will provide a detailed analysis of how hippocampal-cortical coupling patterns and temporal dynamics can be used to differentiate between consolidation and reconsolidation in animals performing spatial and non-spatial memory tasks. This will shed light on the complex interplay and bridge the gap between molecular and systems consolidation processes in the brain's memory formation and stabilization.

References

1. Eichenbaum, H. (2000). A cortical–hippocampal system for declarative memory. *Nature Reviews Neuroscience*, *1*(1), 41–50.
2. Scoville, W. B. & Milner, B. Loss of recent memory after bilateral hippocampal lesions. *J. Neurol. Neurosurg. Psychiatry* 20, 11–21 (1957).
3. Corkin, S. (1984). Lasting consequences of bilateral medial temporal lobectomy: Clinical course and experimental findings in H. M. Sem-inars in Neurology, 4, 249-259
4. Milner, B. Disorders of learning and memory after temporal lobe lesions in man. *Clin. Neurosurg.* 19, 421–446 (1972).
5. Zola-Morgan, S., Squire, L. R. & Amaral, D. G. Human amnesia and the medial temporal region: enduring memory impairment following a bilateral lesion limited to field CA1 of the hippocampus. *J. Neurosci.* **6**, 2950–2967 (1986).
6. Rempel-Clower, N. L., Zola, S. M., Squire, L. R. & Amaral, D. G. Three cases of enduring memory impairment after bilateral damage limited to the hippocampal formation. *J. Neurosci.* **16**, 5233–5255 (1996).
7. Maguire, E. A., Nannery, R., & Spiers, H. J. (2006). Navigation around London by a taxi driver with bilateral hippocampal lesions. *Brain*, *129*(11), 2894–2907.
8. Squire, L. Memory and the hippocampus: A synthesis from findings with rats, monkeys, and humans. Psychol. Rev. 99, 195–231 (1992).
9. Zola-Morgan S, Squire LR. 1990. The primate hippocampal formation: Evidence for a time-limited role in memory storage. Science 250: 288–290.
10. Kim JJ, Fanselow MS. 1992. Modality-specific retrograde amnesia of fear. Science 256: 675–677
11. Olton, D. S., Walker, J. A., & Gage, F. H. (1978). Hippocampal connections and spatial discrimination. *Brain Research*, *139*(2), 295–308.
12. Broadbent, N. J., Squire, L. R., & Clark, R. E. (2006). Reversible hippocampal lesions disrupt water maze performance during both recent and remote memory tests. *Learning & Memory*, *13*(2), 187–191.
13. Squire, L. R., & Alvarez, P. (1995). Retrograde amnesia and memory consolidation: a neurobiological perspective. *Current Opinion in Neurobiology*, *5*(2), 169–177. https://doi.org/10.1016/0959-4388(95)80023-9
14. Buzsáki, G. (1989). Two-stage model of memory trace formation: A role for "noisy" brain states. *Neuroscience*, *31*(3), 551–570.
15. Burwell, R. D. & Amaral, D. G. The cortical afferents of the perirhinal, postrhinal, and entorhinal cortices of the rat. J. Comp. Neurol. 398, 179–205 (1998).
16. Suzuki, W. A. & Amaral, D. G. Perirhinal and parahippocampal cortices of the macaque monkey: Cortical afferents. J. Comp. Neurol. 350, 497–533 (1994).
17. Burwell, R. D., Witter, M. P. & Amaral, D. G. Perirhinal and postrhinal cortices in the rat: A review of the neuroanatomical literature and comparison with findings from the monkey brain. Hippocampus 5, 390–408 (1995)
18. Kahn, I., Andrews-Hanna, J. R., Vincent, J. L., Snyder, A. Z., & Buckner, R. L. (2008). Distinct Cortical Anatomy Linked to Subregions of the Medial Temporal Lobe Revealed by Intrinsic Functional Connectivity. Journal of Neurophysiology, 100(1), 129–139.
19. Diekelmann, S., & Born, J. (2010). The memory function of sleep. *Nature Reviews Neuroscience*, *11*(2), 114–126.

20. Feld, G. B., & Born, J. (2017). Sculpting memory during sleep: concurrent consolidation and forgetting. *Current Opinion in Neurobiology*, *44*, 20–27.
21. Lee, J. L. C. (2009). Reconsolidation: maintaining memory relevance. *Trends in Neurosciences*, *32*(8), 413–420.
22. Nader, K., & Hardt, O. (2009). A single standard for memory: the case for reconsolidation. *Nature Reviews Neuroscience*, *10*(3), 224–234.
23. Hasselmo, M. E. (1999). Neuromodulation: acetylcholine and memory consolidation. *Trends in Cognitive Sciences*, *3*(9), 351–359.
24. O'Keefe, J. & Dostrovsky, J. The hippocampus as a spatial map. Preliminary evidence from unit activity in the freely moving rat. Brain Res. 34, 171–175 (1971).
25. O'Keefe, J., & Recce, M. L. (1993). Phase relationship between hippocampal place units and the EEG theta rhythm. *Hippocampus*, *3*(3), 317–330 h
26. Losonczy, A., Zemelman, B. V., Vaziri, A., & Magee, J. C. (2010).
27. Network mechanisms of theta related neuronal activity in hippocampal CA1 pyramidal neurons. *Nature Neuroscience*, *13*(8), 967–972.
28. Klinzing, J. G., Niethard, N., & Born, J. (2019). Mechanisms of systems memory consolidation during sleep. Nature Neuroscience, 22(10), 1598–1610.
29. Wilson, M. A. & McNaughton, B. L. Reactivation of hippocampal ensemble memories during sleep. Science 265, 676–679 (1994)
30. Skaggs, W. E., & McNaughton, B. L. (1996). Replay of Neuronal Firing Sequences in Rat Hippocampus During Sleep Following Spatial Experience. *Science*, *271*(5257), 1870–1873.
31. O'Neill, J., Pleydell-Bouverie, B., Dupret, D. & Csicsvari, J. Play it again:reactivation of waking experience and memory. Trends Neurosci. 33, 220–229 (2010).
32. Ji, D. & Wilson, M. A. Coordinated memory replay in the visual cortex and hippocampus during sleep. Nat. Neurosci. 10, 100–107 (2007).
33. Nadasdy Z, Hirase H, Czurko A, Csicsvari J, Buzsaki G: Replay and time compression of recurring spike sequences in the hippocampus. J Neurosci 1999, 19:9497-9507
34. Diba, K. & Buzsáki, G. Forward and reverse hippocampal place-cell sequences during ripples. Nat. Neurosci. 10, 1241–1242 (2007).
35. Buzsaki, G., Horvath, Z., Urioste, R., Hetke, J., & Wise, K. (1992). High-frequency network oscillation in the hippocampus. *Science*, *256*(5059), 1025–1027.
36. Skaggs WE, McNaughton BL, Permenter M, Archibeque M, Vogt J, Amaral DG, Barnes CA: EEG sharp waves and sparse ensemble unit activity in the macaque hippocampus. J Neurophysiol 2007, 98:898-910.
37. Bragin A, Engel J, Wilson CL, Fried I, Buzsaki G: High-frequency oscillations in human brain. Hippocampus 1999, 9:137-142.
38. Bliss TVP, Collingridge GL: A synaptic model of memory: long-term potentiation in the hippocampus. Nature 1993, 361:31-39.
39. King C, Henze DA, Leinekugel X, Buzsaki G: Hebbian modification of a hippocampal population pattern in the rat. J Physiol 1999, 521:159-167.
40. Whitlock JR, Heynen AJ, Shuler MG, Bear MF: Learning induces long-term potentiation in the hippocampus. Science 2006, 313:1093-1097.
41. Eschenko O, Ramadan W, Molle M, Born J, Sara SJ: Sustained increase in hippocampal sharp-wave ripple activity during slow-wave sleep after learning. Learn Mem 2008, 15:222-228.

42. Ramadan W, Eschenko O, Sara SJ: Hippocampal sharp wave/ ripples during sleep for consolidation of associative memory. PLoS One 2009, 4:e6697.
43. Axmacher,N.,Elger,C.E.&Fell,J.Ripples in the medial temporal lobe are relevant for human memory consolidation. Brain 131, 1806–1817 (2008).
44. Girardeau G, Benchenane K, Wiener SI, Buzsaki G, Zugaro MB: Selective suppression of hippocampal ripples impairs spatial memory. Nat Neurosci 2009, 12:1222-1223.
45. Ego-Stengel V, Wilson MA: Disruption of ripple-associated hippocampal activity during rest impairs spatial learning in the rat. Hippocampus 2010, 20:1-10
46. Takashima, A., Petersson, K. M., Rutters, F., Tendolkar, I., Jensen, O., Zwarts, M. J., … Fernández, G. (2006). Declarative memory consolidation in humans: A prospective functional magnetic resonance imaging study. *Proceedings of the National Academy of Sciences*, *103*(3), 756–761.
47. Maviel, T., Durkin, T. P., Menzaghi F., & Bontempi, B. (2004). Sites of Neocortical Reorganization Critical for Remote Spatial Memory. Science, 305(5680), 96–99. https://doi.org/10.1126/science.1098180
48. Qin, Y.-L., McNaughton, B. L., Skaggs, W. E. & Barnes, C. A. Memory reprocessing in corticocortical and hippocampocortical neuronal ensembles. Philos. Trans. R. Soc. Lond. B Biol. Sci. 352, 1525–1533 (1997).
49. Nyhus, E., & Curran, T. (2010). Functional role of gamma and theta oscillations in episodic memory. *Neuroscience & Biobehavioral Reviews*, *34*(7), 1023–1035.
50. Buzsáki, G., Draguhn, A., 2004. Neuronal oscillations in cortical networks. Science 304, 1926–1929
51. Fries, P. (2005). A mechanism for cognitive dynamics: neuronal communication through neuronal coherence. Trends in Cognitive Sciences, 9(10), 474–480.
52. Rubino, D., Robbins, K. A., & Hatsopoulos, N. G. (2006). Propagating waves mediate information transfer in the motor cortex. *Nature Neuroscience*, *9*(12), 1549–1557.
53. Siegel, M., Donner, T. H., & Engel, A. K. (2012). Spectral fingerprints of large-scale neuronal interactions. Nature Reviews Neuroscience, 13(2), 121–134. https://doi.org/10.1038/nrn3137
54. Helfrich, R. F., Mander, B. A., Jagust, W. J., Knight, R. T. & Walker, M. P. Old brains come uncoupled in sleep: Slow wave-spindle synchrony, brain atrophy, and forgetting. Neuron 97, 221–230.e4 (2018).
55. Latchoumane, C. V., Ngo, H.-V. V., Born, J. & Shin, H.-S. Thalamic spindles promote memory formation during sleep through triple phase-locking of cortical, thalamic, and hippocampal rhythms. Neuron 95, 424–435.e6 (2017).
56. Siapas AG, Wilson MA: Coordinated interactions between hippocampal ripples and cortical spindles during slow-wave sleep. Neuron 1998, 21:1123-1128.
57. Sirota A, Csicsvari J, Buhl D, Buzsaki G: Communication between neocortex and hippocampus during sleep in rodents. Proc Natl Acad Sci USA 2003, 100:2065-2069.
58. Battaglia FP, Sutherland GR, McNaughton BL: Hippocampal sharp wave bursts coincide with neocortical ‘‘up-state’’ transitions. Learn Mem 2004, 11:697-704
59. Staresina, B. P. et al. Hierarchical nesting of slow oscillations, spindles and ripples in the human hippocampus during sleep. Nat. Neurosci. 18, 1679–1686 (2015).
60. Massimini, M., Huber, R., Ferrarelli, F., Hill, S. & Tononi, G. The sleep slow oscillation as a traveling wave. J.Neurosci. 24, 6862–6870 (2004).

61. Nir, Y. et al. Regional slow waves and spindles in human sleep. Neuron 70, 153–169 (2011).
62. Marshall, L., Helgadóttir, H., Mölle, M., & Born, J. (2006). Boosting slow oscillations during sleep potentiates memory. Nature, 444(7119), 610–613.
63. Chauvette, S., Seigneur, J., & Timofeev, I. (2012). Sleep Oscillations in the Thalamocortical System Induce Long-Term Neuronal Plasticity. *Neuron*, *75*(6), 1105–1113. https://doi.org/10.1016/j.neuron.2012.08.034
64. Ngo, Hong-Viet V., Martinetz, T., Born, J., & Mölle, M. (2013). Auditory Closed-Loop Stimulation of the Sleep Slow Oscillation Enhances Memory. *Neuron*, *78*(3), 545–553. https://doi.org/10.1016/j.neuron.2013.03.006
65. Perrault, A. A. et al. Whole-night continuous rocking entrains spontaneous neural oscillations with benefits for sleep and memory. Curr. Biol. 29, 402–411.e3 (2019).
66. Gais S, Molle M, Helms K, Born J: Learning-dependent increases in sleep spindle density. J Neurosci 2002, 22:6830-6834
67. Eschenko O, Molle M, Born J, Sara SJ: Elevated sleep spindle density after learning or after retrieval in rats. J Neurosci 2006, 26:12914-12920
68. Steriade, M., McCormick, D. A., & Sejnowski, T. J. (1993). Thalamocortical oscillations in the sleeping and aroused brain. Science, 262(5134), 679-685.
69. Varela, C., Kumar, S., Yang, J. Y. & Wilson, M. A. Anatomical substrates for direct interactions between hippocampus, medial prefrontal cortex, and the thalamic nucleus reuniens. Brain Struct. Funct. 219, 911–929 (2014).
70. Maingret, N., Girardeau, G., Todorova, R., Goutierre, M., & Zugaro, M. (2016). Hippocampo-cortical coupling mediates memory consolidation during sleep. Nature Neuroscience, 19(7), 959–964.
71. Vaz, A. P., Inati, S. K., Brunel, N., & Zaghloul, K. A. (2019). Coupled ripple oscillations between the medial temporal lobe and neocortex retrieve human memory. Science, 363(6430), 975–978.
72. Nader, K., Schafe, G. E., & LeDoux, J. E. (2000). The labile nature of consolidation theory. Nature Reviews Neuroscience, 1(3), 216–219.
73. Alberini, C. M. (2005). Mechanisms of memory stabilization: are consolidation and reconsolidation similar or distinct processes? *Trends in Neurosciences*, *28*(1), 51–56. https://doi.org/10.1016/j.tins.2004.11.001
74. McGaugh, J. L. (2000). Memory--a Century of Consolidation. *Science*, *287*(5451), 248–251.
75. Izquierdo, L. A., Barros, D. M., Vianna, M. R. M., Coitinho, A., e Silva, T. deDavid, (2002). *Cellular and Molecular Neurobiology*, *22*(3), 269–287.
76. Izquierdo,et al., Molecular pharmacological dissection of short-and long-term memory. Cell.Mol. Neurobiol.22, 269–287 (2002).
77. Kelly, A. et al. (2003) Activation of mitogen-activate protein kinase/ extracellular signal-regulated kinase in hippocampal circuitry is required for consolidation and reconsolidation of recognition memory. J. Neurosci. 12, 5354–5360
78. Nyberg, L., McIntosh, A. R., Cabeza, R., Habib, R., Houle, S., & Tulving, E. (1996). General and specific brain regions involved in encoding and retrieval of events: what, where, and when. *Proceedings of the National Academy of Sciences*, *93*(20), 11280–11285. https://doi.org/10.1073/pnas.93.20.11280

79. Malenka, R. C., & Nicoll, and R. A. (1999). Long-Term Potentiation--A Decade of Progress? Science, 285(5435), 1870–1874.
80. Khodagholy, D., Gelinas, J. N., & Buzsáki, G. (2017). Learning-enhanced coupling between ripple oscillations in association cortices and hippocampus. *Science*, *358*(6361).

Chapter 2: Disrupted Memory Circuits in Focal Epilepsy

Chapter 1 highlighted the anatomy and physiology of memory networks and how cellular and molecular mechanisms, in complement with systems-level hippocampal-neocortical oscillatory mechanisms, support memory consolidation. This section reviews some of the key human and animal studies that investigate the mechanisms of disrupted memory networks in focal epilepsy.

2.1 Focal Epilepsy

Epilepsy is a neurological disorder that affects millions of people worldwide. It is characterized by recurrent seizures that arise due to abnormal excessive or hypersynchronous neuronal firing in the brain.[1] Depending on the location of the initial event and extent of the abnormal brain activity, the clinical presentation of seizures in patients can vary widely. Based on key signs and symptoms, seizures are classified into focal or generalized onset or unknown onset seizures.[2] Focal-onset seizures originate within networks limited to one hemisphere and may be discretely localized whereas generalized from onset seizures are defined as originating at some point within and rapidly engaging bilaterally distributed networks.

2.2 Interictal epileptiform discharges (IEDs)

One of the hallmark features of focal epilepsy, characterized by with focal-onset seizures, is the presence of interictal epileptiform discharges (IEDs). These interictal spikes are brief (< 250 ms) events produced by synchronous discharges of neurons in the epileptic focus region. [5] IEDs occur between seizures and can have significant impact on brain function. IEDs can not only transiently interrupt cognitive function that results in immediate behavioral effects, but also alter physiological mechanisms that are involved in brain plasticity and memory. Temporal lobe epilepsy (TLE) is the most common form of chronic focal epilepsy. [4] The temporal lobe includes the hippocampus and parahippocampal structures and is a critical brain region for memory

formation and retrieval. In cases of TLE, localized neuropathology in these memory-relevant brain regions often results in significant problems in memory, which is a major cognitive comorbidity.

2.3 IEDs and Memory

The detection and analysis of interictal epileptiform discharges (IEDs) in human patients with epilepsy, as well as experiments conducted on rodent models to explore the relationship between IEDs and memory-dependent behavior, have provided valuable insights into the effects of IEDs on memory and the potential mechanisms underlying these disruptions.

2.3.1 Human Studies

Numerous functional imaging and neuropsychological studies have investigated the effect of IEDs on memory in humans. Techniques such as functional magnetic resonance imaging (fMRI) and positron emission tomography (PET) have been used to non-invasively identify brain areas involved in memory processing in the temporal lobe of both normal and TLE patients, and to predict post-operative memory decline. [6] In a study of left TLE patients who underwent pre-operative fMRI during a memory encoding task, significant reductions in functional connectivity were observed between bilateral MTL, occipital, and left orbitofrontal regions, suggesting roles of specific fibre pathways in functional plasticity of TLE [7].

Studies of children and adults with epilepsy have shown that subjects with frequent IEDs detected on electroencephalography (EEG) were associated with worse performance on tests of attention, memory and executive function compared to those with infrequent IEDs. [8],[9] Hippocampal IEDs detected using depth electrodes in patients during pre-operative seizure localization were associated with decreased memory maintenance and retrieval, but not with encoding, during memory tasks. [10]

Furthermore, IEDs have been found to have enhanced occurrence during NREM sleep relative to wakefulness and REM sleep [13] (Figure 7b). As NREM and SWS sleep play a crucial role in facilitating memory consolidation, reactivations, and oscillatory dialogue, this result suggests that the occurrence of IEDs during this time period has the potential to interfere with key mechanisms. A recent study that aimed to establish the relationship between IEDs and physiological hippocampal sharp wave-ripples (SPW-Rs) during an associative memory task revealed the spatiotemporal impact of IEDs. [11] Patients with hippocampal depth electrodes and subdural intracranial grids covering an extensive portion of the frontal, parietal, occipital, and temporal cortices demonstrated that the occurrence of IEDs during a crucial time window (500-2000 ms) of memory encoding and retrieval decreased the odds of successful memory performance on the task. In addition, hippocampal ripples that followed IEDs showed a transient decrease in rate during encoding and retrieval. These results suggest that IEDs may compete with and even decrease physiological oscillatory patterns crucial for memory encoding and recall.

Finally, combining fMRI and intracranial EEG activity, another study showed that functional connectivity was altered even in brain regions outside of the epileptogenic zone and indices of directionality revealed that these zones exerted influence on non-epileptic zones during the interictal period. Chapter 4 sheds light on the potential mechanism of IEDs to facilitate the spread of epileptic networks and disrupt large-scale inter-cortical communication in humans.

Overall, these human studies have provided evidence that IEDs can lead to changes in functional connectivity between brain regions involved in memory processing, interfere with key mechanisms during sleep crucial for memory consolidation, and compete with physiological oscillatory patterns crucial for memory encoding and recall. Additionally, epilepsy models in rodents have allowed for more in-depth investigation of the specific mechanisms underlying IEDs.

2.3.2 Rodent Studies

To investigate the specific cellular changes associated with spatial memory impairments in epilepsy, one line of work conducted recordings of hippocampal neurons in free moving rats subjected to status epilepticus (SE), which is characterized by continuous or repetitive seizures (Liu et al., 2003). Compared to control rats, SE rats had impaired visual-spatial memory in the Morris water maze as well as less orderly and stable place cells firing patterns. Another study induced seizures in rats during their early postnatal period (between P1-P75) and examined long-term function during adulthood (> P90). [15] They demonstrated that the animals had a reduced capacity for long-term potentiation and impaired spatial learning in a radial maze task.

To investigate the role of IEDs, one group evoked epileptiform activity in the rodent hippocampus through the injection of penicillin.[12] This study provided evidence that IEDs show a phase preference, occurring more frequently during the trough phase of the slow oscillation. (Figure 7a). An epileptic network can also be generated in rodent kindling models by delivering electrical stimulation to a brain structure and lowering the threshold for epileptic activity. Hippocampal IEDs generated by kindling models are precisely coupled with spindle oscillations in the medial prefrontal cortex (mPFC) and this coupling was demonstrated to be more potent than physiological ripple-spindle coupling [16] (Figure 7c-d). More importantly, increased rate of IEDs and IED-spindle coupling during the consolidation period was correlated with impaired spatial memory retrieval performance in kindled rats, compared to control rats. These findings provide important insights that IEDs can participate in memory-dependent oscillatory mechanisms in SWS to potentially disrupt the physiologic memory network necessary for episodic memory consolidation and retrieval.

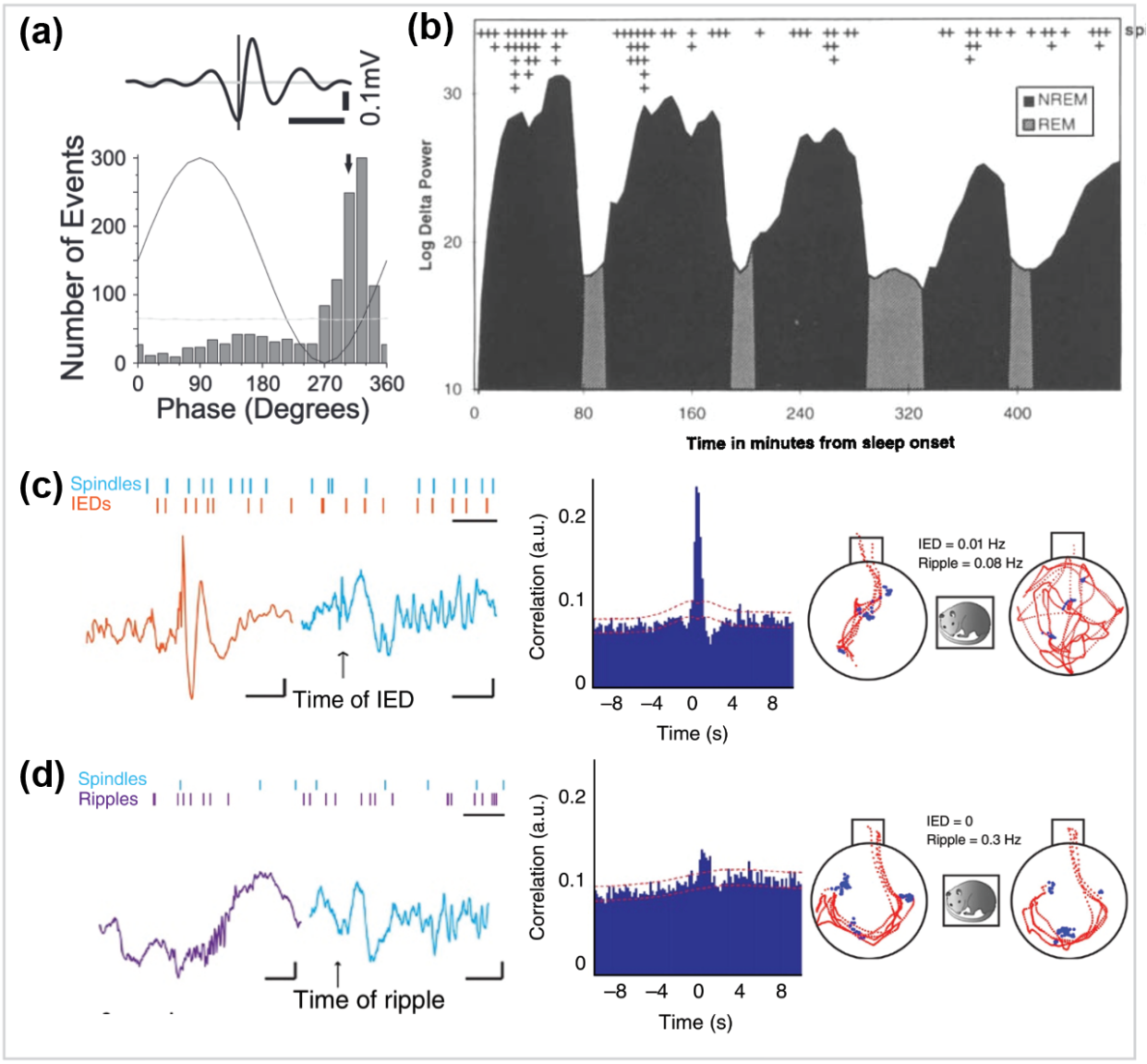

Figure 7: IEDs and their involvement during NREM oscillations governing hippocampal-neocortical information transfer. (a) IED-trigged field averages (top) and phase binning of spike events (bottom). IED spikes occurred preferentially at the negative point of delta-waves (Guzman et al., 2010) **(b)** Moving averages of IEDs (+ symbols) and their log-delta power show increased activity during NREM sleep (Malow et al., 1998) **(c)** Left: Raster plot of mPFC spindles (blue) and hippocampal IEDs (orange) in kindled rats. Scale bar, 10 s. Raw LFP of detected IED (orange; scale bars, 200 µV, 100 ms) and mPFC spindle evoked by IED (blue; scale bars, 100 µV, 500 ms). Middle: Cross-correlation (CCG) of IEDs and spindles show strong coupling. Right: Sample behavioral performance at the end of kindling during training (left) and test (left) shows impaired performance during test. **(d)** Left: Raster plot of mPFC spindles (blue) and hippocampal ripples (purple; scale bar, 10 s) (top). Raw LFP of detected ripple (purple; scale bars, 100 µV, 50 ms) and mPFC spindle associated with ripple (blue; scale bars, 100 µV, 500 ms). Middle: CCG of ripples and spindles showing a weaker coupling than IED-spindle. Right: Baseline behavioral performance of animal during baseline shows intact memory performance during test.

The mechanisms by which IEDs interact with and shape large-scale neural networks in the human brain remain mostly unknown and have implications for associated neuropsychiatric dysfunction and progression of focal epilepsy. Chapter 4 will present our findings on how interactions between IED and spindles in the human brain affected by focal epilepsy modulate neural networks and potentially contribute to cognitive comorbidity in epilepsy.

References

1. Fisher, R. S., Acevedo, C., Arzimanoglou, A., Bogacz, A., Cross, J. H., Elger, C. E., … Wiebe, S. (2014). ILAE Official Report: A practical clinical definition of epilepsy. Epilepsia, 55(4), 475–482
2. Fisher, R. S., Cross, J. H., D'Souza, C., French, J. A., Haut, S. R., Higurashi, N., … Zuberi, S. M. (2017). Instruction manual for the ILAE 2017 operational classification of seizure types. *Epilepsia*, *58*(4), 531–542. https://doi.org/10.1111/epi.13671
3. Kwan, P., & Brodie, M. J. (2000). Early Identification of Refractory Epilepsy. New England Journal of Medicine, 342(5), 314–319.
4. Helmstaedter, C., & Elger, C. E. (2009). Chronic temporal lobe epilepsy: a neurodevelopmental or progressively dementing disease? Brain, 132(10), 2822–2830. https://doi.org/10.1093/brain/awp182
5. Staley, K. J., & Dudek, F. E. (2006). Interictal Spikes and Epileptogenesis. Epilepsy Currents, 6(6), 199–202
6. Robert Powell, H. W., J. Koepp, M., Richardson, M. P., Symms, M. R., Thompson, P. J., & Duncan, J. S. (2004). The Application of Functional MRI of Memory in Temporal Lobe Epilepsy: A Clinical Review. Epilepsia, 45(7), 855–863.
7. Voets, N. L., Adcock, J. E., Stacey, R., Hart, Y., Carpenter, K., Matthews, P. M., & Beckmann, C. F. (2009). Functional and structural changes in the memory network associated with left temporal lobe epilepsy. *Human Brain Mapping*, *30*(12), 4070–4081.
8. Ebus, S., Arends, J., Hendriksen, J., van der Horst, E., de la Parra, N., Hendriksen, R., Aldenkamp, B. (2012). Cognitive effects of interictal epileptiform discharges in children. European Journal of Paediatric Neurology, 16(6), 697–706.
9. Lv, Y., Wang, Z., Cui, L., Ma, D., & Meng, H. (2013). Cognitive correlates of interictal epileptiform discharges in adult patients with epilepsy in China. Epilepsy & Behavior, 29(1), 205–210.
10. Kleen, J. K., Scott, R. C., Holmes, G. L., Roberts, D. W., Rundle, M. M., Testorf, M., … Jobst, B. C. (2013). Hippocampal interictal epileptiform activity disrupts cognition in humans. Neurology, 81(1), 18–24.
11. Henin, S., Shankar, A., Borges, H., Flinker, A., Doyle, W., Friedman, D., … Liu, A. (2021). Spatiotemporal dynamics between interictal epileptiform discharges and ripples during associative memory processing. Brain, 144(5), 1590–1602.
12. de Guzman, P. H., Nazer, F., & Dickson, C. T. (2010). Short-Duration Epileptic Discharges Show a Distinct Phase Preference During Ongoing Hippocampal Slow Oscillations. *Journal of Neurophysiology*, *104*(4), 2194–2202.
13. Malow, B.A., Lin, X., Kushwaha, R. & Aldrich, M.S. Interictal spiking increases with sleep depth in temporal lobe epilepsy. Epilepsia 39, 1309–1316 (1998).
14. Liu, X., Muller, R. U., Huang, L.-T., Kubie, J. L., Rotenberg, A., Rivard, B., … Holmes, G. L. (2003). Seizure-Induced Changes in Place Cell Physiology: Relationship to Spatial Memory. The Journal of Neuroscience, 23(37), 11505–11515.
15. Lynch, M., Sayin, Ü., Bownds, J., Janumpalli, S., & Sutula, T. (2000). Long-term consequences of early postnatal seizures on hippocampal learning and plasticity. European Journal of Neuroscience, 12(7), 2252–2264.

16. Gelinas, J. N., Khodagholy, D., Thesen, T., Devinsky, O., & Buzsáki, G. (2016). Interictal epileptiform discharges induce hippocampal–cortical coupling in temporal lobe epilepsy. Nature Medicine, 22(6), 641–648.

Chapter 3: Hippocampal-cortical coupling differentiates long-term memory processes

In Chapter 1, we reviewed how coupling of hippocampal and cortical activity patterns facilitates initial memory consolidation. However, whether and how these patterns are involved in post-reactivation memory processes is not known. In this study, we monitored the hippocampal-cortical network as rats performed repeated cycles of consolidation and reconsolidation in spatial and nonspatial memory tasks. This chapter highlights the key results from this experiment and provides new insights on how patterns of oscillatory coupling can support the distinct memory processes required to flexibly modulate long-term memories.

Furthermore, we also highlighted that SPW-Rs are a part of large-scale complex system orchestrated by oscillatory networks from different brain regions. However, the interaction of SPW-Rs and spindle oscillations from multiple cortical regions remain elusive primarily due to lack of methodologies that allow simultaneous high spatiotemporal electrophysiological recordings from a wide cast of neocortex. Hence, this chapter also addresses this problem through concurrent hippocampal and multi-site cortical recordings to investigate the full spatial extent of oscillatory activity and its functional role in memory.

3.1 Hippocampal-cortical activity in absence of memory demands

We used a conducting polymer-based conformable microelectrode surface array (NeuroGrid) in tandem with implanted probes to perform concomitant electrophysiological monitoring of cortex and hippocampus in behaving rats (n = 9 rats). We targeted signals derived from posterior parietal cortex (PPC) due to its known interaction with the hippocampus, functional participation in distributed networks involved in formation and retrieval of episodic memory, and its ability to form an enduring cortical engram shortly after learning (27–30). To identify NeuroGrid electrodes

recording from PPC, we combined electrophysiologic and anatomic markers (Figure 1A). We first explored the occurrence of hippocampal and PPC activity patterns during NREM sleep in the absence of a structured task.

Hippocampal traces exhibited characteristic SPW-R, and we detected cortical slow oscillations, spindles (SPI), and CXR from PPC traces (Figure 1B). These oscillatory patterns occurred at expected rates, and detection parameters were optimized for sensitivity and specificity. SPW-R and cortical oscillations have significant temporal coupling (31–34) (Figure 1C) and we aimed to investigate how these coupling dynamics are coordinated. SPW-R and CXR were strongly and precisely coupled, compared to a more modest coupling between SPW-R and SPI (Figure 1D). We determined the extent to which all three patterns were jointly correlated by identifying the CXR that co-occurred with SPI and performing cross-correlation with SPW-R (Figure 1E). This tripartite coupling was statistically significant, and its strength was comparable to that of SPW-R / SPI coupling. Furthermore, when we eliminated SPI that were additionally coupled to CXR, the correlation between SPW-R / SPI significantly decreased (Figure 1F). In contrast, significant SPW-R / CXR coupling was sustained despite elimination of SPI co-occurring with CXR (Figure 1F). The relationship between CXR and SPI was also preserved under this manipulation. Taken together, these results suggest that hippocampal-cortical interactions in the absence of a consequential behavioral experience are dominated by SPW-R / CXR coupling, but display joint modulation of SPW-R, CXR, and SPI.

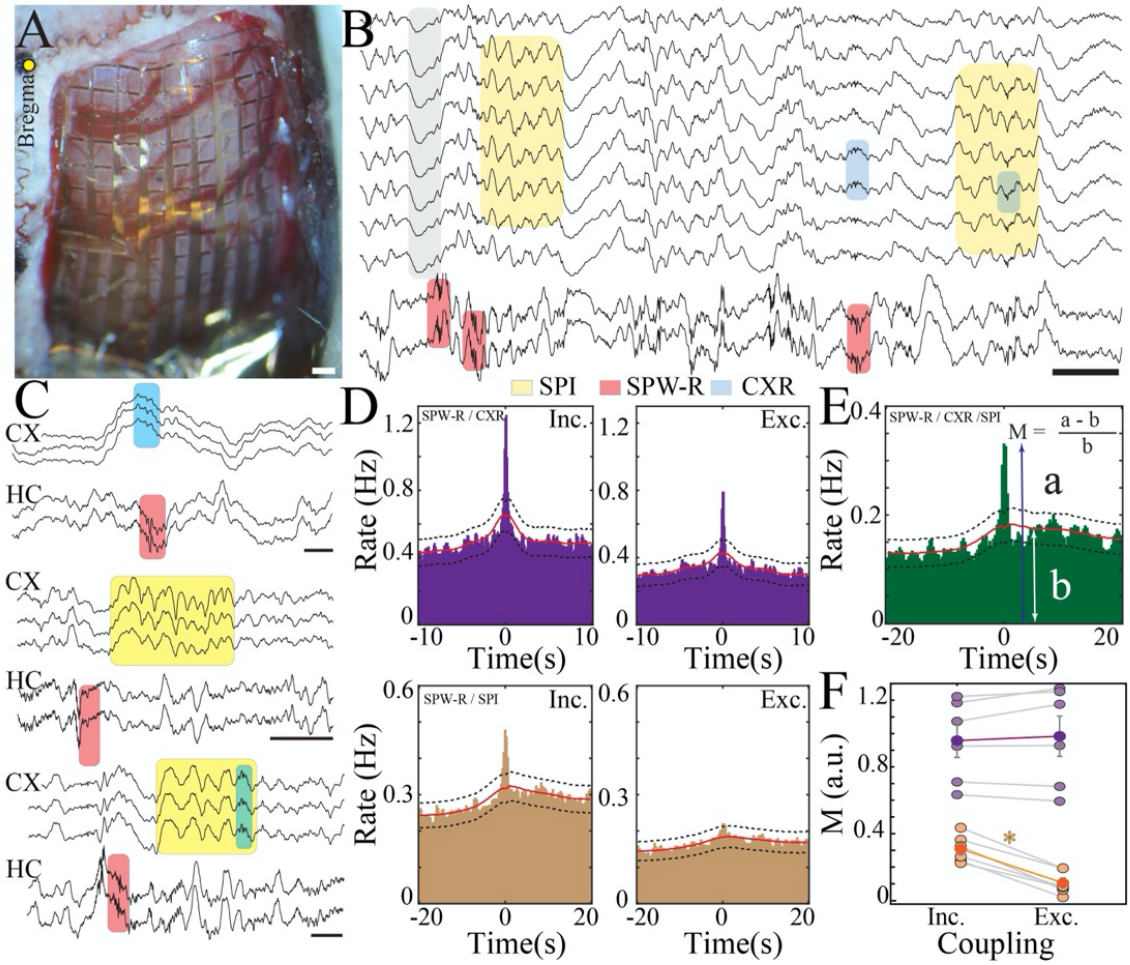

Figure 1. Hippocampal-cortical interactions are jointly modulated in the absence of memory demand. (A) NeuroGrid array conforming over the dorsal cortical surface of a rat from bregma (yellow dot) anteriorly to lambda posteriorly (scale bar, 1 mm).(B) Sample wide-band LFP traces (0.1 to 1250 Hz) simultaneously acquired from multiple cortical areas and hippocampus using NeuroGrid and a silicon probe, respectively. Shaded boxes highlight SPW-R (red), delta waves (gray), SPI (yellow) and CXR (blue; scale bar, 0.5 s). (C) Sample recording traces from hippocampus and PPC electrodes illustrating various hippocampal-cortical oscillatory interactions; SPW-R / CXR (top; scale bar: 60 ms), SPW-R / SPI (middle; scale bar: 0.5 s) and tripartite coupling (bottom; scale bar, 0.2 s). (D) Sample cross-correlograms (CCGs) between SPW-R / CXR (top) and SPW-R / SPI (bottom) during baseline NREM sleep (time 0 = occurrence of SPW-R; red lines indicate mid-point of upper and lower boundary of 95% confidence intervals shown as black-dotted lines; single session in one rat). Exclusive SPW-R / CXR CCG (top; right; 1,852 SPW-R, 1,892 CXR) was calculated by eliminating any CXR co-occurring with SPI in the inclusive CCG (top; left; 1,852 SPW-R, 2,805 CXR). Similarly, exclusive SPW-R / SPI CCG (bottom, right; 1,852 SPW-R, 968 SPI) was calculated by eliminating SPI co-occurring with CXR in the inclusive CCG (bottom, left; 1,852 SPW-R, 1,660 SPI). (E) Sample CCG between SPW-R, SPI, and CXR demonstrating tripartite coupling (time 0 = occurrence of SPW-R; single session in one rat; 1,852 SPW-R, 2,805 CXR and 1,660 SPI). Parameter *a* represents the peak of the CCG at time 0 whereas *b* represent average expected value at time 0. Coupling modulation (*M*) is calculated as (a –b)/b.(F) Group statistics demonstrating changes in coupling modulation (n = 6 rats, paired sample t-test; *P < 0.05 between two groups). Significant difference between inclusive-exclusive SPW-R / SPI coupling modulation (orange; $P = 1.04 \times 10^{-4}$) but not inclusive-exclusive SPW-R / CXR coupling modulation (purple; $P = 0.324$). Gray lines show mean values for individual rats.

3.2 Long-term memories in a spatial memory task

We next asked how these oscillatory relationships were affected by behavioral experience sufficient to induce long-term memory. Both SPW-R / SPI and SPW-R / CXR coupling are altered by learning(24, 25), but whether these changes are manifestations of a unified underlying process and how their temporal dynamics modulate across memory phases remain unknown. To address these questions, we designed a behavioral protocol based on variations of the cheeseboard maze task (CB(33, 35)). This task is amenable to within-animal repetition, with a robust new memory generated by changing the spatial locations associated with rewards. We leveraged this structure to examine dynamic memory processes within a consistent task schema. New memories for spatial locations were established with training trials, consolidated overnight, and then retrieved the following day in a set of test trials. Different reward locations were trained later the same day, initiating a subsequent memory cycle (Figure 2A). We found that rats effectively sustained these memory cycles, with consistently high behavioral performance during retrieval the following day for each new memory. To evaluate the interaction between previously consolidated reward locations and new reward locations, we tracked the rat's trajectory across the maze during training (Figure 2B). Initial training trials with new reward locations were characterized predominantly by searching at the previously rewarded locations. After an average of 5 trials, the rat shifted to a random searching strategy for new rewards, followed by subsequent trials consistent with gradual encoding of the new reward locations. Over the course of 15-20 trials, rats developed a stereotyped, efficient trajectory to navigate to the reward locations. Memory for these reward locations was successfully retrieved the subsequent day (Figure 2C). These results demonstrate the rats' ability to flexibly, accurately, and repetitively generate new long-term memories based on the changing salient stimuli.

We also designed several variations of the CB task to parse its component memory processes. Firstly, we explored the relationship between extent of training and memory performance. Rats were trained on new reward locations only until they could demonstrate an accurate, effective navigation trajectory. After this truncated training session, rats were tested for recall of the reward locations the following day. We found that these sessions resulted in significantly impaired memory performance compared to completion of the full training session (**Figure 2D**), indicating that a threshold of training must be attained to ensure robust formation of long-term memory. We next investigated the contrasting behavioral scenario, by training rats on the same reward locations for two consecutive memory cycles. In this case of repeat learning, performance reached a plateau during the first memory cycle that was sustained throughout the subsequent training and testing sessions of the second memory cycle. Memory performance was not different between the first

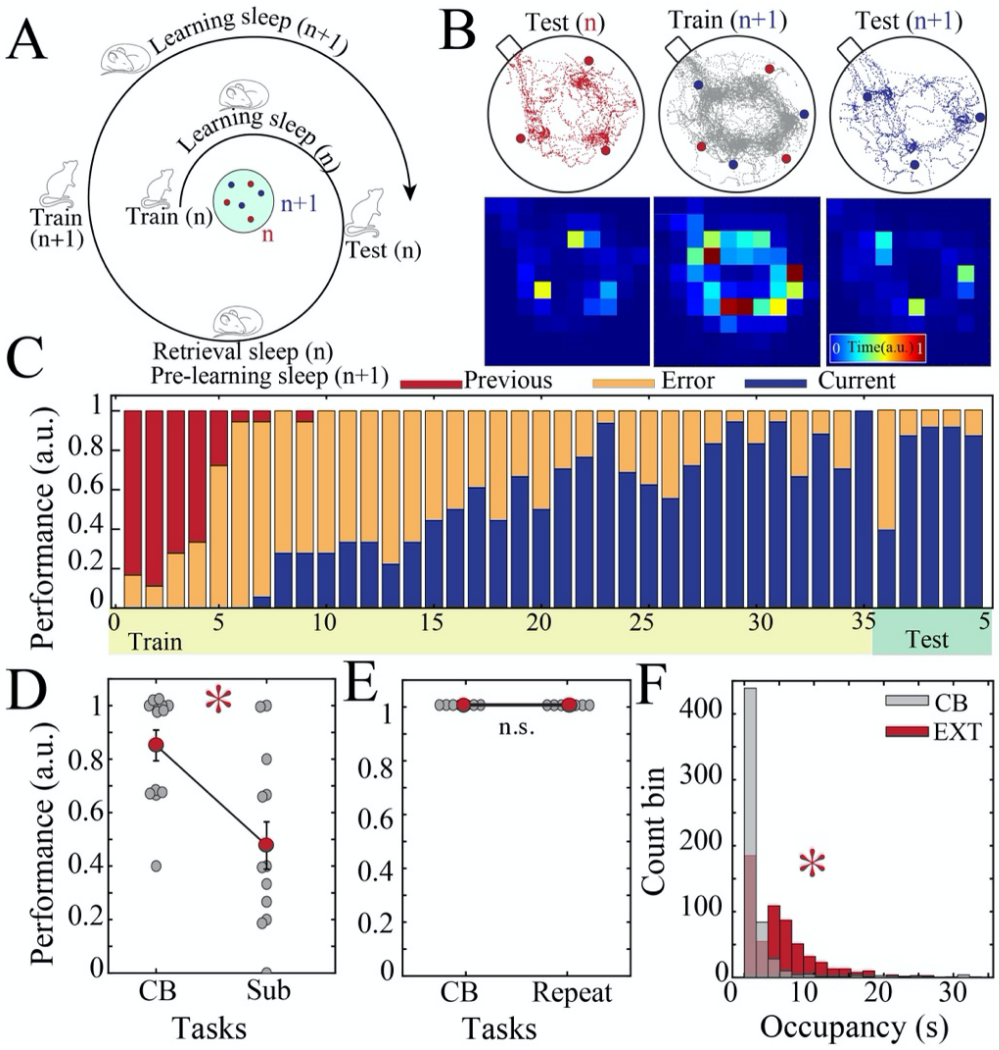

Figure 2. Rats demonstrate ability to flexibly update long-term memories in a spatial memory task. (A) Schematic of behavioral protocol for CB task. (B) Sample CB behavioral performance. Top: trajectory of a rat across the maze during five trials of test session$_{(n)}$ (red), during 25 trials of training session$_{(n+1)}$ (gray), and during five trials of test session$_{(n+1)}$ (blue). Red and blue circles indicate reward configuration$_{(n)}$ and reward configuration$_{(n+1)}$, respectively. Bottom: color map shows spatial distribution of time spent by the rat on the maze surface. Warmer colors represent the locations where the rat spent proportionally more time during the session. (C) Performance of rats across training and testing trials for CB task (n = 6 rats). Red boxes represent proportion of trials when the rats directly searched for the previously rewarded wells (reward configuration$_{(n)}$). Orange boxes represent proportion of trials when the rats had a predominantly random exploration strategy. Blue boxes represent proportion of trials where the rat directly navigated to the locations of currently rewarded wells (reward configuration$_{(n+1)}$). (D) Memory performance of rats was significantly decreased for subthreshold (sub) compared to regular CB training (paired t-test, $P = 0.003$, n = 13 sessions). (E) Memory performance of rats was identical when the same reward configuration was used for two consecutive memory cycles (paired t-test, $P = 1$, n = 7 sessions). (F) During extinction training sessions, rats spent more time exploring the maze compared to CB training sessions where rats spent minimum time in non-rewarded locations. (K-S test, $P << 0.001$, n = 6 sessions).

and second testing session, consistent with the notions that a single training session is sufficient to establish a robustly recalled long-term memory and that additional training does not further enhance behavior (Figure 2E). Lastly, we conducted training sessions with the goal of extinguishing the previously recalled memory without encoding new reward locations. To accomplish this, we randomized reward locations on each training trial. Rats initially searched the previously recalled reward locations, but in the absence of rewards at these locations, they then embarked on a random foraging strategy that resulted in a lack of stereotyped trajectory across the maze by the end of this session (Supplementary Figure 3). In this manner, we were able to diminish the salience of the previous reward locations without introducing a novel learning demand (Figure 2F).

These tasks allowed us to investigate how hippocampal-cortical communication is modulated across memory phases. Neurophysiologic recordings were performed after each behavior session, and we analyzed the trajectory of oscillatory coupling during NREM sleep. To track changes within individual animals with sensitivity to each training-testing cycle, our analysis was based on comparisons between a sleep session and its chronologically subsequent sleep session, generating unique paired datapoints. Sleep quality was similar between sleep sessions that occurred after the different behavioral sessions, and we did not identify circadian patterns that could drive behavior-independent changes in oscillatory coupling

3.3 Role of ripple-ripple coupling in long-term memory

We first examined changes in SPW-R / CXR coupling as rats progressed through the memory cycle. We observed that this coupling was strongest after a long-term memory was retrieved, compared to when the memory was first established (Figure 3A-B). In contrast, SPW-R / CXR coupling was decreased by the transition from a previously learned reward configuration to a new

reward configuration (Figure 3C-D). When we quantified this interaction at an intermediate timepoint during training, we found that SPW-R / CXR coupling progressively increased after additional learning trials and peaked after successful memory retrieval. Rat that underwent the subthreshold training (as in Figure 2D) did not display significant changes in the SPW-R / CXR interaction, though trends were present that tracked the direction of change that occurred with a full training session (Figure 3E). This pattern of modulation was specific for newly established long-term memory, because repeat training of the previously learned and recalled reward locations (as in Figure 2E) did not induce significant coupling modulation (Figure 3F). An extinction training session (as in Figure 2F, Supplementary Figure 3) was also insufficient to change SPW-R / CXR coupling (Figure 3G). In addition, the enhanced SPW-R / CXR coupling observed after memory retrieval occurred in the absence of a parallel increase in oscillation occurrence rates, indicating a specific alteration in temporal precision. Taken together, these results demonstrate that long-term memory processes drive specific, phase-specific modulations in SPW-R / CXR coupling.

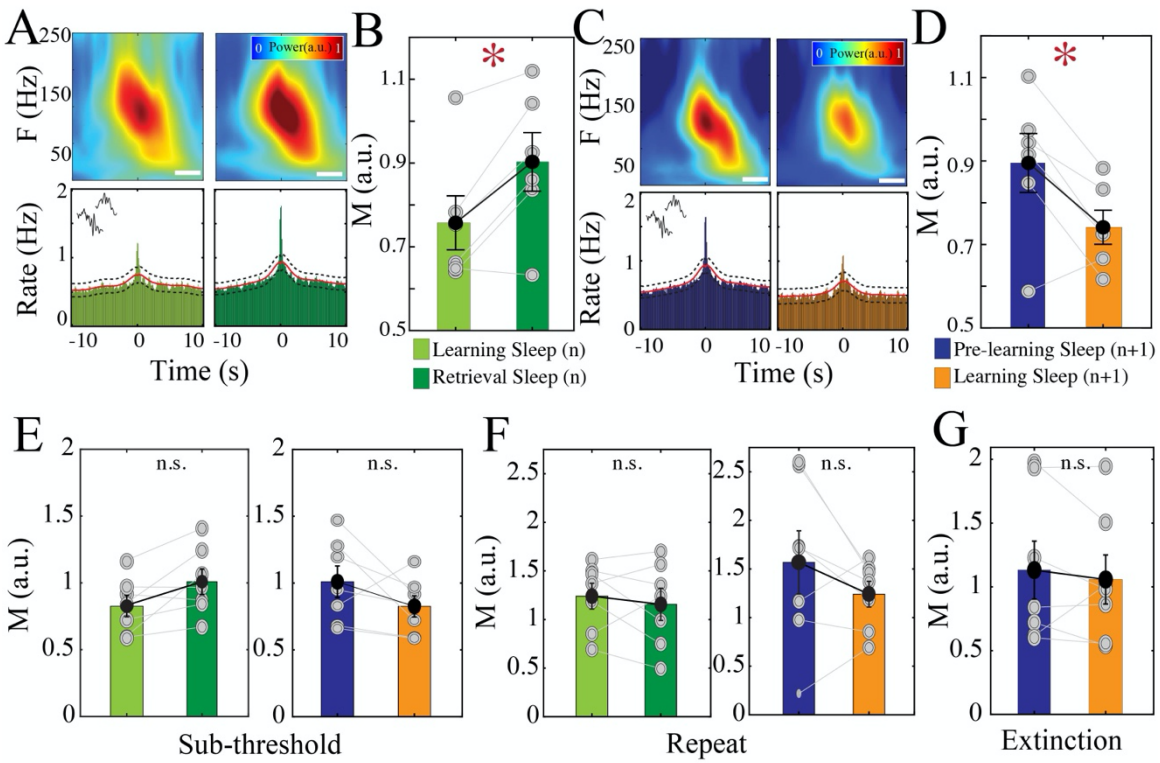

Figure 3. Coupling of SPW-R with CXR is specifically upregulated after retrieval of newly established long-term spatial memory.

(A) PPC spectrogram trigger-averaged on occurrence time of SPW-R from sample rat (top) reveals temporally locked increase in power in the ripple band that is more prominent in retrieval sleep$_{(n)}$ (right) compared to learning sleep$_{(n)}$ (left) on the CB task. Corresponding CCGs demonstrating change in SPW-R / CXR coupling (bottom) during learning sleep$_{(n)}$ (left; 1,555 SPW-R, 2,569 CXR) compared to retrieval sleep$_{(n)}$ (right; 1,999 SPW-R, 4,263 CXR). Time 0 is the occurrence of SPW-R; scale bar, 25 ms. (B) SPW-R / CXR coupling modulation in learning sleep$_{(n)}$ vs. retrieval sleep$_{(n)}$ (bars; mean ± s.e.m) on the CB task. Gray lines indicate mean change in individual rats (n = 6 rats, paired t-test, $P = 0.0174$, * = $P < 0.05$). (C) PPC spectrogram trigger-averaged on occurrence time of SPW-R from sample rat (top) reveals temporally locked increase in power in the ripple band that is more prominent in pre-learning sleep$_{(n+1)}$ (left) compared to learning sleep$_{(n+1)}$ (right). Corresponding CCGs demonstrating change in SPW-R / CXR coupling (bottom) during paired pre-learning sleep$_{(n+1)}$ (left; 1,936 SPW-R, 4,737 CXR) and learning sleep$_{(n+1)}$ stages (right; 1,139 SPW-R, 1,662 CXR; scale bar, 25 ms). (D) SPW-R / CXR coupling modulation in pre-learning sleep$_{(n+1)}$ vs. learning sleep$_{(n+1)}$ on the CB task (n = 6 rats; paired t-test, $P = 0.028$, * = $P < 0.05$). (E) SPW-R / CXR coupling modulation on the sub-threshold CB task variation for learning sleep$_{(n)}$ vs. retrieval sleep$_{(n)}$ (left; n = 7 sessions, paired t-test, $P = 0.052$) and pre-learning sleep$_{(n+1)}$ vs. learning sleep$_{(n+1)}$ (right; n = 7 sessions, paired t-test, $P = 0.16$). (F) SPW-R / CXR coupling modulation on the repeat CB task variation for learning sleep$_{(n)}$ vs. retrieval sleep$_{(n)}$ (left; n = 7 sessions, paired t-test, $P = 0.52$) and pre-learning sleep$_{(n+1)}$ vs. learning sleep$_{(n+1)}$ (right; n = 7 sessions, paired t-test, $P = 0.23$). (G) SPW-R / CXR coupling modulation on the extinction CB task variation for pre-learning sleep$_{(n+1)}$ sleep vs. learning sleep$_{(n+1)}$ (n = 7 sessions, paired t-test, $P = 0.50$).

3.4 Role of ripple-spindle coupling in long-term memory

We next examined SPW-R / SPI coupling across the memory cycle. In contrast to SPW-R / CXR coupling, we found that this coupling was significantly increased after learning but dropped after retrieval (Figure 4A-D).

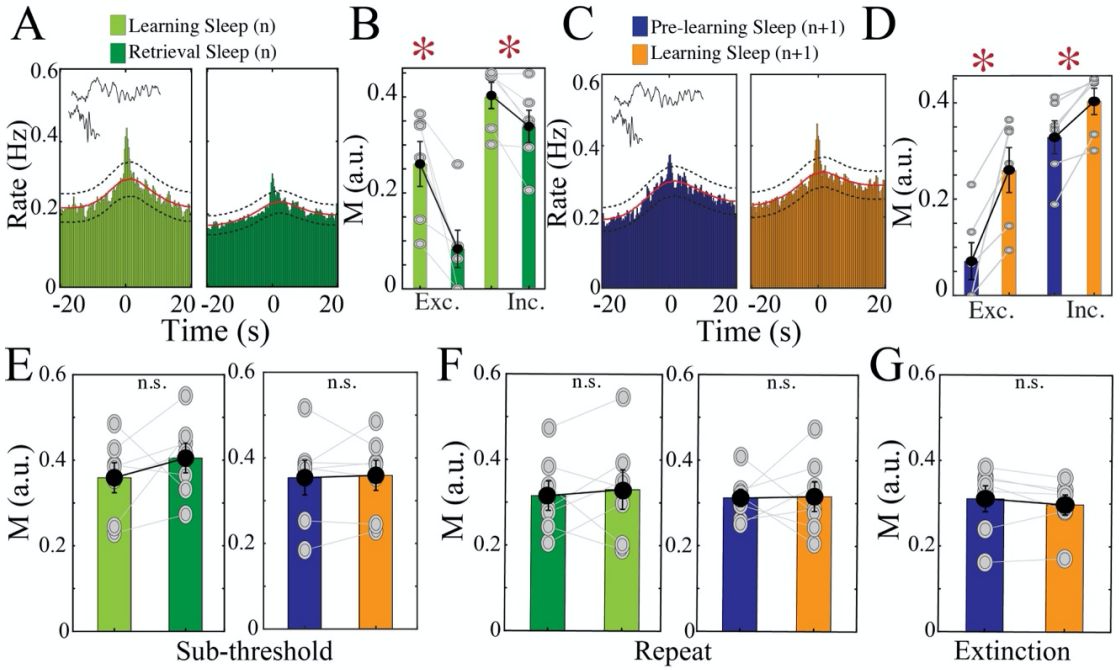

Figure 4. Coupling of SPW-R with SPI is specifically upregulated after learning of newly established long-term memory
(**A**) Sample SPW-R / SPI CCGs demonstrating a decrease in modulation during learning sleep$_{(n)}$ (left; 1,668 SPW-R, 1,312 SPI) vs. retrieval sleep$_{(n)}$ (right; 2,025 SPW-R, 1,353 SPI) on the CB task. (**B**) Significant change in coupling modulation between learning sleep$_{(n)}$ and retrieval sleep$_{(n)}$ for exclusive and inclusive SPW-R / SPI coupling on the CB task (left; exclusive, $P = 0.0127$; right; inclusive, $P = 0.032$; paired t-test, * $P < 0.05$; n = 6 rats). (**C**) Sample SPW-R / SPI CCGs demonstrating an increase in modulation during pre-learning sleep$_{(n+1)}$ (left; 1,473 SPW-R, 1,009 SPI) vs. learning sleep$_{(n+1)}$ (right; 1,318 SPW-R, 1,020 SPI) on the CB task.(**D**) Significant change in coupling modulation between pre-learning sleep$_{(n+1)}$ and learning sleep$_{(n+1)}$ for exclusive (left; paired t-test, $P = 0.012$) and inclusive (right; paired t-test, $P = 0.010$) SPW-R / SPI coupling on the CB task. * $P < 0.05$; n = 6 rats.(**E**) SPW-R / SPI coupling modulation on the sub-threshold CB task variation for learning sleep$_{(n)}$ vs. retrieval sleep$_{(n)}$ (left; n = 7 sessions, paired t-test, $P = 0.33$) and pre-learning sleep$_{(n+1)}$ vs. learning sleep$_{(n+1)}$ (right; n = 7 sessions, paired t-test, $P = 0.82$). (**F**) SPW-R / SPI coupling modulation on the repeat CB task variation for learning sleep$_{(n)}$ vs. retrieval sleep$_{(n)}$ (left; n = 7 sessions, paired t-test, $P = 0.69$) and pre-learning sleep$_{(n+1)}$ vs. learning sleep$_{(n+1)}$ (right; n = 7 sessions, paired t-test, $P = 0.92$). (**G**) SPW-R / SPI coupling modulation on the extinction CB task variation for pre-learning sleep$_{(n+1)}$ sleep vs. learning sleep$_{(n+1)}$ (n = 7 sessions, paired t-test, $P = 0.32$).

These changes were enhanced when instances of tripartite coupling were eliminated, in contrast to what was observed in the absence of memory demand (Figure 4B, D). Behavioral experiences that:

i) were subthreshold for long-term memory expression; ii) repeated previously trained information; or iii) served to extinguish previous memory in the absence of new information were all insufficient to generate significant changes in SPW-R / SPI coupling (Figure 4E-G). Although occurrence rates of SPW-R and SPI paralleled their coupling modulation across the memory cycle, the precise oscillatory pairing exceeded that predicted by rate. Thus, SPW-R / SPI coupling is strongly induced by long-term memory with a different time course across memory phases compared to SPW-R / CXR coupling. Of note, direct interaction between CXR and SPI did not change with any memory phase.

3.5 Coupling patterns in long-term non-spatial memory

To investigate how these oscillatory coupling patterns could be influenced by the type of task, we conducted similar analyses for a non-spatial object association task (OA(36)). Rats learned to associate a particular object with a reward over the course of training trials, and successfully retrieved memory for this object the following day (Figure 5A-B). Similar to our findings with the CB task, SPW-R / CXR coupling was significantly increased during sleep following retrieval compared to learning (Figure 5C). This change was also specific for new information because it was abolished by repeating the same object-reward association on consecutive memory cycles (Figure 5D). However, significant alteration of SPW-R / SPI coupling was not observed for any

stage of this memory task (Figure 5E-F). These results suggest a conserved role for SPW-R/ CXR in long-term memory, but a task-specific function of SPW-R / SPI coupling.

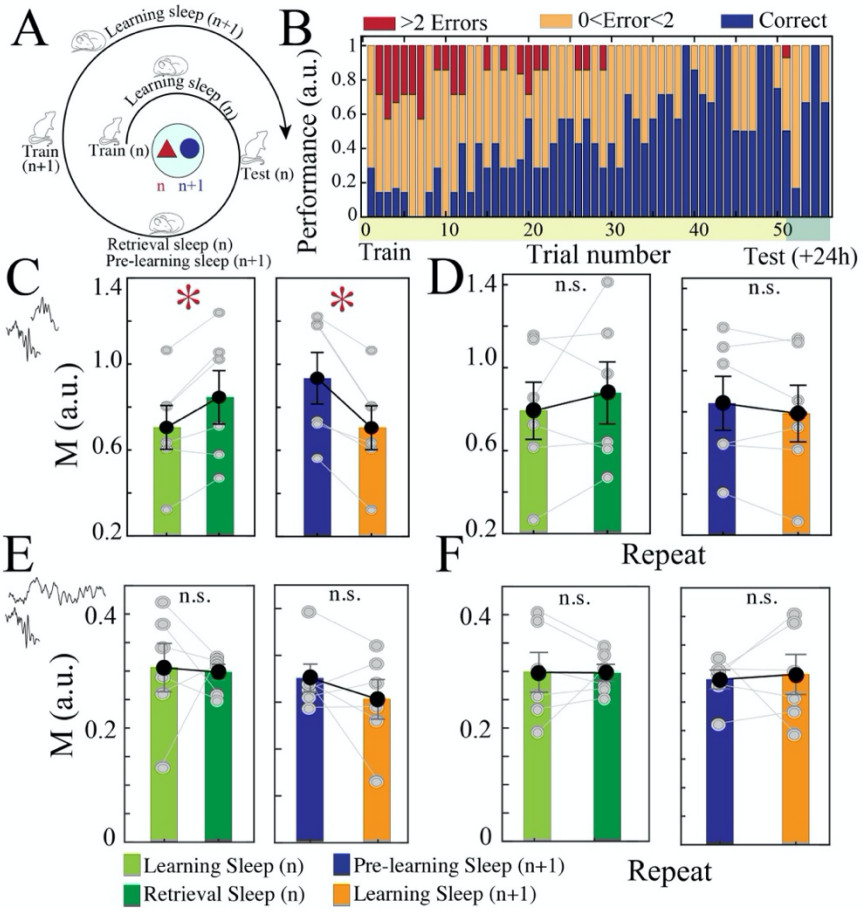

Figure 5. Coupling of SPW-R with CXR is specifically upregulated after retrieval of established long-term non-spatial memory

(**A**) Schematic of behavioral protocol for a non-spatial OA task. (**B**) Performance of rats across training and testing trials for the OA task (n = 6 rats). Red boxes indicate proportions of trials where rats explored >2 incorrect reward objects before finding the correct object. Orange boxes indicate trials where rats explored at most 2 incorrect objects. Blue boxes represent proportion of trials where rat directly located the correct object. (**C**) SPW-R / CXR coupling modulation in learning $sleep_{(n)}$ vs. retrieval $sleep_{(n)}$ (left; paired t-test, $P = 0.019$) and pre-learning $sleep_{(n+1)}$ vs. learning $sleep_{(n+1)}$ (right; paired t-test, $P = 0.0067$) on the OA task. Gray lines indicate mean change in individual rats (bars; mean ± s.e.m; n = 6 rats, * = $P < 0.05$) (**D**) SPW-R / CXR coupling modulation in the repeat variation of the OA task for learning $sleep_{(n)}$ vs. retrieval $sleep_{(n)}$ (left; paired t-test, $P = 0.47$) and pre-learning $sleep_{(n+1)}$ vs. learning $sleep_{(n+1)}$ (right; paired t-test, $P = 0.28$). (**E**) SPW-R / SPI coupling modulation in learning $sleep_{(n)}$ vs. retrieval $sleep_{(n)}$ (left; paired t-test, $P = 0.87$) and pre-learning $sleep_{(n+1)}$ vs. learning $sleep_{(n+1)}$ (right; paired t-test, $P = 0.30$) on the OA task. (**F**) SPW-R / SPI coupling modulation in the repeat variation of the OA task for learning $sleep_{(n)}$ vs. retrieval $sleep_{(n)}$ (left; paired t-test, $P = 0.47$) and pre-learning $sleep_{(n+1)}$ vs. learning $sleep_{(n+1)}$ (right; paired t-test, $P = 0.29$).

3.6 Consolidation versus Reconsolidation

Given these findings, we further characterized the dynamics of SPW-R / CXR coupling across individual sleep sessions after behavior on the CB and OA tasks. We found that in the sleep session after learning for both the spatial and nonspatial tasks, coupling rates were initially high, but exhibited a steady decline over subsequent NREM sleep (Figure 6A-B, light colors). In contrast, the sleep after retrieval of a spatial or nonspatial long-term memory was associated with a similar initial peak, but then a sustained plateau in coupling (Figure 6A-B, dark colors). These data indicate that the temporal recruitment of SPW-R / CXR coupling is time-limited and specific to whether memory was previously encoded or retrieved. We then aimed to synthesize these results into neural signatures characteristic of different stages within the memory cycle. We classified changes that occurred after learning and prior to retrieval as related to consolidation, and changes that occurred after retrieval but prior to any new learning as reconsolidation. For CB and OA tasks, the principal indicator of reconsolidation was a surge in SPW-R / CXR coupling. This increase was accompanied by a decrease in SPW-R / SPI coupling that was only significant for the CB task. In contrast, consolidation was characterized by a joint enhancement of SPW-R / SPI coupling for the CB task only. Unsupervised k-means clustering based on SPW-R / CXR and SPW-R / SPI coupling modulations resulted in an accurate classification of memory processes across animals (Figure 6C). When examined chronologically, these patterns resulted in a cyclic, task-specific modulation of oscillatory coupling that was appreciable at the level of an individual rat (Figure 6C-D). Therefore, hippocampal-cortical communication occurs in independent streams that are differentially modulated both by memory phase and the spatial demand of the task. These results

support the notion that oscillatory coupling facilitates memory-specific information flow and shed light onto the mechanisms that govern long-term memory in a dynamic environment.

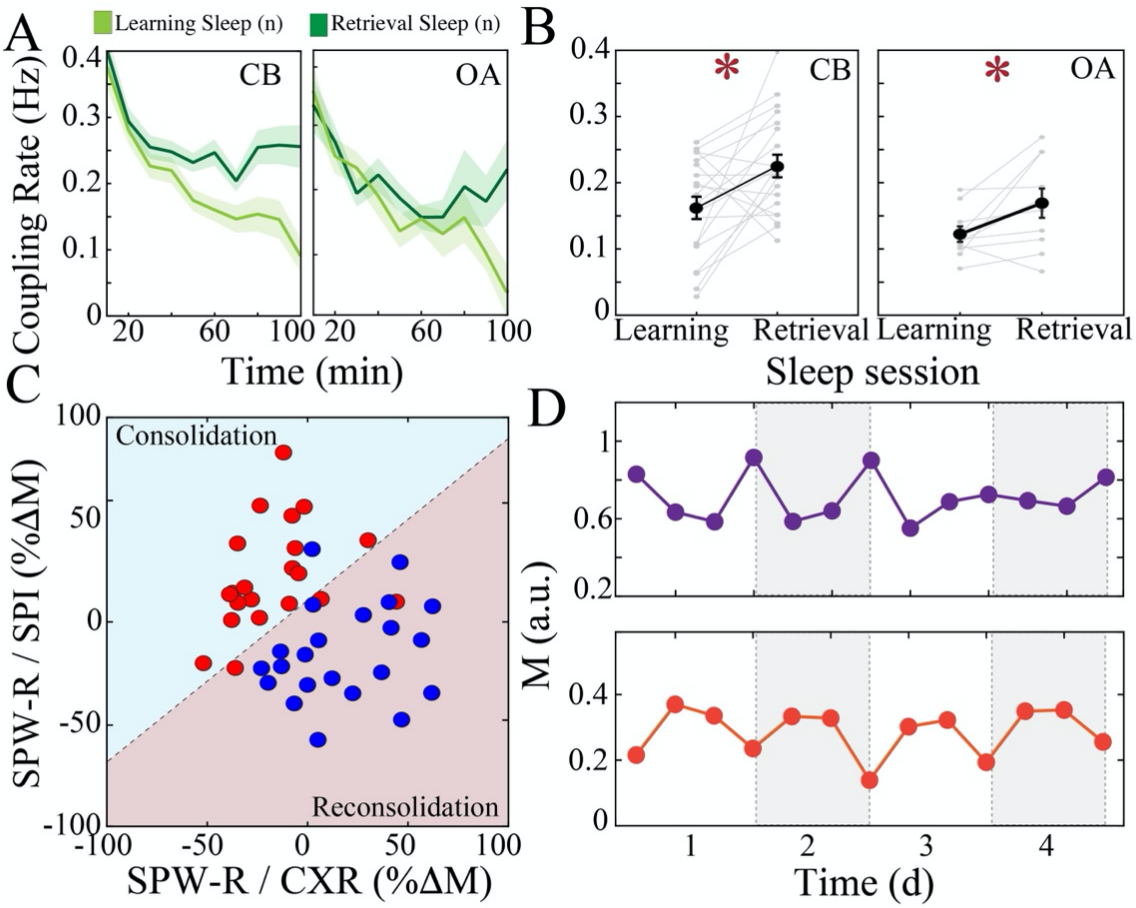

Figure 6. Memory consolidation and reconsolidation are differentiable on the basis of hippocampal-cortical coupling patterns.
(A) Joint occurrence rate of SPW-R and CXR across NREM sessions reveal different temporal trajectories for learning sleep$_{(n)}$ vs. retrieval sleep$_{(n)}$ on the CB task (left; n = 23 sessions) and the OA task (right; n = 12 sessions). Lines and shaded bars represent mean ± s.e.m. (B) Increase in joint occurrence rate of SPW-R and CXR from learning sleep$_{(n)}$ vs. retrieval sleep$_{(n)}$ on the CB task (left; n = 20 sessions; paired t-test P = 0.012) and OA task (right; n = 10 sessions; paired t-test P = 0.037). Data represented as mean ± s.e.m; gray lines are individual sessions; * $P < 0.05$. (C) Unsupervised K-means clustering of the percentage changes in the coupling modulation of SPW-R / CXR and SPW-R / SPI between sleep sessions after memory phases on the CB task shows accurate classification (n = 6 rats, accuracy = 86.36%) (D) Cyclical modulation of SPW-R / CXR coupling (top) and SPW-R / SPI coupling (bottom) across the memory cycle for CB task (sample rat).

3.7 Large-scale investigation of cortical spindles

To characterize large-scale oscillatory networks in the cortex, we utilized a conducting polymer-based conformable microelectrode surface array (NeuroGrid) to simultaneously monitor multi-site activity from the cortical surface in behaving rats (n = 6 rats). By combining electrophysiologic and anatomic markers, we identified electrodes in different cortical sites (Figure 7A), including primary neocortical regions such as motor, somatosensory, retrosplenial, posterior parietal and visual cortices. Our objective was to investigate the spatial patterns of spindle oscillations within the cortex and explore the functional relationship between sharp wave-ripple complexes (SPW-Rs) and topographically specific spindles, given the crucial role of ripple-spindle coordination in long-term memory processes.

3.7.1 Spindles have a wide distribution of spatial extent over the neocortex

Visual inspection of the raw traces revealed that spindle events were not uniformly distributed across the cortical surface. Instead, we observed spindle events that were concentrated in mostly one cortical site, or encompassed one or more adjacent brain regions, or were globally present. To quantify the distribution of spindle spatial extent, we calculated the deviation of each spindle event's median spatial power from the threshold criterion for detection of spindles. This approach allowed us to categorize spindles into three distinct groups based on their spatial extent: localized (low), intermediate, and global (high) spindles. The resulting distribution confirmed a wide range of spindle spatial extents, with a spectrum that ranged from low to high spatial extent spindles. Our findings suggest that spindle activity is not confined to specific regions of the brain but instead can occur in topographically distinctive networks with varying spatial extents. This observation

was consistent with all animals in our cohort.

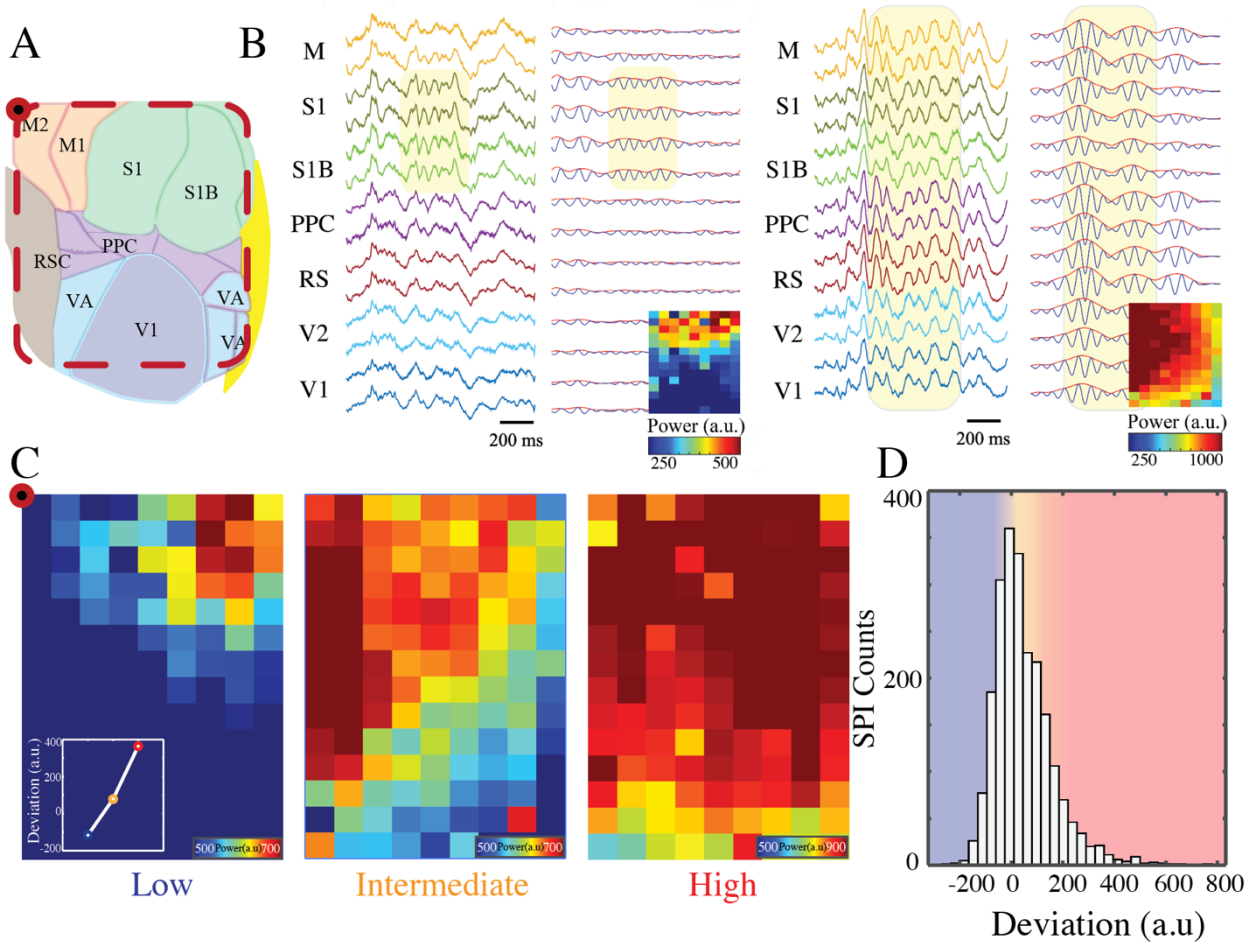

Figure 6. Spindles have a wide distribution of spatial extent on the cortical surface (A) NeuroGrid array (dashed red) coverage over the dorsal cortical surface of a rat from bregma (red dot) anteriorly to lambda posteriorly. Simultaneous recording can be made from multiple brain regions including motor (M1, M2), somatosensory (S1, S1B), posterior parietal cortex (PPC), retrosplenial (RSC) and visual cortex (V1, VA). (B) Sample raw, filtered (blue) and Hilbert (red) traces of a localized spindle event (left) and a global spindle event (right). Inset spindle-triggered power maps show the location of spindles on the grid. Warmer colors indicate high spindle power. Blue color indicates absence of spindle. Spindle threshold power is 450 a.u. for these samples. (C) Sample spindle grid power maps showing local (low), intermediate and global (high) spatial extent of spindle events. Red dot indicates the location of bregma. Inset plot represents the deviation of median spatial power of the three samples from the threshold detection power (450 a.u.). (D) Distribution of the spindle power deviation of 2,360 spindle events from a sample session. Lower deviation represents localized SPI events. As deviation value progressively increases, SPIs events higher spatial extent.

3.7.2 Hippocampal ripples are preferentially coupled to global spindles after learning

We then wanted to examine the coupling patterns between SPW-Rs and topographically specific SPI and whether they play a preferential role in memory consolidation. We extracted equal number of SPI events from low, intermediate, and high category of spatial extent distribution and performed their cross-correlation with SPW-Rs in each session. In general, we found that SPW-R / SPI coupling progressively increased for SPI with increasing spatial extent in all our sessions. We observed that the coupling was strongest for global SPI compared to low spatial extent SPI and significant during the learning sleep in CB task. These results suggest that large-scale spindles reflect a more coordinated activation of neocortical circuits and may provide a more favorable context for the hippocampal to communicate with multiple cortical regions simultaneously. During learning sleep, consolidation of memory requires communication between hippocampus and distributed neocortical networks. Our findings suggest that global spindles, with their synchronized wide-spread activity, may be a mechanism that hippocampal SPW-Rs employ to facilitate this information transfer.

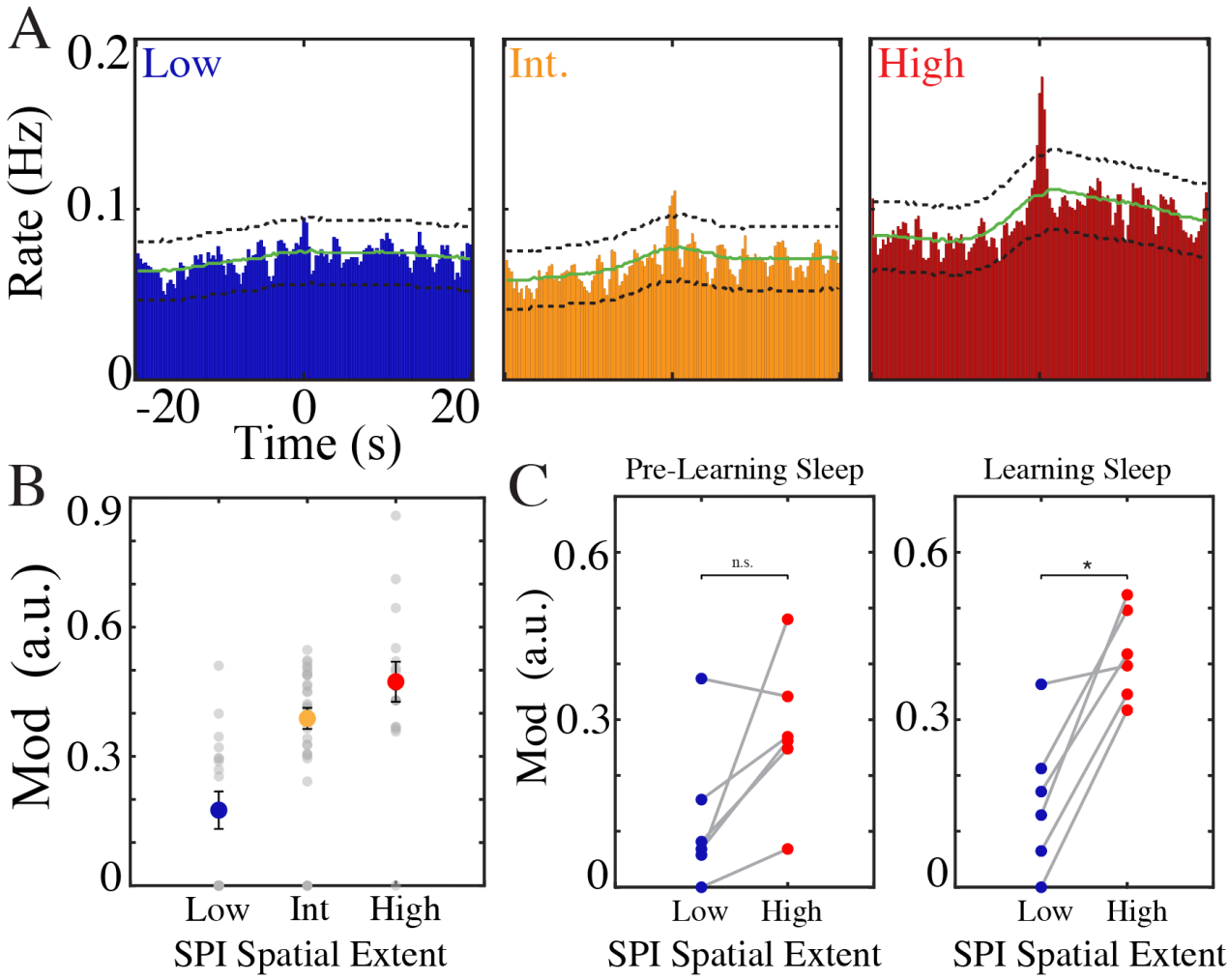

Figure 7. Hippocampal SPW-Rs are preferentially coupled towards global spindles during learning sleep (A) Sample CCGs of low (400 SPIs), intermediate (400 SPIs) and high (400 SPIs) spatial extent spindles with hippocampal SPW-Rs (1,698 SPW-Rs) show progressively increasing coupling strength with the spatial extent. (B) Summary for all sleep sessions from one animal illustrating the coupling modulation (M) of SPW-R / SPI coupling. Data represented as mean ± s.e.m; gray dots are individual sessions (C)Summary from all rats (n = 6) during pre-learning sleep (left) and learning (sleep) show significant SPW-R / global SPI compared SPW-R / local SPI only for learning sleep (paired t-test $P = 0.002$; * $P < 0.05$)

3.8 Discussion

Here, we investigated oscillatory dynamics between hippocampus and cortex as long-term memories were consolidated, strengthened, and updated during sleep after a behavioral experience. We found that in the absence of memory demand, SPW-R, CXR, and SPI were jointly modulated in these regions. Offline consolidation of spatial, but not nonspatial, memory was correlated with

independent recruitment of SPW-R / SPI coupling. Subsequent retrieval and reconsolidation initiated a shift toward enhanced SPW-R / CXR interactions for both memory types. This shift only occurred for recently established long-term memories; in the absence of new learning within 24 hours, no changes were evoked. The stage of memory processing could be identified by the relative prominence of oscillatory coupling patterns, as well as their post-behavior dynamics. These findings suggest the ability of such interactions to specifically, flexibly, and repetitively support memory processes required for adaptation to a changing environment.

Memory consolidation requires protein synthesis(37, 38) and reactivation of a previously consolidated memory is postulated to restore its lability, as demonstrated by an additional window of susceptibility to protein synthesis blockade in certain conditions(39–41). These processes are partially differentiable on the basis of identified molecular mechanisms and involved anatomic circuits(4, 42, 43). Our data, which demonstrate a contrast between hippocampal-cortical oscillatory interactions after learning and retrieval supports the notion that these experiences can be functionally and mechanistically distinguished. Furthermore, we observed that a retrieval experience characterized by reinforcement of previous associations resulted in a different pattern of oscillatory coupling than a retrieval experience that weakened previous associations and established new ones within the same schema. Such patterns may therefore provide insight into whether a behavioral experience has served to strengthen or extinguish a memory. Repetitive training and retrieval of the same associations over two days eliminated oscillatory coupling differences during the subsequent offline epochs, suggesting either a time-limited role in both consolidation and reconsolidation, or a requirement for proximal new learning. Further behavioral experiments that extend the examination of an individual memory could facilitate disambiguation of these possibilities.

Significant modification of hippocampal-cortical coupling occurred with spatial and nonspatial tasks, in keeping with evidence supporting the role for the hippocampus and distributed cortical regions in offline processing for both these types of memory(14, 44, 45). However, SPW-R / SPI coupling was more strongly modulated across consolidation and reconsolidation of the spatial, compared to the nonspatial, task. We propose that this form of coupling is most prominent with PPC for tasks that heavily rely on spatial context information(46, 47), whereas SPW-R / CXR coupling is more generally activated within complex, distributed circuits involved in strengthening of long-term representations(48, 49). It is possible that this SPW-R / SPI coupling is locally upregulated in cortical regions outside of PPC during the nonspatial task.

In keeping with previous studies, we found that occurrence rates of SPW-R and SPI were modestly modulated by previous salient behavioral experiences(50–54). However, we found evidence to support independent regulation of oscillation occurrence rate and temporal coupling. Changes in coupling strength utilized were selected to normalize for rate measures(55, 56), and during specific memory stages coupling strength was increased when oscillation occurrence rate decreased. Because SPW-R, CXR, and SPI have all individually been associated with reactivation of behaviorally-relevant neural spiking patterns and cellular plasticity(17, 57–59), these parameters could be differentially engaged to modify local or distributed processes depending on memory phase and task demand.

Rodents established long-term memory for our tasks within a single day of training and efficiently updated these memories within a previously learned schema when reward associations were changed. This task structure allowed us to focus on the dynamics of the memory process, in contrast to tasks where prolonged training requirements, strong aversive responses, or habituation can hinder repeated cycles of memory formation within an individual animal(33, 35, 60).

Oscillation occurrence rates and strength of oscillatory coupling demonstrated memory-driven fluctuation around a setpoint, suggestive of homeostatic limits on modulation of these parameters over the course of days. On a shorter timescale, coupling was highest in the sleep epochs immediately following a behavior, consistent with the effectiveness of closed-loop manipulations performed for only the first hour of the consolidation period in modifying memory and evidence for rapid establishment of cortical engrams(22, 24, 47, 61). During reconsolidation, SPW-R / CXR coupling was also increased in later sleep epochs, raising a potential parallel with the delayed window of memory-modulating effects for cortically administered pharmacologic substances(62–64).

The fate of a long-term memory is determined by subsequent experience and is dynamic over a prolonged period. Our results show that three prominent network patterns implicated in memory (hippocampal sharp wave-ripples, cortical spindles, and cortical ripples) undergo dynamic comodulation across the cycle of memory consolidation, reconsolidation, and updating. We hypothesize that temporal links between these plasticity-related oscillations in different brain structures provide the network infrastructure for cellular and molecular changes associated long-term memory processing. These oscillatory coupling patterns present an opportunity for design of novel closed-loop investigations to manipulate memory across distributed neural networks and enhance understanding of disorders characterized by impaired and over-active information retention(65, 66).

3.9 Materials and Methods

Probe fabrication and preparation

The fabrication of conducting polymer-based NeuroGrids has been discussed in previous publications(25, 67). In brief, a projection exposure system was used to pattern parylene C, Au,

Pt, Ti and PEDOT:PSS films. The NeuroGrid was attached to a custom printed circuit board using mixed conducting particulate composites(68). The board contained an RHD2164 die (Intan Technologies) for the purpose of amplification, digitization and transmission of the acquired neural signals via a serial peripheral interface protocol to a computer interface board (RHD2000 evaluation board; Intan Technologies). All back-end electronics were covered with silicone elastomer as an encapsulation layer.

Animal surgical procedure

All animal experiments were approved by the Institutional Animal Care and Use Committee at Columbia University. Nine male Long Evans rats (200-350 g) were used for intracranial implantation. Rats were kept on a regular 12h/12h light dark cycle and housed in pairs prior to implantation, but separated afterward. Prior experimentation was not performed on these animals. The animals were initially anaesthetized with 2% isoflurane and maintained under anesthesia with 0.75-1% isoflurane during the surgery. Silicon probes and/or wires were implanted into hippocampus (-3.5 AP, 3.0 ML). A NeuroGrid electrocorticography array was placed over the dorsal cortical surface of the contralateral hemisphere relative to the wires. Screws in the skull, overlying cerebellum, served as ground electrodes. The craniotomies were covered by Gelfoam and sealed using a 10:1 mixture of paraffin and mineral oil. Rats recovered for 4-5 days prior to initiation of experimentation. Hippocampal electrodes were adjusted in the dorsal/ventral axis to target CA1 pyramidal cell layer based on characteristic appearance of hippocampal sharp-wave ripples.

Neurophysiology data acquisition and processing

All rats underwent a protocol consisting of neurophysiologic recordings and behavioral tasks. Recordings were started at a fixed time, timed after each behavioral intervention.

Neurophysiological signals were amplified, digitized continuously at 20 kHz using a head-stage directly attached to the probe (RHD2000 Intan technology), and stored for off-line analysis with 16-bit format. Data were analyzed using MATLAB (MathWorks) and visualized using Neuroscope.

Behavioral training

Rats were placed on a water deprivation schedule for 3-5 days prior to intracranial implantation to ensure they could receive water through a hand-held syringe. Rats were weighed daily during water deprivation to ensure that body weight did not decrease to <85% of pre-deprivation measurements. Three additional rats underwent only behavioral training.

Behavior for all tasks was tested on a cheeseboard maze, consisting of a 1.5 m diameter open circular arena that was painted a uniform green and stood 70 cm above the floor. A total of 177 water wells (7 mm in diameter, 3 mm in depth) were drilled 8 cm apart in the maze surface, forming evenly distributed, parallel columns and rows. One wall of the starting box (23 cm wide x 30 cm long x 48 cm high) functioned as a gate that could be raised and lowered to control the rat's access to the maze.

Prior to surgery, water-deprived rats were first familiarized with exploring the maze environment to obtain water. Initially, the rat was placed in the center of the maze and allowed to explore and retrieve multiple (~25) randomly placed hidden water rewards. Over the next 3 days, the number of available water rewards on the maze was gradually reduced, and a trial structure introduced such that the rat received a food reward (0.5-1 Froot Loop) after successful retrieval of all water rewards. The rat was then trained to return to the starting box after retrieving water to obtain its food reward. After 2-4 days of this repeated procedure, the rat would consistently explore the maze to obtain 3 spatially distinct water rewards and then independently return to the starting box. To

prevent use of odor-mediated searching, the maze was wiped with a towel soaked in 70% ethanol and rotated by a random multiple of 90 degrees relative to the starting box between all trials. Plastic toys of varying shapes and colors were then introduced onto the maze surface. Rats were exposed to the objects initially to ensure that there were no intrinsic preferences for any given object. Rats learned to displace the objects and obtain water from the well directly under the object. This phase of general training ended when the rat could complete 35-50 trials per day. Behavior sessions were monitored by an overhead video camera (20 fps), and tracking of the rat's location was facilitated by blue and red LEDs attached to its cap. Rats had neurophysiological recording in their home cage after each behavioral session. Several rats performed both CB and OA tasks, with each rat typically completing 2-4 memory cycles per task.

Cheeseboard maze task

Each memory cycle on this task was completed over 2 days. On the first of the two days, the rats learned the location of 3 hidden water rewards placed in a single, randomly selected set of water wells over the course of ~35 trials (25 trial session, then ~1h home cage rest, then 10 trial session). All rats obtained > 80% performance averaged over 5 trials by the end of the training session. On the second of the two days, the rat was given a 5-trial test with water rewards located in the same location as the first day to assess memory for the spatial configuration of the reward locations. After 4 hours in the home cage, the rat was brought back to the maze to learn 3 different water reward locations. Behavior was scored by tracking the animal's trajectory across the maze. During training sessions, the trajectory was compared to that of the test session performed earlier in the day (wherein the rat tracks to the previous day's rewards) and an idealized minimal distance trajectory between the new reward locations. Memory performance in the test session was scored

by determining the number of rewards obtained in < 30 seconds per trial, weighted by trial number (with higher weight to the initial trials).

Object association task

On the first day for this task, rats learned to associate one out of five objects placed at random locations on the cheeseboard maze surface over the course of ~50 trials. The number of trials and temporal arrangement was slightly modified compared to the CB task due to different amounts of water obtained by the rat per trial (affecting motivational status) and number of trials required to meet learning criterion (> 80% performance averaged over 5 trials). On the second day, the rat was given a 5-trial test with water rewards associated with the same object as the first day to assess this memory. After 4 hours in the home cage, the rat was brought back to the maze to complete another training session, which consisted of either a new object-reward association or re-training with the same object-reward association from the previous day. Behavior was scored by tracking the animal's interactions with the objects. Direct navigation to the correct object was scored the highest, with progressively lower scores for each incorrect object explored prior to the correct object.

Task variations

A series of variations on the behavioral protocols were conducted.

Subthreshold

A subthreshold memory cycle took place over three days. The first day consisted of a normal CB task training followed by a test session on the morning of the second day. Approximately 4 hours after this test session, a single "subthreshold" training session was performed. In subthreshold training, the animal was taught a new spatial reward configuration, but with fewer training trials. Once the animal was able to successfully navigate to all reward locations on 3 consecutive trials

in < 30 seconds, the session was terminated and the animal was placed in the home cage to sleep. On the third day, the animal was tested on the reward configuration used in the subthreshold training.

Repeat

In this case, the animal was trained on reward configurations that had been used in the previous training/testing sessions. Performance was assayed by a subsequent test session the following day.

Extinction

An extinction cycle took place over two days. The first day consisted of a normal CB task training followed by a test session on the morning of the second day. Approximately 4 hours after this test session, a single "extinction" training session was performed. In extinction training, the general task structure was unchanged, but reward locations were randomized for each individual trial of the session. The trials were continued until the animal consistently no longer navigated in a directed manner to the reward locations from the previous training/testing sessions, and instead foraged the maze randomly. Use of the reward locations from previous training/testing sessions were avoided during reward location randomization to prevent reinforcement of the prior trajectory.

Preprocessing

The electrophysiological data was resampled to 1250 Hz to facilitate LFP analysis. We identified epochs of sleep by first detecting immobility in the motion signal of the accelerometer attached to the head-stage and absence of EMG artifacts. NREM sleep epochs were then detected by locating periods of elevated delta (0.5-4 Hz) amplitude in the neocortex at times of immobility. REM epochs were distinguished by an increased theta/delta band frequency ratio in the iEEG spectrograms in the hippocampus. Sleep scored epochs were then visually inspected and manually

adjusted using whitened spectrograms and raw traces to eliminate short epochs containing movement artifacts.

Region selection

The anatomical location of each NeuroGrid electrode was estimated by first determining the stereotactic position of the anteromedial electrode, which sits closest to bregma. Then by following the inter-channel distance we interpolated the anatomical position of each electrode based on the rat stereotactic atlas. We corroborated these anatomical regions with physiologic markers. Electrodes demonstrating high rate of cortical ripples overlapped with channels marked as PPC based on anatomical mapping. Only the detected events in the channels identified in the PPC region were considered for analysis. We visually inspected the recordings on NeuroScope to eliminate noisy electrodes.

LFP event detection

SPW-R, SPI, and CXR, were detected based on the Free Moving Animal (http://fmatoolbox.sourceforge.net) toolbox sequential detection algorithm. Detection of SPW-R was initiated by visually determining a channel where SPW-R were present and then band-pass filtering this hippocampal channel between 100 - 250 Hz. The filtered signal was then rectified and instantaneous power was extracted using the Hilbert transform. Events where the filtered envelope was 2 standard deviations (s.d.) above the baseline s.d. of the filtered traces and where peaks reached 5 times the s.d. were selected. Only events longer than 20 ms duration were selected and the duration between two SPW-R events had to be a minimum of 30 ms. Events common to the ripple channel and an EMG electrode noise channel were eliminated.

To detect SPI in the PPC, a PPC channel was filtered between 10-20 Hz, followed by signal rectification and enveloping. Events where the filtered envelope was greater than 3 s.d. above

baseline for a minimum of 300 ms and a maximum of 4 s were detected. The duration between two SPI events had to be a minimum of 450 ms.

CXR were detected by filtering a PPC channel between 110-180 Hz, rectifying and extracting instantaneous power using the Hilbert transform. CXR were identified when the envelope was greater than 5 s.d. above baseline for a minimum of 20 ms and a maximum of 90 ms. The duration between two CXR events was set to a minimum of 30 ms.

All detections were visually inspected for accuracy for each recording session.

Rate calculation

Rate of SPW-R was calculated by dividing the number of detected SPW-R in the hippocampal channel by the duration of NREM sleep. For CXR and SPI, the detected events were pooled together from all the PPC channels and any repeating event timepoints were eliminated. This allowed us to identify all the unique events occurring in the PPC region. Dividing the number of unique events by the NREM duration provided us with the rate of CXR and SPI.

CCG calculation

To determine coupling between detected oscillations, cross-correlograms (CCG) were calculated and the statistical significance was determined using a modified convolution method(56). The CCG was calculated from the counts of the under-investigation event E_2 at specific time delays with respect to the occurrence of the reference event E_1 which quantifies the temporal correlation between two detected events.

By convolving the cross-correlation histogram with a partially hollowed window, we estimated the co-occurrence of the two events when the occurrence of the two events is independent[54]. The confidence interval was estimated from a Poisson distribution with mean lambda value determined from the convolution.

The peak of the CCG (a) above the confidence interval and expected-value level (b) at time zero allow us to compute the coupling modulation (M) as a normalized ratio of the peak exceeding the confidence interval at chance.

$$M = \frac{a - b}{b}$$

Consider the scenario where the entire length of neural recording was divided into time bins without overlap. For each time bin, suppose that E_2 occurs with a probability p_1 if event E_1 is present but with probability p_2 if event E_1 is absent. The degree of difference of the two probabilities can be quantified through the log odds ratio (R) (55):

$$R = \log\left(\frac{p_1}{1 - p_1} \Big/ \frac{p_2}{1 - p_2}\right)$$

where the statistical parameter R quantifies the tendency of the two events to co-occur. In our case, both p_1 and p_2 are much lower than 1 based on the small-time bins comprising the CCG, compared to the length of the entire recording. The ratio can then be simplified as:

$$R = \log\left(\frac{p_1}{p_2}\right)$$

From the cross-correlograms, probability p_1 and p_2 are directly proportional to the significant number of co-occurring events per second a and the number of co-occurring events at chance b, respectively.

$$\frac{p_1}{p_2} \propto \frac{a}{b}$$

The coupling strength we defined can be seen as equivalent to the exponential of co-occurrence index *R* with a shift (*a / b -1)*. The coupling strength thus quantifies the co-occurrence of two events and is independent of the occurrence rate of both event 1 and event 2.

To determine validity across different statistical approaches, we compared CCG quantification with another methodology demonstrated to reliably assess correlation (affinity metric) as described in (69). Both CCG quantification and the affinity metric account for oscillation occurrence rates, and gave concordant results. Joint occurrence rates of oscillations do not account for oscillation occurrence rates, but also demonstrated similar directional modulation in a subset of data tested. CCG quantification was selected as an appropriate statistical representation of oscillatory coupling and used for all analyses.

CCG dynamics across sleep epochs

To examine the dynamics of SPW-R / CXR coupling over sleep, we looked at events occurring within every 10-minute, non-overlapping NREM window across the entire recording session with NREM duration longer than 80 min. We calculated the co-occurrence by counting the number of SPW-R and CXR events that coincided temporally within 100 ms of their peak times. We divided the count by the nominal occurrence rate of SPW-R.

Statistics

We conducted statistical analyses across the different memory sleep stages following training or test sessions, for both CB and OA tasks. To test the null hypothesis that there is no significant difference in the coupling strength between memory stages, we used paired t-test. Kolmogorov-Smirnov (KS) testing was used to compared distributions. Significance was taken as $P < 0.05$. Unsupervised k-means algorithm was used to cluster patterns of oscillatory coupling modulation.

References

1. J. L. McGaugh, Memory - A century of consolidation. *Science* **287**, 248–251 (2000).
2. Nader K, Schafe GE, le Doux JE, The labile nature of consolidation theory. *Nature* **406** (2000).
3. C. M. Alberini, Mechanisms of memory stabilization: Are consolidation and reconsolidation similar or distinct processes? *Trends Neurosci* **28** (2005).
4. J. L. C. Lee, B. J. Everitt, K. L. Thomas, Independent Cellular Processes for Hippocampal Memory Consolidation and Reconsolidation. *Science* **304** (2004).
5. J. L. C. Lee, Reconsolidation: maintaining memory relevance. *Trends Neurosci* **32** (2009).
6. H. Eichenbaum, A cortical–hippocampal system for declarative memory. *Nat Rev Neurosci* **1** (2000).
7. M. G. Zhao, *et al.*, Roles of NMDA NR2B subtype receptor in prefrontal long-term potentiation and contextual fear memory. *Neuron* **47** (2005).
8. T. Kitamura, S. K. Ogawa, D. S. Roy, T. Okuyama, Engrams and circuits crucial for systems consolidation of a memory. *Science* **356**, 73–78 (2017).
9. T. Okuyama, T. Kitamura, D. S. Roy, S. Itohara, S. Tonegawa, Ventral CA1 neurons store social memory. *Science* **353** (2016).
10. J. J. Quinn, Q. D. Ma, M. R. Tinsley, C. Koch, M. S. Fanselow, Inverse temporal contributions of the dorsal hippocampus and medial prefrontal cortex to the expression of long-term fear memories. *Learning and Memory* **15** (2008).
11. J. Lopez, *et al.*, Context-dependent modulation of hippocampal and cortical recruitment during remote spatial memory retrieval. *Hippocampus* **22** (2012).
12. T. Maviel, T. P. Durkin, F. Menzaghi, B. Bontempi, Sites of neocortical reorganization critical for remote spatial memory. *Science* **305** (2004).
13. P. W. Frankland, B. Bontempi, L. E. Talton, L. Kaczmarek, A. J. Silva, The Involvement of the Anterior Cingulate Cortex in Remote Contextual Fear Memory. *Science (1979)* **304**, 881–883 (2004).
14. A. Sawangjit, *et al.*, The hippocampus is crucial for forming non-hippocampal long-term memory during sleep. *Nature* **564** (2018).
15. L. R. Squire, Memory and the hippocampus: A synthesis from findings with rats, monkeys, and humans. *Psychol Rev* **99** (1992).
16. A. Peyrache, M. Khamassi, K. Benchenane, S. I. Wiener, F. P. Battaglia, Replay of rule-learning related neural patterns in the prefrontal cortex during sleep. *Nat Neurosci* **12** (2009).
17. D. Mao, *et al.*, Hippocampus-dependent emergence of spatial sequence coding in retrosplenial cortex. *Proc Natl Acad Sci U S A* **115** (2018).
18. M. P. Walker, R. Stickgold, Sleep-dependent learning and memory consolidation. *Neuron* **44** (2004).
19. B. P. Staresina, *et al.*, Hierarchical nesting of slow oscillations, spindles and ripples in the human hippocampus during sleep. *Nat Neurosci* **18** (2015).
20. D. R. Euston, M. Tatsuno, B. L. McNaughton, Fast-forward playback of recent memory sequences in prefrontal cortex during sleep. *Science* **318** (2007).
21. M. A. Wilson, B. L. McNaughton, Reactivation of hippocampal ensemble memories during sleep. *Science* **265** (1994).

22. G. Girardeau, K. Benchenane, S. I. Wiener, G. Buzsáki, M. B. Zugaro, Selective suppression of hippocampal ripples impairs spatial memory. *Nat Neurosci* **12** (2009).
23. S. P. Jadhav, C. Kemere, P. W. German, L. M. Frank, Awake hippocampal sharp-wave ripples support spatial memory. *Science* **336**, 1454–1458 (2012).
24. N. Maingret, G. Girardeau, R. Todorova, M. Goutierre, M. Zugaro, Hippocampo-cortical coupling mediates memory consolidation during sleep. *Nat Neurosci* **19** (2016).
25. D. Khodagholy, J. N. Gelinas, G. Buzsáki, Learning-enhanced coupling between ripple oscillations in association cortices and hippocampus. *Science (1979)* **358** (2017).
26. A. P. Vaz, S. K. Inati, N. Brunel, K. A. Zaghloul, Coupled ripple oscillations between the medial temporal lobe and neocortex retrieve human memory. *Science* **363**, 975–978 (2019).
27. C. Sestieri, M. Corbetta, G. L. Romani, G. L. Shulman, Episodic memory retrieval, parietal cortex, and the default mode network: Functional and topographic analyses. *Journal of Neuroscience* **31** (2011).
28. C. S. Keene, D. J. Bucci, Contributions of the Retrosplenial and Posterior Parietal Cortices to Cue-Specific and Contextual Fear Conditioning. *Behavioral Neuroscience* **122** (2008).
29. J. L. Rogers, R. P. Kesner, Hippocampal-parietal cortex interactions: Evidence from a disconnection study in the rat. *Behavioural Brain Research* **179** (2007).
30. S. Brodt, *et al.*, Fast track to the neocortex: A memory engram in the posterior parietal cortex. *Science* **362** (2018).
31. A. Sirota, J. Csicsvari, D. Buhl, G. Buzsáki, Communication between neocortex and hippocampus during sleep in rodents. *Proc Natl Acad Sci U S A* **100** (2003).
32. A. G. Siapas, M. A. Wilson, Coordinated interactions between hippocampal ripples and cortical spindles during slow-wave sleep. *Neuron* **21** (1998).
33. J. N. Gelinas, D. Khodagholy, T. Thesen, O. Devinsky, G. Buzsáki, Interictal epileptiform discharges induce hippocampal-cortical coupling in temporal lobe epilepsy. *Nat Med* **22** (2016).
34. D. Khodagholy, J. N. Gelinas, G. Buzsáki, Learning-enhanced coupling between ripple oscillations in association cortices and hippocampus. *Science* **358**, 369–372 (2017).
35. D. Dupret, J. O'Neill, B. Pleydell-Bouverie, J. Csicsvari, The reorganization and reactivation of hippocampal maps predict spatial memory performance. *Nat Neurosci* **13** (2010).
36. M. W. Brown, E. C. Warburton, J. P. Aggleton, Recognition memory: Material, processes, and substrates. *Hippocampus* **20** (2010).
37. H. P. Davis, L. R. Squire, Protein synthesis and memory: A review. *Psychol Bull* **96** (1984).
38. Y. Dudai, Consolidation: Fragility on the road to the engram. *Neuron* **17** (1996).
39. M. E. Judge, D. Quartermain, Characteristics of retrograde amnesia following reactivation of memory in mice. *Physiol Behav* **28** (1982).
40. K. Nader, G. E. Schafe, J. E. le Doux, Fear memories require protein synthesis in the amygdala for reconsolidation after retrieval. *Nature* **406** (2000).
41. J. R. Misanin, R. R. Miller, D. J. Lewis, Retrograde amnesia produced by electroconvulsive shock after reactivation of a consolidated memory trace. *Science* **160** (1968).
42. L. Nyberg, *et al.*, General and specific brain regions involved in encoding and retrieval of events: What, where, and when. *Proc Natl Acad Sci U S A* **93** (1996).

43. P. J. Hernandez, K. Sadeghian, A. E. Kelley, Early consolidation of instrumental learning requires protein synthesis in the nucleus accumbens. *Nat Neurosci* **5** (2002).
44. S. J. Cohen, *et al.*, The rodent hippocampus is essential for nonspatial object memory. *Current Biology* **23** (2013).
45. G. Riedel, *et al.*, Reversible neural inactivation reveals hippocampal participation in several memory processes. *Nat Neurosci* **2** (1999).
46. P. Piterkin, E. Cole, M. P. Cossette, S. Gaskin, D. G. Mumby, A limited role for the hippocampus in the modulation of novel-object preference by contextual cues. *Learning and Memory* **15** (2008).
47. S. Brodt, *et al.*, Fast track to the neocortex: A memory engram in the posterior parietal cortex. *Science (1979)* **362** (2018).
48. S. Tonegawa, M. D. Morrissey, T. Kitamura, The role of engram cells in the systems consolidation of memory. *Nat Rev Neurosci* **19** (2018).
49. I. Izquierdo, J. H. Medina, Memory formation: The sequence of biochemical events in the hippocampus and its connection to activity in other brain structures. *Neurobiol Learn Mem* **68** (1997).
50. S. Gais, M. Mölle, K. Helms, J. Born, Learning-dependent increases in sleep spindle density. *Journal of Neuroscience* **22** (2002).
51. O. Eschenko, M. Mölle, J. Born, S. J. Sara, Elevated sleep spindle density after learning or after retrieval in rats. *Journal of Neuroscience* **26** (2006).
52. G. Girardeau, A. Cei, M. Zugaro, Learning-induced plasticity regulates hippocampal sharp wave-ripple drive. *Journal of Neuroscience* **34** (2014).
53. O. Eschenko, W. Ramadan, M. Mölle, J. Born, S. J. Sara, Sustained increase in hippocampal sharp-wave ripple activity during slow-wave sleep after learning. *Learning and Memory* **15** (2008).
54. Y. Norman, *et al.*, Hippocampal sharp-wave ripples linked to visual episodic recollection in humans. *Science (1979)* **365** (2019).
55. K. P. Mainali, E. Slud, M. C. Singer, W. F. Fagan, "A better index for analysis of co-occurrence and similarity" (2022).
56. E. Stark, M. Abeles, Unbiased estimation of precise temporal correlations between spike trains. *J Neurosci Methods* **179** (2009).
57. L. A. Johnson, D. R. Euston, M. Tatsuno, B. L. McNaughton, Stored-trace reactivation in rat prefrontal cortex is correlated with down-to-up state fluctuation density. *Journal of Neuroscience* **30** (2010).
58. C. W. Dickey, *et al.*, Travelling spindles create necessary conditions for spike-timing-dependent plasticity in humans. *Nat Commun* **12** (2021).
59. G. Buzsáki, Hippocampal sharp wave-ripple: A cognitive biomarker for episodic memory and planning. *Hippocampus* **25** (2015).
60. E. Cole, A. Simundic, F. P. Mossa, D. G. Mumby, Assessing object-recognition memory in rats: Pitfalls of the existent tasks and the advantages of a new test. *Learn Behav* **47** (2019).
61. Y. Novitskaya, S. J. Sara, N. K. Logothetis, O. Eschenko, Ripple-triggered stimulation of the locus coeruleus during post-learning sleep disrupts ripple/spindle coupling and impairs memory consolidation. *Learning and Memory* **23** (2016).

62. T. Luft, G. S. Pereira, M. Cammarota, I. Izquierdo, Different time course for the memory facilitating effect of bicuculline in hippocampus, entorhinal cortex, and posterior parietal cortex of rats. *Neurobiol Learn Mem* **82** (2004).
63. P. Ardenghi, *et al.*, Late and prolonged post-training memory modulation in entorhinal and parietal cortex by drugs acting on the cAMP/protein kinase A signalling pathway. *Behavioural Pharmacology* **8** (1997).
64. J. I. Rossato, *et al.*, Retrograde amnesia induced by drugs acting on different molecular systems. *Behavioral Neuroscience* **118** (2004).
65. O. Hardt, K. Nader, L. Nadel, Decay happens: The role of active forgetting in memory. *Trends Cogn Sci* **17** (2013).
66. R. K. Pitman, *et al.*, Biological studies of post-traumatic stress disorder. *Nat Rev Neurosci* **13** (2012).
67. D. Khodagholy, *et al.*, NeuroGrid: Recording action potentials from the surface of the brain. *Nat Neurosci* **18** (2015).
68. P. Jastrzebska-Perfect, *et al.*, Mixed-conducting particulate composites for soft electronics. *Sci Adv* **6** (2020).
69. K. P. Mainali, E. Slud, M. C. Singer, W. F. Fagan, A better index for analysis of co-occurrence and similarity. *Sci Adv* **8**, 9204 (2022).

Chapter 4: Interictal epileptiform discharges shape large-scale intercortical communication

In Chapter 2, we reviewed how intercortical communication is disrupted in the neural networks of patients with focal epilepsy, and epileptic activity, characterized by seizures and IEDs can exert widespread effects within the brain. However, the mechanisms by which epileptic activity interacts with and shapes these large-scale neural networks in the human brain remain mostly unknown and have implications for associated neuropsychiatric dysfunction and progression of focal epilepsy. In this study, we analyzed intracranial EEG (iEEG) data from patients with focal epilepsy who required large-scale electrophysiological monitoring to localize seizures during clinical work-up for epilepsy surgery. This chapter highlights the key results from this study on how IEDs can drive spatiotemporally specific patterns of abnormally coordinated brain activity and provide new insights on how such mechanisms of large-scale disruption and potentially contribute to impairment of memory processes.

4.1 IEDs induce spindles in patients with focal epilepsy

To explore the influence of IEDs on large-scale cortical networks, we analyzed sleep iEEG data from patients with implanted subdural grid arrays combined with subdural strips and depth electrodes to localize seizure foci before resective surgery. We first detected and localized electrodes expressing IEDs for each patient and identified co-occurring activity patterns across all other brain regions. IEDs arose beneath electrodes reflecting the onset zone and propagated to areas within the epileptic network. In accordance with previous results (Gelinas *et al.*, 2016), some electrodes displayed an increase in spindle power (9-16 Hz) within 1 second of IED occurrence, whereas others showed no change in any power band (Fig. 1A). We hypothesized that this IED-

spindle coupling reflects a pathologic connectivity that enables epileptic activity to disrupt function beyond the network of IED and seizure propagation.

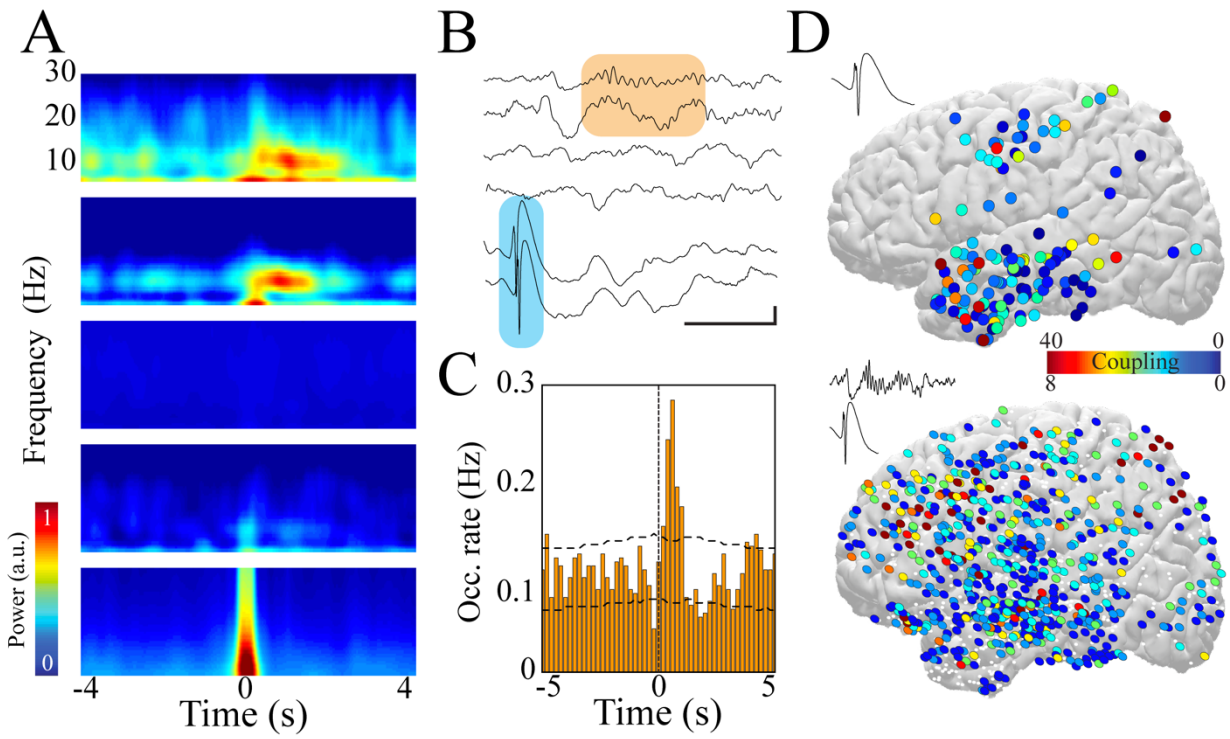

Figure 1: IEDs induce spindles in patients with focal epilepsy.
(A) IED trigger-averaged spectrograms derived from different electrodes reveal distinct patterns of activity: coupled spindle (upper 2 panels), no change (middle 2 panels), temporally locked IED (bottom panel). (B) Sample raw traces of detected IEDs (shaded blue box) and coupled cortical spindles (shaded orange box); scale bar 1 s, 200 μV. (C) Sample cross-correlogram demonstrating significant IED-spindle coupling. IED occurrence times served as reference (time = 0, vertical dashed line) and horizontal dashed lines represent 95% confidence intervals. (D) Anatomical location of electrodes expressing IEDs that couple to spindles across all patients (top) and anatomical location of electrodes expressing spindles that are coupled to IEDs across all patients (bottom) projected onto lateral cortical surface (left hemisphere view; right hemisphere locations converted to left for display purposes). Color represents number of significant IED-spindle coupling interactions per electrode location across patients. White dots show electrode locations that do not express IED-spindle coupling.

To test this hypothesis, we quantified and characterized the interaction between IEDs and spindles across the full spatial extent of recorded brain regions. Cross-correlation of detected IED and spindle events revealed a subset of electrodes with significant temporal interaction between these neural patterns (spindle (SPI)-coupled electrodes; Fig. 1B-C). Coupled spindles were initiated following IEDs at a mean latency of 0.51 ± 0.005 s. The strength of IED-spindle coupling was

defined as the occurrence of spindles exceeding the 95th percentile of cross-correlation within 1 s after IED occurrence. IEDs located in diverse brain regions demonstrated spindle coupling, and coupled spindles were similarly expressed in numerous areas (Fig. 1D). Nearly all IED electrodes could generate spindles, but the proportion of electrodes expressing spindles temporally coupled to IEDs ranged from 15-67% across patients.

4.2 IED-spindle coupling spans medium and long-range connections

We then investigated the anatomical distribution of IED-spindle coupling by localizing each IED and coupled spindle electrode to parcellated cortical areas (Desikan *et al.*, 2006). IEDs occurring in each lobe could induce spindles, with temporal lobe IEDs (within lateral temporal and limbic cortex) inducing the greatest number of coupled responses (Fig. 2A). Lateral temporal and frontal brain regions most commonly expressed spindle coupling (Fig. 2B). Because IEDs were more common in the temporal lobe compared to other areas, we also estimated IED induction and SPI response potency by normalizing based on the number of electrodes capable of expressing IEDs or spindles respectively in each brain region. This normalization revealed similar potency across lobes, with the exception of the occipital lobe, which was less likely to participate in IED-spindle coupling.

To gain insight into the anatomical substrate of IED-spindle coupling, we examined the pairs of IED-generating and SPI-coupled brain regions. A pair was identified if IEDs in a parcellated brain region resulted in a significant (> 95th percentile) cross-correlation with spindles in a brain region (Fig. 2C). Most SPI-coupled electrodes did not have detectable IEDs (90.2 ± 0.04%); only 7.6% of pairs were within the same parcellated brain region. IED-SPI pairs typically spanned more than one lobe (Fig. 2D), with the exception of frontal lobe IEDs, which tended to couple with other frontal cortical regions. Across all patients, the average distance between IED-SPI coupled

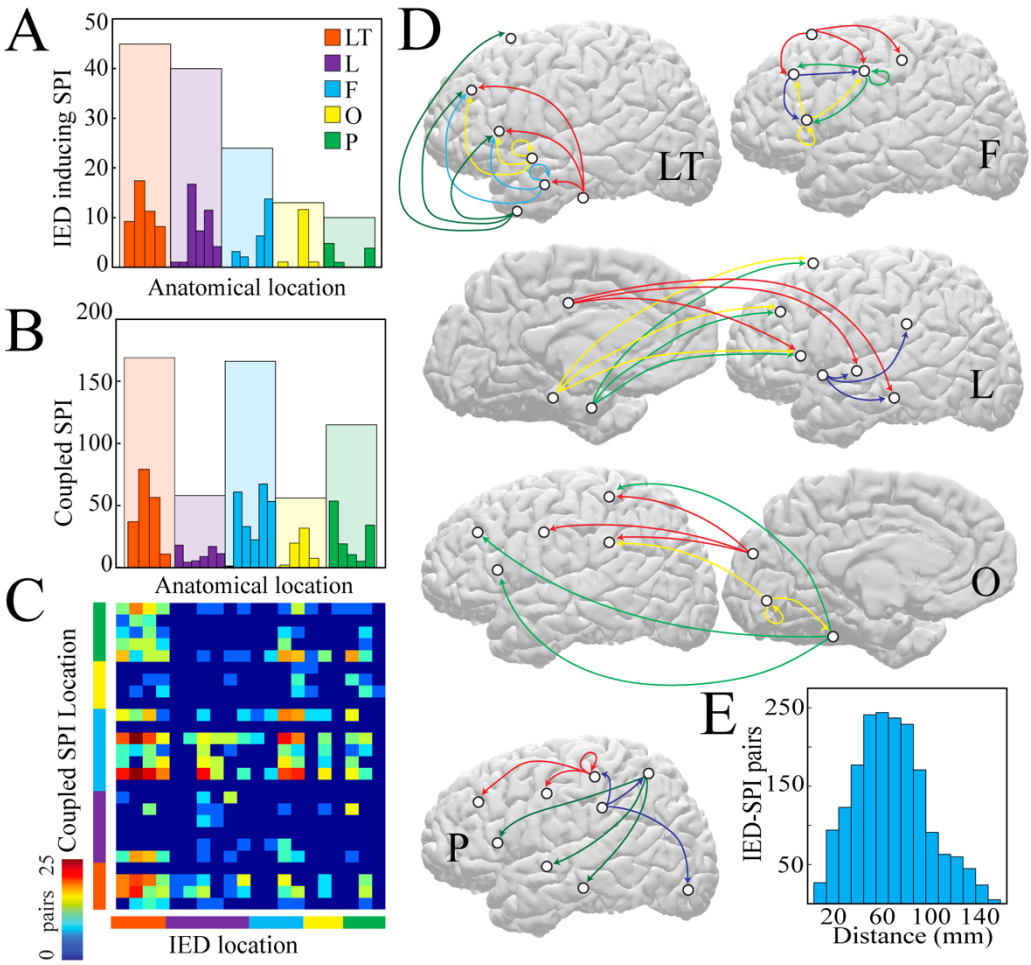

Figure 2: Medium and long-range connections are implicated in IED-spindle coupling.
(A) Number of electrodes expressing IEDs that couple to spindles across all patients divided by anatomical lobe. (B) Number of electrodes expressing spindles that are coupled to IEDs across all patients divided by lobe. (C) Number of IED-spindle pairs per brain region; lobes color-coded as in A) and B). Warmer colors indicate more pairs; ordered list of individual brain regions is in Supplementary Table 2. (D) Schematics showing the most prominent IED-spindle anatomical pairings across patients for each brain region expressing IEDs, separated by lobe and projected onto lateral and medial cortical surfaces (left hemisphere view; right hemisphere locations converted to left for display purposes). Origin of arrow indicates location of IED electrode; destination indicates location of coupled SPI electrode. White circles show location of each brain region and colors separate pairings of individual IED electrode locations. (E) Histogram of average distance between pairs of electrodes that interact via IED-spindle coupling.

electrodes was 6.2 ± 0.7 cm (Fig. 2E), suggesting that this pathologic coordinated brain activity often spans medium to long distances, rather than remaining a local network phenomenon. Anatomically and temporally separate populations of IEDs could produce distinct IED-spindle

coupling patterns within an individual patient (Supplementary Fig. 2), establishing the regional specificity of these interactions.

4.3 IED-spindle coupling patterns are outside the ictal network

We next examined the relationship between IEDs, IED-coupled spindles, and seizure activity. Electrodes were classified into 5 zones: seizure onset (earliest change from iEEG baseline), initial propagation (recruitment to ictal discharge within ≤ 1 s), middle propagation (recruitment within ≤ 5 s), late propagation zone (recruitment within ≤ 30 s) (de Curtis and Avoli, 2015), and unrecruited zone. The degree of colocalization between IEDs and seizure onset zone was highly variable across patients, but brain regions expressing IED-coupled spindles were consistently unlikely to participate in the initial stages of ictal activity (Fig. 3A-C). These areas were also relatively resistant to recruitment into seizure propagation (Fig. 3D), and were located an average of 6.1 ± 1.8 cm from the seizure onset center (Fig. 3E). Thus, the network interactions established through IED-spindle coupling are distinct from the ictal network.

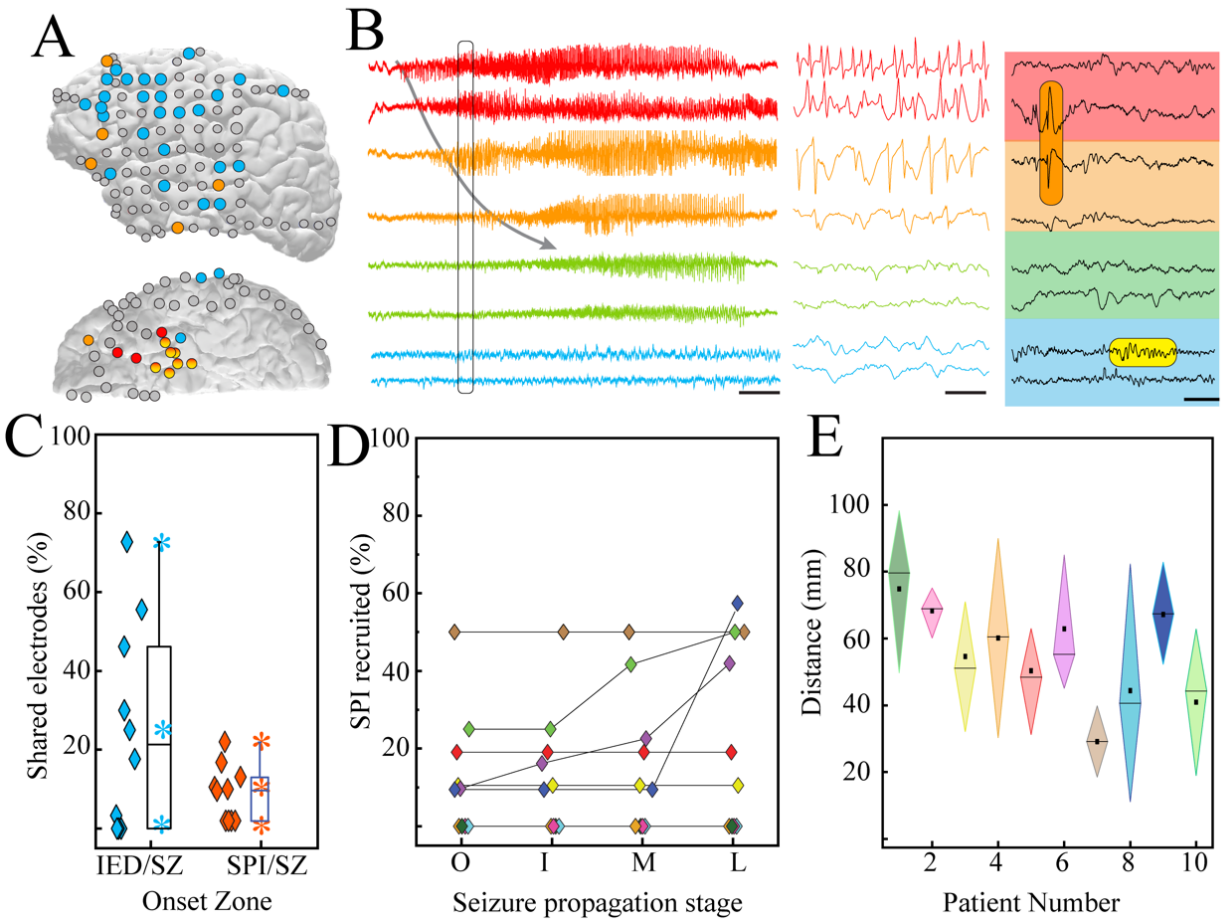

Figure 3: Brain regions that demonstrate spindles coupled to IEDs are located outside of the ictal network. (**A**) Sample patient brain (lateral and inferior views) displaying localization of seizure onset zone (red), IED foci (orange), and regions with spindles coupled to IEDs (blue). (**B**) Raw compressed (left, scale bar 5 s) and expanded (middle, from section of left panel defined by black box, scale bar 125 ms) traces revealing the onset and propagation of ictal activity from electrodes in the seizure onset zone (red), middle propagation zone (orange), and late propagation zone (green). Traces from the IED-spindle coupling zone (blue) are not recruited into the ictal rhythm. Right panel shows interictal activity from these same electrodes, highlighting an IED (orange shaded box) and coupled spindle (yellow shaded box; scale bar 200 ms) during NREM sleep. (**C**) Percentage of overlap between electrodes across patients constituting the seizure onset zone and those expressing IEDs (blue) as well as those expressing IED-coupled spindles (orange). Box shows 25th, median, and 75th percentiles; stars show range and mean. Diamonds are individual data points for each patient. (**D**) Percentage of total electrodes expressing IED-coupled spindles that are recruited into successive stages of ictal activity (colors represent individual patients; O = onset; I = initial propagation; M = middle propagation; L = late propagation). (**E**) Measures of centrality and dispersion for distance between electrodes expressing IED-coupled spindles and centroid of seizure onset zone (diamond shows 25th, median, and 75th percentiles; square is mean).

4.4 IED-spindle coupling is associated with broader spindle spatial extent across the cortical surface

We investigated whether the IED-coupled spindles exhibited different oscillation characteristics than spontaneous spindles. The trigger-averaged spectrograms of coupled and uncoupled spindles were indistinguishable. Coupled spindles were marginally longer, higher amplitude, and lower frequency, though differences were not significant across all patients (Supplementary Fig. 3). Therefore, the temporal and morphological characteristics do not permit separation of IED-coupled and spontaneous spindles.

Spindles are commonly regional events, with restricted spatial distribution across cortex (Dehghani *et al.*, 2010; Andrillon *et al.*, 2011; Halassa *et al.*, 2011; Nir *et al.*, 2011). The broad and contiguous intracranial electrode coverage of brain regions allowed us to investigate spatial properties of IED-coupled spindles. Spindle waveform spatial extent was non-uniformly distributed across cortex (Fig. 4A-B). To quantify spatial extent, we used two complementary approaches: spindle cross-correlation and spindle band coherence (Supplementary Fig. 4). In each case, values were calculated for each pair of electrodes, and the amount of significant correlation or coherence resulting from each comparison was summated to provide an overall indication of spatial extent for each electrode. These approaches gave consistent locations of maximal extent for each patient (Supplementary Fig. 4). This location varied considerably between patients, (Fig. 4C) supporting a patient-specific factor driving spindle spatial extent variability. Most patients had significant correlation between the spatial extent of spindles in a region and the degree to which this region expressed spindles coupled to IEDs (Fig. 4D-E). Together, these results suggest that IEDs may regionally modify cortical networks to enable broad expression of local oscillations.

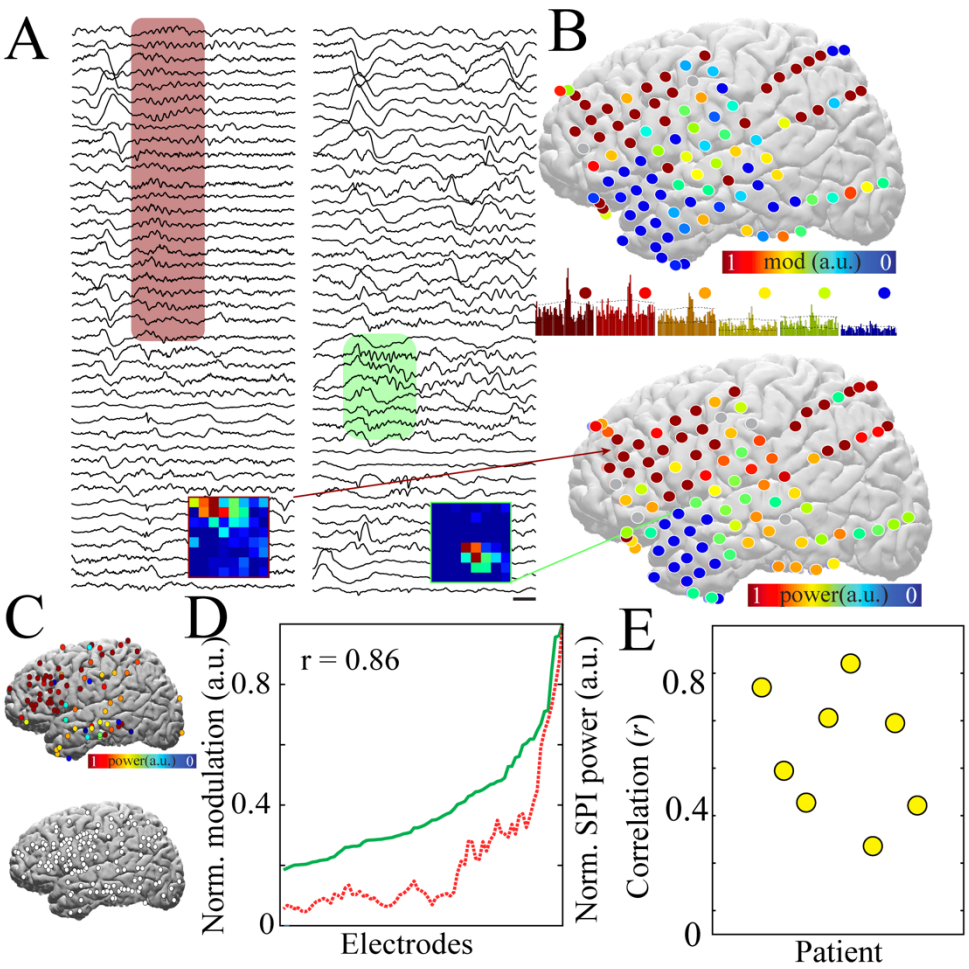

Figure 4: IED-spindle coupling is associated with broader spindle spatial extent across the cortical surface. (**A**) Sample raw traces from 41 electrodes in a sample patient demonstrating a spatially extensive spindle (red shaded box, left) and spatially restricted spindle (green shaded box, right). Scale bar 250 ms. Insets show the amount of spindle-spindle cross-correlation across the subdural grid using a reference electrode from the spatially extensive and restricted regions respectively; warmer colors indicate higher zero-bin significant cross-correlation. (**B**) Comparison of electrode locations demonstrating spindles highly coupled with IEDs (top, warmer colors) and electrode locations with broad spindle spatial extent (bottom, warmer colors) from a sample patient. IED-spindle cross-correlograms with a range of significant correlations corresponding to electrode colors (middle; 10 s duration). (**C**) Normalized spindle spatial extent for all spindle electrodes (top) and spatially extensive spindle electrodes only (top 50th percentile, bottom) summated across patients and plotted on lateral cortical surface, revealing no anatomical preference for spindle spatial extent and existence of spatially extensive spindles in all lobes. (**D**) Significance of IED-spindle coupling (red) and spindle spatial extent (green) are highly correlated across electrodes for patient visualized in A-B). (**E**) Correlation between IED-spindle coupling and spindle spatial extent for all patients with greater than 20 significant IED-spindle pairs, n = 8).

4.5 Spindles travel across the cortical surface

Increased oscillatory spatial extent can be produced by a larger area expressing synchronous oscillations or by an enhanced capacity for oscillation propagation. We used phase gradient directionality (PGD), which measures the alignment of phase gradients between neural oscillations (Rubino *et al.*, 2006; Zhang *et al.*, 2018), to investigate these mechanistic possibilities. We empirically defined the spatial geometry over which to probe the PGD as the largest symmetrical electrode grid that consistently displayed simultaneous increases in spindle band power (cluster of 3 × 3 electrodes; Supplementary Fig. 4-5). By calculating the PGD for each overlapping electrode cluster contained within the 8 × 8 iEEG subdural grid implanted in each patient, we determined whether spindles were significantly propagating in a given region by comparing to a distribution of shuffled phases. 59.3 ± 1.4% of spindles had significant PGD values, indicating that they traveled across cortex (Fig. 5A-B, Supplementary Fig. 5). Traveling spindles variably had preferred direction(s) of travel (16% no preferred direction; 27% one preferred direction; 57% two preferred directions; 0% > 2 preferred directions; Fig. 5C,E). We derived a measure to jointly reflect proportion of spindles with significant traveling and strength of directional travel (modulation index; Fig. 5C-D). The modulation index was calculated for each electrode cluster, and it displayed spatial variation across each patient's subdural grid (Fig. 5D), indicating that spindles exhibited maximal directional propagation in specific regions that overlapped with the zone expressing spindles coupled to the patient's IEDs (Fig. 5F).

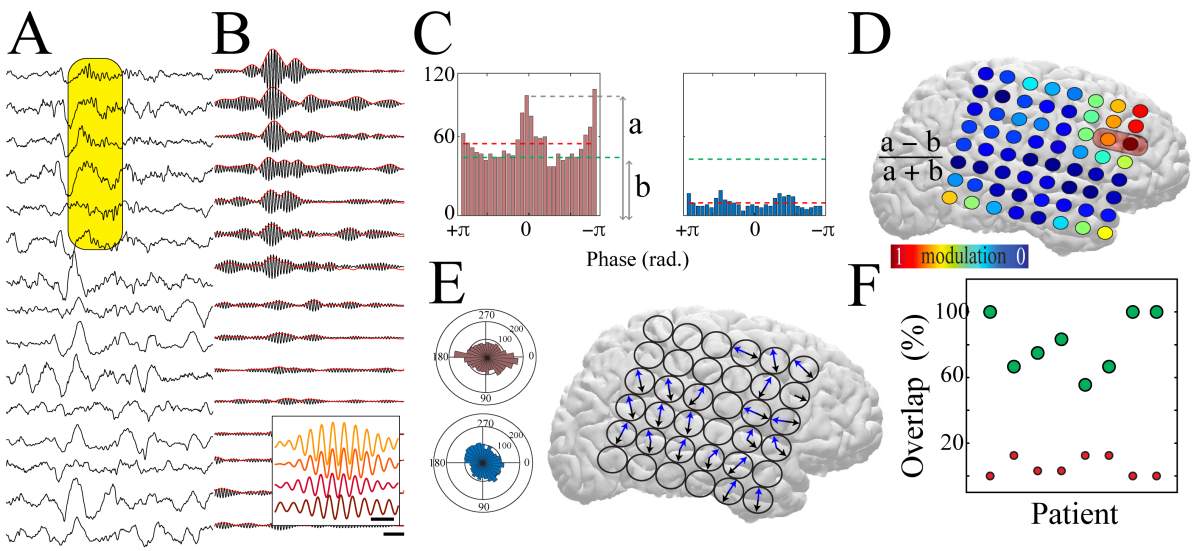

Figure 5: Localized spindles travel across the cortical surface in regions with IED-spindle coupling: (**A**) Sample raw traces from 15 electrodes of a subdural grid revealing a spatially localized propagating spindle (shaded yellow box; scale bar 250 ms). (**B**) Traces from A) filtered at spindle band (10 to 15 Hz) with rectified envelope in red. Inset shows expanded filtered traces from four electrodes within shaded yellow box, revealing consistent phase shifts (scale bar, 150 ms). (**C**) Modulation index extracted from the distribution of significant propagation angles from sample highly modulated electrode cluster (left) and minimally modulated electrode cluster (right). Dashed green line indicates the mean of the significant propagation angles across all the electrode clusters within the subdural grid (global mean) and dashed red line indicates the mean of the significant propagation angles in the individual electrode cluster (local mean). 'a' and 'b' represent the measures used to calculate modulation index (see Methods). (**D**) Modulation index across a sample subdural grid; warm colors represent high modulation index. Red shaded box shows region displaying maximal IED-spindle coupling. (**E**) Polar plots demonstrating the propagation directions for the electrode clusters shown in C) (left). Directions of preferred spindle traveling for all electrode clusters across a sample subdural grid are shown (right); note that the majority of clusters have 2 preferred directions of travel (blue and black arrows). (**F**) The majority of electrodes expressing spindles coupled to IEDs fall within the zone of maximal traveling modulation index (green circles). Red circles show the percentage of high modulation index electrodes outside of the IED-spindle coupling zone.

4.6 Spindle spatial extent and traveling predict brain regions influenced by IEDs

Electrodes with the largest spatial extent of spindles and highest propensity for spindle propagation were significantly colocalized (Fig. 6A, Supplementary Fig. 6), suggesting that enhanced traveling could account for the broad spatial coverage. Given the overlap of these properties with expression of IED-induced spindles, we hypothesized that maximal spindle spatial extent and traveling could predict brain regions influenced by IEDs. Using a predictor based on the intersection between spatial extent and propensity to travel, we found that $81.7 \pm 0.08\%$ electrodes with significant IED-spindle coupling could be accurately predicted (Fig. 6B-C). Thus, IED-induced spindles are associated with regionally enhanced spatial extent and traveling.

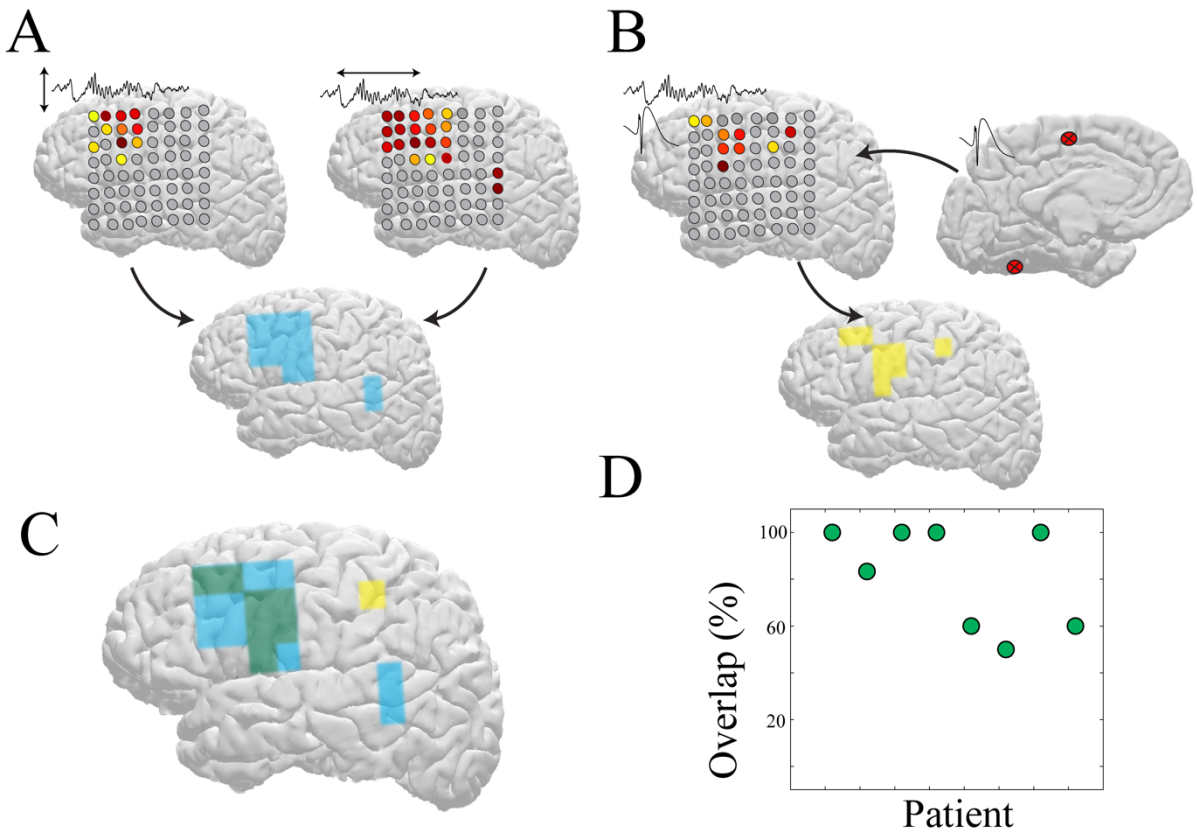

Figure 6: Maximal spindle spatial extent and traveling predict brain regions influenced by IEDs. (**A**) Region of maximal spindle spatial extent (left) and maximal spindle traveling modulation index (right) obtained by watershed analysis of a sample patient's subdural grid. The regions representing the union between these measures are identified in blue (bottom). (**B**) Regions of significant spindle coupling (left) to IEDs generated at regions marked on the right for the same patient as in A). Regions of IED-spindle coupling are identified in yellow (bottom). (**C**) Overlap between regions of maximally extensive propagating spindles and regions expressing spindles coupled to IEDs (green). (**D**) Percentage of overlap between regions of maximally extensive propagating spindles and regions expressing spindles coupled to IEDs across all patients with greater than 20 significant IED-spindle pairs (n = 8).

4.7 Discussion

We demonstrate that IEDs functionally interact with diverse and remote cortical regions in the human brain via induction of coupled spindles. Anatomical patterns of IED-spindle coupling are patient specific, but consistently localized outside of the seizure onset zone. Further, spindles in

brain regions targeted by IEDs have larger spatial extent and higher tendency to propagate compared to spindles in regions unaffected by IEDs. These altered spindle properties predict brain regions distinct from the epileptic network that express neural activity patterns coordinated with IEDs, reflecting interictal network dysfunction that could possibly contribute to cognitive comorbidities and disease progression.

We found IED-induced spindles in each patient of our cohort, suggesting that it represents a conserved reaction to epileptiform activity in cortical networks. Spindles can be induced by synchronous synaptic input to cortical circuits, as occurs in response to physiologic oscillations (for instance, hippocampal sharp wave ripples) (Siapas and Wilson, 1998; Wierzynski *et al.*, 2009), as well as exogenous electrical or magnetic stimulation (Massimini *et al.*, 2007; Vyazovskiy *et al.*, 2009). The hypersynchronous neural firing associated with an IED likely generates a similar effect in cortical tissue (Bragin *et al.*, 1999), resulting in a coupled spindle oscillation. We demonstrated that spindles occur within a well-defined time interval after IEDs in humans, and that IEDs can drive cortical neural spiking at monosynaptic latencies in animals (Gelinas *et al.*, 2016). These characteristics suggest that pathologic neural firing conveyed through synaptic interactions initiate IED-spindle coupling. However, IED-related neural firing could be conveyed to cortex via cortico-cortical or thalamocortical synapses (Alarcon *et al.*, 1997; Bourien *et al.*, 2005), and subsequent expression of spindles should recruit thalamocortical circuits (Steriade *et al.*, 1993). The similarity in the duration, frequency, and amplitude between coupled and uncoupled spindles supports the same basic neural substrate in their generation.

Insight into the pathways that support IED-spindle coupling can be gained by examining the anatomical relationship between pairs of regions that demonstrate these interactions. We were optimally positioned to assess these relationships due to the broad cortical electrode coverage in

each patient, reducing bias associated with restricted sampling of neural signals. Pairs were located on average more than 6 cm apart (substantially larger than the width of a gyrus (Thompson *et al.*, 1996)) and typically consisted of two distinct brain regions based on cortical parcellation. Thus, IED-spindle coupling in the human brain involves predominantly medium to long-range, rather than local, connections.

IED-spindle interactions were consistent with white matter connectivity patterns (Hagmann *et al.*, 2008; Jung *et al.*, 2017). There were prominent interactions between limbic/temporopolar cortex and ventrolateral frontal cortex (Sedat and Duvernoy, 1990), as well as between lateral temporal, dorsolateral prefrontal, and parietal cortices (Schmahmann *et al.*, 2007), in keeping with tractography defined networks (Dosenbach *et al.*, 2007). However, the anatomical distribution of IED-spindle coupling was also highly individualized. Similar variability occurs in the propagation of seizures and IEDs across patients with anatomically comparable epileptogenic lesions (Alarcon *et al.*, 1997; Proix *et al.*, 2017), and even in resting state functional connectivity across normal subjects (Mueller *et al.*, 2013).

Another factor that predicted IED-spindle coupling was the location of the epileptic network. Spindles coupled to IEDs were consistently observed in brain regions that did not generate IEDs and seizures. These regions were also unlikely to be recruited into early stages of seizure propagation. Therefore, expression of spindles temporally locked to IEDs likely reflects a directional interaction from the epileptic to the non-epileptic zone. The brain regions outside of the active ictal area during a seizure (Englot *et al.*, 2008; Schevon *et al.*, 2012) or immediately surrounding an IED focus (Serafini and Loeb, 2015) display neural firing and oscillations suggestive of increased inhibition. IED-spindle coupling in rats is associated with a strong inhibition of neural firing for hundreds of milliseconds prior to the start of the spindle oscillation

(Gelinas *et al.*, 2016). Regions of IED-spindle coupling "surround" the epileptic network, suggesting that these areas receive synaptic activity generated by IEDs, but can mount an inhibitory response that prevents IED propagation.

Cross-correlation and coherence analysis of spindles in our patients supports the strong local expression patterns of these oscillations (Caderas *et al.*, 1982; Nishida and Walker, 2007; Dehghani *et al.*, 2010; Andrillon *et al.*, 2011; Halassa *et al.*, 2011), though some spindles have a more global distribution (Muller *et al.*, 2016). We also found evidence that regionally restricted spindles can travel across the cortical surface, consistent with traveling waves in other frequencies in the awake human brain (Takahashi *et al.*, 2011; Zhang *et al.*, 2018). We found that spindles in brain regions expressing IED-spindle coupling have a larger spatial extent and higher propensity to travel compared to those in brain regions without IED-coordinated activity. Increased frequency-specific coherence between functionally related brain regions and traveling waves correlate with successful task-based information processing (Hipp *et al.*, 2011; Samaha and Postle, 2015; Rohenkohl *et al.*, 2018; Zhang *et al.*, 2018). In contrast, lack of functionally segregated network activity is associated with immature neural networks and impaired neurocognitive performance (Dosenbach *et al.*, 2010; Ibrahim *et al.*, 2014). IED-induced increases to coherence and traveling of spindles could disrupt the spatiotemporal specificity of these oscillations and impair functional neural computation.

Focal epilepsy is associated with brain dysfunction that extends beyond the epileptic network (Bettus *et al.*, 2011; Englot *et al.*, 2016; Lagarde *et al.*, 2018; Tong *et al.*, 2019). This dysfunction may contribute to cognitive impairments in these patients (Hermann *et al.*, 2006) and prime the brain for further spread of the epileptic network (Sato *et al.*, 1998; Velisek and Moshe, 2003), but lack of mechanistic understanding limits approaches to treatment. Our results identify IED-spindle

coupling as a consistent but individualized pattern of dynamically coordinated interactions between the epileptic network and surrounding brain regions. Brain regions that exhibit this coupling also display altered capacity for oscillatory expression and propagation that persists beyond the epochs of coupling, allowing them to be identified even the absence of IEDs. IED-spindle coupling may therefore play a role in establishing the altered global connectivity observed in patients with focal epilepsy. Detection and manipulation of these patterns of coordinated brain activity (Maingret *et al.*, 2016) will permit causal testing of this hypothesis and may present new opportunities for therapies to address distributed network dysfunction in epilepsy

4.8 Methods

Subjects

We analyzed intracranial electroencephalography (iEEG) recordings from 10 patients with focal epilepsy who underwent clinical electrode placement as part of the work-up for epilepsy surgery. Gathering and analysis of this data was approved by the Institutional Review Board at New York University Langone Medical Center (NYULMC), and all data collection occurred at this institution. Informed written consent was obtained from all patients according to the Declaration of Helsinki. Each patient had a configuration of electrodes implanted based on clinical need, including subdural grids and strips, as well as depth electrodes. Patients with focal epilepsy with continuous high quality iEEG recordings that included at least one 8 x 8 subdural grid (1 cm electrode spacing, center to center) in the absence of major cortical lesions were eligible for analysis. The majority of patients had normal neuroimaging; when lesions were identified they were pathologically identified as focal cortical dysplasia or low-grade tumor. All patients had a

similar number of electrodes available for analysis. Recordings included waking and sleep epochs; no task-related data was analyzed.

Clinical reports

We obtained the clinical iEEG reports for each patient's hospital admission. Each report detailed the date, time, semiology, onset and propagation of seizures, as well as clinical localization of IEDs. Data was clinically interpreted using a combination of referential montage (referenced to epidural electrodes) and bipolar montage (based on pairs of neighboring electrodes). Epochs of iEEG data corresponding to these seizures were identified for further analysis.

iEEG data pre-processing and detections

Epochs of sleep were identified by immobility (lack of change in a motion vector extracted from synchronized video files) in concert with increased delta/gamma frequency ratio in the iEEG spectrogram. Referential data was imported into Matlab and resampled from 512 to 1250 Hz for compatibility with previously validated analytical toolboxes. IED detection was performed on all electrodes, using a combination of frequency, amplitude, and duration parameters: (i) band-pass filtering at 25–80 Hz and signal rectification; (ii) detection of events where the filtered envelope was > 3 times above baseline; (iii) elimination of events where the unfiltered envelope was < 3 times above baseline; (iv) elimination of IEDs occurring within 500 ms of another IED to prevent over-correlation due to a run of IEDs (Gelinas *et al.*, 2016). Detected IEDs had waveforms consistent with typical interictal spikes and/or sharp waves, and were variably associated with an aftergoing slow wave (Supplementary Fig. 1). Spindle detection was performed based on wavelet derived power and duration parameters. A ratio of normalized autoregressive wavelet-based P_{AR} as first calculated based on the following equation:

$$P_{AR} = (P_{spi} - (P_{low} + P_{high}))/(P_{spi} + (P_{low} + P_{high}))$$

where spindle band power (P_{spi}) was based on 10-20 Hz, low band power was based on 2-8 Hz (P_{low}), and high band power was based on 25-40 Hz (P_{high}). Spindle events were identified when the ratio crossed zero and was greater than 0.1 for a minimum of 300 ms and a maximum of 3 s. We detected both fast (13-15 Hz) and slow (9-12 Hz) spindles using this approach. All detections were visually inspected for accuracy for each recording session.

iEEG electrode localization

Localization of intracranial electrodes was performed based on reconstruction of subject specific pial surfaces, co-registration of pre- and post-implant MRI images, a combination of manual and automatic localization of electrodes, and subsequent co-registration to a standard template brain (Yang *et al.*, 2012). MNI coordinates and the gyral location of electrodes (determined based on cortical parcellation using the Desikan-Killiany atlas (Desikan *et al.*, 2006)) were used for across subject localization comparisons. For visualization of group data, electrode MNI coordinates from patients with right hemisphere electrodes were converted to corresponding left hemisphere coordinates.

iEEG spatiotemporal analysis

We used a combination of freely available, online Matlab toolboxes (Freely Moving Animal Toolbox; http://fmatoolbox.sourceforge.net; Chronux; http://chronux.org) and custom Matlab code. Cross-correlograms, calculated using a modified convolution method (Stark and Abeles, 2009), enabled temporal correlation between detected events. Spindles were designated as coupled to an IED if they occurred within 1 second after the IED. Power was extracted using wavelet transformation (Gabor). Spatial extent of oscillations was determined by two methods, which provided complementary results: i) cross-correlation of detected events and identification of

electrodes with significant zero time lag values; ii) determination of wavelet-based coherence at the time of detected events.

iEEG phase analysis

i) Initial processing. To extract spindle phase, we first applied a third order 10-15 Hz bandpass Butterworth filter to the local field potential recordings from all the electrodes within the 8 × 8 subdural grid at the time of each detected spindle (spindle trial). Filtered data was downsampled to 125 Hz and Hilbert transform was performed to extract the instantaneous phase of the spindles. We compared this method to cycle-by-cycle time domain analysis (Cole and Voytek, 2018). The peaks, troughs, and flank midpoints in individual spindle cycles were identified and a phase time series was estimated by interpolating between the theoretical phases at these points. We obtained similar results in the instantaneous phases and their gradients extracted using these two methods (Supplementary Fig. 4D-E). We did not incorporate electrodes of subdural strips or depths in this analysis, due to their inconsistent geometry relative to adjacent electrodes.

ii) Calculation of phase gradient directionality (PGD). We computed the PGD to quantitatively assess whether spindles behaved as traveling waves across the cortex. PGD is a measure of the alignment of phase gradients of oscillations over space (Rubino *et al.*, 2006). If the PGD exceeds a threshold value, the oscillations in that space exhibit wave-like traveling for which the direction can be estimated. We sought to determine PGD values across a spatial extent that consistently demonstrated amplitude coherent spindles to minimize spurious phase values that could be elicited by filtering. Across patients, this spatial extent was found to be a cluster of 3×3 electrodes (Supplementary Fig. 4). We verified expected variations in PGD based on cluster size, with smaller clusters exhibiting higher PGD values (consistent with phase gradients that are highly aligned over a short distance), and larger clusters exhibiting lower PGD values (consistent with the primarily

spatially localized nature of the oscillations; Supplementary Fig. 5). Therefore, we characterized systematic variations in the spindle phase across a region of nine electrodes organized in a 3×3 cluster. By sliding this window over the entire 8 × 8 electrode space, we obtained a total of 36 oscillation clusters for each patient grid. For each cluster and its corresponding number of spindle trials, the instantaneous phase at the start time point of the spindle was extracted. Having obtained a spatial array of instantaneous phase values, we computed the PGD as:

$$PGD = \|\overline{\nabla\varphi}\| / \overline{\|\nabla\varphi\|}$$

If a cluster contained noisy or missing electrodes, the instantaneous phase for those electrodes were interpolated using neighboring phase values. We identified the spindle trials that demonstrated significant PGD values (PGD > threshold) and estimated the propagation directions across those trials by calculating the angle between the average horizontal and vertical phase gradients of that cluster.

iii) Determination of threshold for PGD significance. For each patient's subdural grid, we computed a single threshold to determine the significant PGD values in all oscillation clusters. We identified five test clusters located on the corners and center regions of the grid. For each cluster and spindle trial, we shuffled the phase values across the 3 × 3 region for 500 iterations per spindle trial and computed the median PGD for each iteration. The 95th percentile of this shuffled phase distribution signified the PGD threshold for that cluster. We averaged the threshold values across the five test clusters to obtain the final PGD threshold for each patient's grid electrodes. PGD values that exceeded this threshold in each 3×3 cluster were classified as significant.

iv) Consistency of directional travel. For significant PGD values, we calculated the consistency of directional travel (i.e. the degree to which spindles traveled in preferred direction(s)). Because the preferred traveling direction of a population of spindle events is not necessarily unimodal, we

convolved the histogram of the spindle direction angles with a finite gaussian window and estimated the 95th percent confidence intervals using a Poisson distribution (Stark and Abeles, 2009). The maximum of the angle bins that surpassed the upper bound of the confidence interval represented preferred direction(s) of spindle traveling in each cluster. To determine clusters that expressed both a high proportion of traveling spindles and highly preferred direction(s) of travel, we calculated a modulation index (MI) based on the histogram of spindle propagation angles as follows:

$$MI = hist_{max} - hist_{mean} / hist_{max} + hist_{mean}$$

For each patient, we determined the histogram mean per cluster (local mean), and the mean of all cluster histograms combined (global mean). When the local and global means differed by more than an order of magnitude, the global mean was used to calculate the modulation index; otherwise the local mean was used. This approach enabled identification of the region with the highest number traveling spindles with consistent direction of travel regardless of the variability in this property across the grid.

Statistical analysis

Differences between groups were calculated using non-parametric ranksum (Wilcoxon) or ANOVA (Kruskal-Wallis with Bonferroni correction) depending on the nature of the data analyzed. Probability distributions were compared using two-sample Kolmogorov-Smirnov tests. Correlations were calculated using a correlation coefficient matrix based on the covariance of input variables. Error bars represent s.e.m. Significance level was $P < 0.05$.

References

1. Alarcon G, Garcia Seoane JJ, Binnie CD, Martin Miguel MC, Juler J, Polkey CE, et al. Origin and propagation of interictal discharges in the acute electrocorticogram. Implications for pathophysiology and surgical treatment of temporal lobe epilepsy. Brain 1997; 120 (Pt 12): 2259-2282.
2. Andrillon T, Nir Y, Staba RJ, Ferrarelli F, Cirelli C, Tononi G, et al. Sleep spindles in humans: insights from intracranial EEG and unit recordings. J Neurosci 2011; 31: 17821-17834.
3. Bartolomei F, Lagarde S, Wendling F, McGonigal A, Jirsa V, Guye M, et al. Defining epileptogenic networks: Contribution of SEEG and signal analysis. Epilepsia 2017; 58: 1131-1147.
4. Benchenane K, Peyrache A, Khamassi M, Tierney PL, Gioanni Y, Battaglia FP, et al. Coherent theta oscillations and reorganization of spike timing in the hippocampal-prefrontal network upon learning. Neuron 2010; 66: 921-936.
5. Bettus G, Ranjeva JP, Wendling F, Benar CG, Confort-Gouny S, Regis J, et al. Interictal functional connectivity of human epileptic networks assessed by intracerebral EEG and BOLD signal fluctuations. PLoS One 2011; 6: e20071.
6. Bourien J, Bartolomei F, Bellanger JJ, Gavaret M, Chauvel P and Wendling F. A method to identify reproducible subsets of co-activated structures during interictal spikes. Application to intracerebral EEG in temporal lobe epilepsy. Clin Neurophysiol 2005; 116: 443-455.
7. Bragin A, Engel J, Jr., Wilson CL, Fried I and Mathern GW. Hippocampal and entorhinal cortex high-frequency oscillations (100--500 Hz) in human epileptic brain and in kainic acid--treated rats with chronic seizures. Epilepsia 1999; 40: 127-137.
8. Buzsaki G and Schomburg EW. What does gamma coherence tell us about inter-regional neural communication? Nat Neurosci 2015; 18: 484-489.
9. Caderas M, Niedermeyer E, Uematsu S, Long DM and Nastalski J. Sleep spindles recorded from deep cerebral structures in man. Clin Electroencephalogr 1982; 13: 216-225.
10. Cole S and Voytek B. Cycle-by-cycle analysis of neural oscillations. bioRxiv 2018; 302000.
11. de Curtis M and Avoli M. Initiation, Propagation, and Termination of Partial (Focal) Seizures. Cold Spring Harb Perspect Med 2015; 5: a022368.
12. Dehghani N, Cash SS, Chen CC, Hagler DJ, Jr., Huang M, Dale AM, et al. Divergent cortical generators of MEG and EEG during human sleep spindles suggested by distributed source modeling. PLoS One 2010; 5: e11454.
13. Desikan RS, Segonne F, Fischl B, Quinn BT, Dickerson BC, Blacker D, et al. An automated labeling system for subdividing the human cerebral cortex on MRI scans into gyral based regions of interest. Neuroimage 2006; 31: 968-980.
14. Diekelmann S and Born J. The memory function of sleep. Nat Rev Neurosci 2010; 11: 114-126.
15. Dosenbach NU, Fair DA, Miezin FM, Cohen AL, Wenger KK, Dosenbach RA, et al. Distinct brain networks for adaptive and stable task control in humans. Proc Natl Acad Sci U S A 2007; 104: 11073-11078.
16. Dosenbach NU, Nardos B, Cohen AL, Fair DA, Power JD, Church JA, et al. Prediction of individual brain maturity using fMRI. Science 2010; 329: 1358-1361.

17. Englot DJ, Konrad PE and Morgan VL. Regional and global connectivity disturbances in focal epilepsy, related neurocognitive sequelae, and potential mechanistic underpinnings. Epilepsia 2016; 57: 1546-1557.
18. Englot DJ, Mishra AM, Mansuripur PK, Herman P, Hyder F and Blumenfeld H. Remote effects of focal hippocampal seizures on the rat neocortex. J Neurosci 2008; 28: 9066-9081.
19. Frauscher B, von Ellenrieder N, Ferrari-Marinho T, Avoli M, Dubeau F and Gotman J. Facilitation of epileptic activity during sleep is mediated by high amplitude slow waves. Brain 2015; 138: 1629-1641.
20. Fries P. A mechanism for cognitive dynamics: neuronal communication through neuronal coherence. Trends Cogn Sci 2005; 9: 474-480.
21. Gais S, Molle M, Helms K and Born J. Learning-dependent increases in sleep spindle density. J Neurosci 2002; 22: 6830-6834.
22. Gelinas JN, Khodagholy D, Thesen T, Devinsky O and Buzsaki G. Interictal epileptiform discharges induce hippocampal-cortical coupling in temporal lobe epilepsy. Nat Med 2016; 22: 641-648.
23. Hagmann P, Cammoun L, Gigandet X, Meuli R, Honey CJ, Wedeen VJ, et al. Mapping the structural core of human cerebral cortex. PLoS Biol 2008; 6: e159.
24. Halassa MM, Siegle JH, Ritt JT, Ting JT, Feng G and Moore CI. Selective optical drive of thalamic reticular nucleus generates thalamic bursts and cortical spindles. Nat Neurosci 2011; 14: 1118-1120.
25. Hermann BP, Seidenberg M, Dow C, Jones J, Rutecki P, Bhattacharya A, et al. Cognitive prognosis in chronic temporal lobe epilepsy. Ann Neurol 2006; 60: 80-87.
26. Hipp JF, Engel AK and Siegel M. Oscillatory synchronization in large-scale cortical networks predicts perception. Neuron 2011; 69: 387-396.
27. Ibrahim GM, Cassel D, Morgan BR, Smith ML, Otsubo H, Ochi A, et al. Resilience of developing brain networks to interictal epileptiform discharges is associated with cognitive outcome. Brain 2014; 137: 2690-2702.
28. Igarashi KM, Lu L, Colgin LL, Moser MB and Moser EI. Coordination of entorhinal-hippocampal ensemble activity during associative learning. Nature 2014; 510: 143-147.
29. Johnson LA, Euston DR, Tatsuno M and McNaughton BL. Stored-trace reactivation in rat prefrontal cortex is correlated with down-to-up state fluctuation density. J Neurosci 2010; 30: 2650-2661.
30. Jung J, Cloutman LL, Binney RJ and Lambon Ralph MA. The structural connectivity of higher order association cortices reflects human functional brain networks. Cortex 2017; 97: 221-239.
31. Lagarde S, Roehri N, Lambert I, Trebuchon A, McGonigal A, Carron R, et al. Interictal stereotactic-EEG functional connectivity in refractory focal epilepsies. Brain 2018; 141: 2966-2980.
32. Maingret N, Girardeau G, Todorova R, Goutierre M and Zugaro M. Hippocampo-cortical coupling mediates memory consolidation during sleep. Nat Neurosci 2016; 19: 959-964.
33. Massimini M, Ferrarelli F, Esser SK, Riedner BA, Huber R, Murphy M, et al. Triggering sleep slow waves by transcranial magnetic stimulation. Proc Natl Acad Sci U S A 2007; 104: 8496-8501.
34. Mueller S, Wang D, Fox MD, Yeo BT, Sepulcre J, Sabuncu MR, et al. Individual variability in functional connectivity architecture of the human brain. Neuron 2013; 77: 586-595.

35. Muller L, Piantoni G, Koller D, Cash SS, Halgren E and Sejnowski TJ. Rotating waves during human sleep spindles organize global patterns of activity that repeat precisely through the night. Elife 2016; 5:
36. Nir Y, Staba RJ, Andrillon T, Vyazovskiy VV, Cirelli C, Fried I, et al. Regional slow waves and spindles in human sleep. Neuron 2011; 70: 153-169.
37. Nishida M and Walker MP. Daytime naps, motor memory consolidation and regionally specific sleep spindles. PLoS One 2007; 2: e341.
38. Proix T, Bartolomei F, Guye M and Jirsa VK. Individual brain structure and modelling predict seizure propagation. Brain 2017; 140: 641-654.
39. Rohenkohl G, Bosman CA and Fries P. Gamma Synchronization between V1 and V4 Improves Behavioral Performance. Neuron 2018; 100: 953-963 e953.
40. Rosenow F and Luders H. Presurgical evaluation of epilepsy. Brain 2001; 124: 1683-1700.
41. Rubino D, Robbins KA and Hatsopoulos NG. Propagating waves mediate information transfer in the motor cortex. Nat Neurosci 2006; 9: 1549-1557.
42. Samaha J and Postle BR. The Speed of Alpha-Band Oscillations Predicts the Temporal Resolution of Visual Perception. Curr Biol 2015; 25: 2985-2990.
43. Sato T, Yamada N, Morimoto K, Uemura S and Kuroda S. A behavioral and immunohistochemical study on the development of perirhinal cortical kindling: a comparison with other types of limbic kindling. Brain Res 1998; 811: 122-132.
44. Sawangjit A, Oyanedel CN, Niethard N, Salazar C, Born J and Inostroza M. The hippocampus is crucial for forming non-hippocampal long-term memory during sleep. Nature 2018; 564: 109-113.
45. Schevon CA, Weiss SA, McKhann G, Jr., Goodman RR, Yuste R, Emerson RG, et al. Evidence of an inhibitory restraint of seizure activity in humans. Nat Commun 2012; 3: 1060.
46. Schmahmann JD, Pandya DN, Wang R, Dai G, D'Arceuil HE, de Crespigny AJ, et al. Association fibre pathways of the brain: parallel observations from diffusion spectrum imaging and autoradiography. Brain 2007; 130: 630-653.
47. Sedat J and Duvernoy H. Anatomical study of the temporal lobe. Correlations with nuclear magnetic resonance. J Neuroradiol 1990; 17: 26-49.
48. Serafini R and Loeb JA. Enhanced slow waves at the periphery of human epileptic foci. Clin Neurophysiol 2015; 126: 1117-1123.
49. Siapas AG and Wilson MA. Coordinated interactions between hippocampal ripples and cortical spindles during slow-wave sleep. Neuron 1998; 21: 1123-1128.
50. Stark E and Abeles M. Unbiased estimation of precise temporal correlations between spike trains. J Neurosci Methods 2009; 179: 90-100.
51. Steriade M, McCormick DA and Sejnowski TJ. Thalamocortical oscillations in the sleeping and aroused brain. Science 1993; 262: 679-685.
52. Takahashi K, Saleh M, Penn RD and Hatsopoulos NG. Propagating waves in human motor cortex. Front Hum Neurosci 2011; 5: 40.
53. Thompson PM, Schwartz C, Lin RT, Khan AA and Toga AW. Three-dimensional statistical analysis of sulcal variability in the human brain. J Neurosci 1996; 16: 4261-4274.
54. Tong X, An D, Xiao F, Lei D, Niu R, Li W, et al. Real-time effects of interictal spikes on hippocampus and amygdala functional connectivity in unilateral temporal lobe epilepsy: An EEG-fMRI study. Epilepsia 2019; 60: 246-254.

55. Ujma PP, Halasz P, Kelemen A, Fabo D and Eross L. Epileptic interictal discharges are more frequent during NREM slow wave downstates. Neurosci Lett 2017; 658: 37-42.
56. Velisek L and Moshe SL. Temporal lobe epileptogenesis and epilepsy in the developing brain: bridging the gap between the laboratory and the clinic. Progression, but in what direction? Epilepsia 2003; 44 Suppl 12: 51-59.
57. Vyazovskiy VV, Faraguna U, Cirelli C and Tononi G. Triggering slow waves during NREM sleep in the rat by intracortical electrical stimulation: effects of sleep/wake history and background activity. J Neurophysiol 2009; 101: 1921-1931.
58. Wierzynski CM, Lubenov EV, Gu M and Siapas AG. State-dependent spike-timing relationships between hippocampal and prefrontal circuits during sleep. Neuron 2009; 61: 587-596.
59. Yang AI, Wang X, Doyle WK, Halgren E, Carlson C, Belcher TL, et al. Localization of dense intracranial electrode arrays using magnetic resonance imaging. Neuroimage 2012; 63: 157-165.
60. Zhang H, Watrous AJ, Patel A and Jacobs J. Theta and Alpha Oscillations Are Traveling Waves in the Human Neocortex. Neuron 2018; 98: 1269-1281 e1264.

Conclusions

The fate of a long-term memory is determined by subsequent experience and is dynamic over a prolonged period. Our results show that three prominent network patterns implicated in memory (SPW-R, SPI, and CXR) undergo dynamic comodulation across the cycle of memory consolidation, reconsolidation, and updating. We hypothesize that temporal links between these plasticity-related oscillations in different brain structures provide the network infrastructure for cellular and molecular changes associated with long-term memory processing. Enhanced SPW-R / SPI coupling was associated with consolidation of memories whereas reconsolidation was influenced by upregulation of SPW-R / CXR coupling. These oscillatory coupling patterns serve as neurophysiologic biomarkers that differentiate consolidation and reconsolidation memory processes. Furthermore, global SPI patterns that are coordinated across multiple neocortical regions are strongly correlated with SPW-R and enhanced with learning. Our findings present an opportunity for design of novel closed-loop investigations to manipulate memory across distributed neural networks and enhance understanding of disorders characterized by impaired and overactive information retention. For example, in cases where individuals have impaired information retention, such as in memory disorders associated with aging or neurological disorders, cognitive interventions or pharmacological treatments aimed at enhancing SPW-R / SPI coupling can aid in memory formation and consolidation. Such interventions could aim to enhance the neural processes involved in consolidation by stimulating multiple neocortical sites at the time of SPW-R to generate global SPIs. Similarly, in cases where individuals have overactive information retention, such as in post-traumatic stress disorder (PTSD) or phobias, modifying SPW-R / CXR interactions, a key neurophysiologic marker of memory reconsolidation, could help identify potential targets for therapeutic interventions aimed at weakening or erasing maladaptive

fear memories. Our results from human epilepsy studies identified IED-spindle coupling as a biomarker of pathological activity which plays a role in establishing the altered global connectivity observed in patients with focal epilepsy. These IEDs, like physiologic SPW-Rs, also induce cortical delta waves and spindles. Modulating spindle expression around the time of IEDs in rodent kindling models can provide a causal link between the IED-spindle and memory, paving way for new opportunities for therapies to address disruption of large-scale intercortical communication in epilepsy.